Non-Linear FE Analysis of RC Slabs with and without Openings Subjected to In- Plane and Out- of- Plane Loads

by Rouzbeh Khajehdehi, Bachelor of Science

A Thesis Submitted in Partial
Fulfillment of the Requirements
for the Degree of
Master of Science
in the field of Civil Engineering

Advisory Committee:

Dr. Nader Panahshahi, Chair

Dr. Brad Cross

Dr. Jianpeng Huang

Graduate School
Southern Illinois University Edwardsville
August, 2013

ABSTRACT

NON-LINEAR FE ANALYSIS OF RC SLABS WITH AND WITHOUT OPENINGS SUBJECTED TO IN- PLANE AND OUT- OF- PLANE LOADS

by

ROUZBEH KHAJEHDEHI

Chairperson: Professor Nader Panahshai

There are two primary methods to investigate the response of reinforced concrete (RC) structural components. Experimental testing method has been widely used to study the behavior of RC members under different loading conditions, while the results obtained have a high degree of accuracy, it is sometimes very time consuming and also can be very costly. Finite element (FE) analysis method as a numerical based solution technique, also is widely used to analyze behavior of structural components, and although the use of this method was very time consuming in several decades ago, however utilizing existing powerful software and hardware capabilities has made it easier nowadays.

An investigation is conducted on two-way RC beam-supported slabs using FE analysis technique to study their inelastic behavior when subjected to in- plane and out- of- plane loads. Two- way RC slab models were constructed for solid slab panels tested by Nakashima (1981) and the results obtained from FE analysis were compared with the experimental data.

Non-linear 3-D ANSYS models with smeared and discrete reinforcing steel were used. The obtained results from FE method indicated an acceptable agreement with experimental data. The verified FE model then was used to investigate the effect of floor openings on inelastic behavior of two-way RC slabs subjected to in-plane and out-of-plane loads. The opening was placed in the mid-region of the slab panel, where its size was varied from 6.25% to 25% of

the panel area. To satisfy the strength requirements Section 13.4 of the American Concrete Institute code (ACI 318-11), additional reinforcement were placed in the slab around the opening. The results are presented and discussed.

It is observed that the failure mechanism changes in slab with larger opening where the steel yielding starts in rebars at the opening corners, and the failure damage at the ultimate load is more distributed. It is concluded that as the opening size increases, effect of out-of-plane (gravity) load on in-plane load capacity reduction of the slab decreases while the ultimate displacement at failure increases.

ACKNOWLEDGEMENTS

It is an honor for me to heartily thank my advisor, Dr. Nader Panahshahi, whose encouragement, patience and generous support from the beginning to the very last days enabled me to develop an understanding of the subject. Professor Panahshahi who has the attitude and substance of an effective supervisor has continually conveyed a spirit of research in regard to this topic. I must honestly say that without his help this thesis would not have been complete.

I also would like to thank Dr. Brad Cross for his continuing support through my master's study; I will always cherish the memories of working for him as a Teacher Assistant for more than two years.

Last but not least, I offer my best regards and blessings to my family especially my dad, Dr. Ali Khajehdehi, M.D., and all of those who supported me in any respect towards the completion of my thesis.

TABLE OF CONTENTS

LIST OF FIGURES

Figure Page

LIST OF TABLES

Table Page

CHAPTER 1

INTRODUCTION

1.1 General

Understanding the behavior of RC components in structures subjected to different loading conditions is very important in order to obtain a comprehensive knowledge to design a safe and functional structure.

There are several methods to analyze the response of RC structural components. Experimental testing is one the most reliable methods to understand the behavior of structures. While this method yields a high degree of accuracy, it is time consuming and always entails a high cost. Use of FE analysis method has become popular in recent years; it is fast and saves time and money. Although the use of this method was time consuming because of low processing capability of computers before, it is much easier these days with existing of faster computers in terms of both software and hardware capabilities.

The results obtained from FE analysis must be scrutinized very carefully. To fully understand the results of a FE analysis program; one must closely check the results and compare them with experimental data or other methods of analysis such as reliable and reasonable hand calculation methods. The validity of FE model must be verified first.

In this study, two-way RC slabs with and without openings were modeled using commercial software package ANSYS to understand the inelastic behavior of slabs with and without openings when subjected to in-plane and out-of-plane loads.

1.2 Statement of the Problem

Within every building, there are multiple elements that are used to transmit and resist lateral forces. These transmitting and resisting elements define the building's lateral-load path. There are two orientations of primary elements in the load path: those that are vertical, such as shear walls, braced frames, and moment frames, and those that are essentially horizontal, such as the roof, floors, and foundation. The roof and floor elements are known as diaphragm

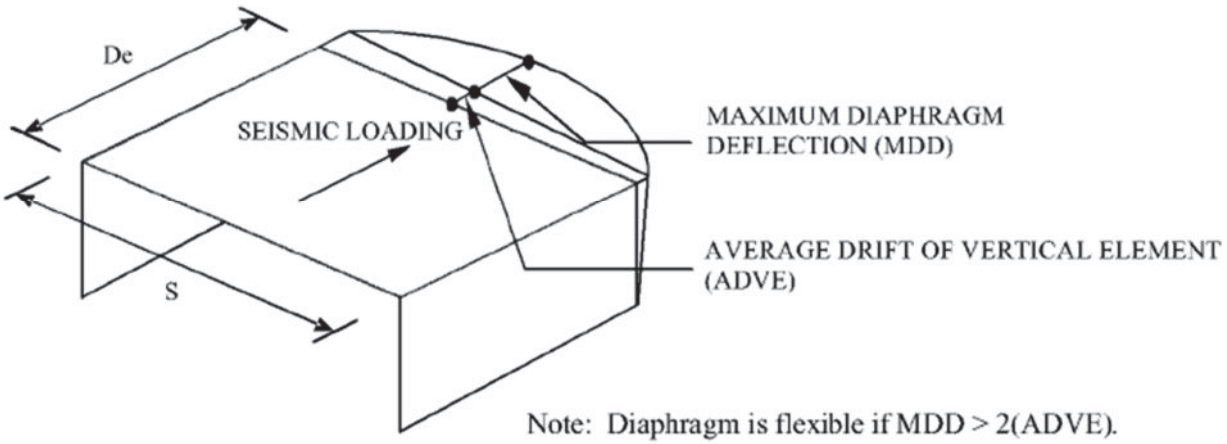

Figure 1.1: Floor Diaphragms (ASCE, 2010)

A floor diaphragm may be classified as rigid, semi-rigid or flexible. A diaphragm may be considered as rigid when its midpoint displacement, "MDD" as shown in Figure 1.1, under lateral load, is less than one half of the average displacements at its ends, "ADVE/2" (ASCE, 2000). Rigid diaphragm distributes the horizontal forces to the vertical load resisting elements in direct proportion to their relative rigidities. It is based on the assumption that the diaphragm in-plane deformation is negligible, and it will cause vertical elements to deflect laterally the same amount when no torsion is present. A diaphragm is considered flexible, when the midpoint displacement under lateral load, "MDD", exceeds twice the average displacement of the end support, "2ADVE" (ASCE, 2010). It is assumed here that the

relative stiffness of the end supports is large compared to that of diaphragm. For the cases where diaphragm deflections and resisting members' deflections are in the same order of magnitude, then such diaphragm is categorized as a Semi-Rigid diaphragm, which basically represents a diaphragm condition between Rigid and Flexible.

At present, the ASCE/SEI 7-10, "Minimum Design Loads for Buildings and Other Structures" (ASCE, 2010) allows the use of a rigid floor assumption in concrete buildings with plan aspect ratio equal or less than 3:1, where no horizontal plan irregularities exist. The assumption that the concrete floor slab is infinitely rigid in its own plane has frequently been adopted in structural analyses due to the simplicity of the analysis procedure and lack of understanding of the in-plane behavior of RC floor systems. However, experience and research have clearly demonstrated the importance of the influence of in-plane diaphragm deformations on the seismic response of many types of buildings. This influence is more pronounced for long rectangular low-rise buildings, particularly where a dual bracing system, consisting of moment-resisting frame and stiff shear-walls is used (Panahshahi et al., 1991). Thus, an understanding of the in-plane behavior of RC floor slabs and their influence on the dynamic characteristics and response of structures (i.e., fundamental period and distribution of the lateral forces in the vertical elements) is necessary. This understanding can be obtained by using both experimental and analytical investigations. In this research study three dimensional non-linear load deformation characteristics of RC slabs with and without openings are evaluated and the results are compared with experimental results, when available.

1.3 Motivation and Objectives

The main goal of this project is to use an analytical method for predicting the in-plane characteristics of concrete floor diaphragms subjected to the gravity loads and in-plane seismic loads and to provide meaningful information for analysis and design of the concrete buildings with semi-rigid concrete diaphragms. This study is concentrated on the floor slab system with edge beams, referred to as the beam-supported slab (slab-on-beam) system. Both slabs with and without openings are investigated.

Previous research conducted at State University of New York at Buffalo has proved that the distribution of earthquake loads is greatly influenced by in- plane deformation of floor diaphragms in rectangular buildings when a dual bracing lateral force resisting system consisting of moment resisting frame and stiff shear walls is used (Panahshahi et al., 1991 & 1994). It was observed that occurrence of significant in-plane cracking and yielding in floor diaphragms affects their in-plane capacity and lateral force distribution in them.

Panahshahi et al. (1991 & 1994) have indicated that cracking and in-plane yielding of RC floor systems is likely to happen in low-rise rectangular buildings with dual bracing systems when aspect ratio of the plan exceeds 3:1. In the those buildings, interior columns failure may occur as a culmination of strength and ductility demands put on them caused by premature failure and yielding of floor diaphragms while shear walls may stand still.

Damage due to diaphragm action was experienced in numerous cases. The collapse of Taiyo Fisheries in Japan was based on the same failure mode mentioned above. Premature failure of interior columns was followed after partial collapse of floor diaphragm while the shear walls remained standing. The damage observed in a department store in Northridge Fashion

Center was associated with diaphragm response. A parking structure in Santa Monica experienced same failure scenario (Philips 1993).

A three dimensional analytical model was developed based on non-linear FE technique using ANSYS for concrete floor system to identify the important parameters governing the in-plane load-deformation characteristics of the floor system with and without openings. The accuracy of this model is checked by comparing the results obtained from experiments conducted on solid slabs at Lehigh University (Nakashima, 1981).

CHAPTER 2

REVIEW OF THE LITERATURE

2.1 General

In this chapter latest data available related to current study was addressed. Also latest contribution of FE Analysis method in RC field and other efforts that were done before but are related to the current study was reviewed.

2.2 FE Analysis of RC Members

In terms of FE analysis contributions, Shing and Tanabe (2001) and Willam and Tanabe (2001) have done numerous studies related to non-linear FE analysis of RC structures subjected to seismic and cyclic loads, rebar bond analysis, and shear failure of RC members.

Tavarez (2001) describes and compares three existing methods to simulate the rebar behavior of a RC member in a FE analysis: the embedded, smeared and discrete model (Figure 2.1).

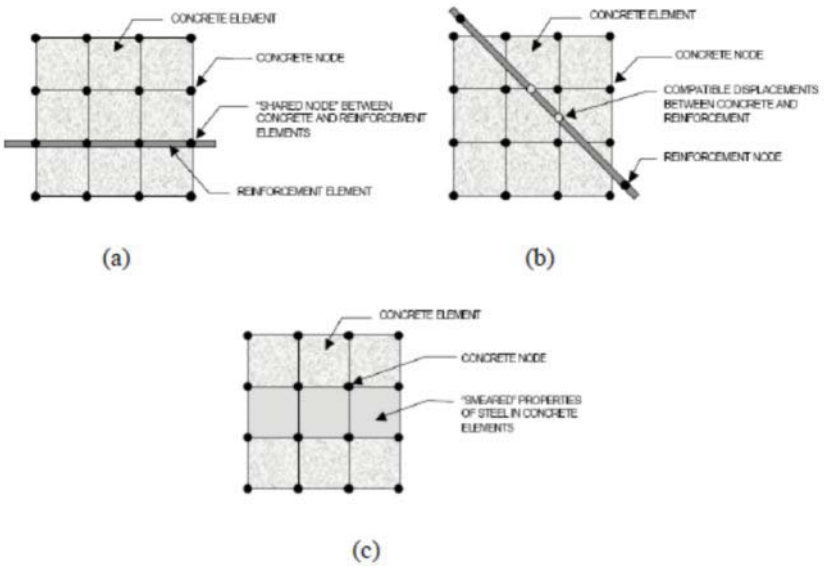

Figure 2.1: Rebar Models in RC Members: a) Discrete; b) Embedded; c) Smeared, (Tavareaz, 2001)

Smeared model (Figure 2.1c) distributes the rebar thorough the concrete element which is an appropriate assumption for type of models which their response is not highly dependent on steel reinforcements, or models that are evaluated up to service level and no yielding of rebars occur. The embedded model (Figure 2.1b) is very accurate but will increase the computational cost because it will introduce more nodes. While discrete modeling (Figure 2.1a) may not have the accuracy of the embedded model, but since it is sharing the nodes the analysis time may be less than discrete one. According to Fanning (2001) discrete and embedded reinforcement models work best for rebar modeling in RC members.

2.3 Flexural Behavior of RC Slabs

Floor systems in multistory building serve for several purposes, they transfer gravity loads through their out-of-plane action, and lateral loads (e.g., caused by earthquakes) through their in-plane action to the vertical elements. Out-of- plane behavior of the floor systems have extensively been studied in the past. Clear and complete design procedures are present in chapter thirteen of American Concrete Institute (ACI) Building Code, ACI 318-11. Through floor system's so called diaphragm action, they play another important task; interconnecting all vertical elements and transferring lateral loads to lateral load resisting systems such as shear walls. Diaphragm function of the floor systems are controlled by their in-plane and relative stiffness with respect to lateral load resisting systems. Under cyclic loads such as earthquakes, inertia forces generated in floor systems are transferred through diaphragm action of floor systems to lateral load resisting systems such as shear walls (Nakashima et al, 1984).

It is the earthquake loads (in-plane) which will push the slab to its inelastic range and even failure (Panahshahi et al., 1991). This emphasizes the need for more information on behavior of various RC diaphragms when subjected to both in-plane and out-of-plane loads.

The presence of openings in floor diaphragms for the architectural, staircase and elevator shaft purposes sometimes is inevitable. These openings will results in diaphragm stiffness reduction and can cause stress concentration in their corners. These types of diaphragms are usually designed ignoring the above effects, therefore, their response maybe inadequate when subjected to earthquake loads. In other words presence of openings even makes the in-plane behavior of the floor diaphragms more complicated, and simplified design guidelines are needed.

American Concrete Institute (ACI) Building Code, ACI 318-11, Section 11.11.6, briefly explains the effect of openings on floor diaphragms in very broad terms. The section introduces certain restrictions for the size and location of the opening. According to this section any reinforcement interrupted by an opening must be placed one half on each side of it. This section however does not explain the effect of opening on the diaphragm actions.

J. Jiangt and F. A. Mirzaf (1993) studied the non-linear behavior of RC slabs without openings using a discrete FE approach. The study dealt with cracking pattern, bond-slippage of rebars and the difference between using a discrete and smeared cracking pattern. The results were compared with experimental results; however, the mentioned characteristics were only evaluated when slabs were subjected to out-of-plane loads.

Ola Enochsson et al. (2006) Investigated behavior of slabs with openings. They have focused on the structural behavior of two-way RC slabs with openings, subjected to distributed service loads. However the effect of in-plane loads was not considered in that study.

Koh Heng Boon et al. (2009) have investigated the behavior of RC slabs with openings, the study focused on the lack of enough information for designing the RC slabs with openings in the ACI code. The main objective was to evaluate the behavior of slabs with openings with different sizes at different locations, and the fact that openings with relatively large sizes will have considerable effect on capacity of the slab. However, the slabs were only subject to out-of-plane loads and the effect of in-plane loads was not studied.

Joel M. Barron et al. (2004) started with the fact that there is little information available in order to validate the efficiency of the assumption of using a rigid diaphragm for RC floor diaphragms. The study dealt with evaluation of the seismic response of four different RC buildings with different seismic characteristics to determine if assuming a rigid floor system yields an acceptable design result. A case study was developed and the four models were analyzed using a rigid floor assumption, then the analysis was conducted using a flexible floor assumption. Linear static, linear dynamic and non-linear dynamic scenarios were used to analyze the models. The analysis concluded that floor flexibility is more obvious in short rectangular buildings. However, the study did not include the effect of openings.

Hosam A. Daham (2010) investigated non-linear behavior of RC two-way slabs with openings using FE software package ANSYS. The study focused on the lack of enough information in building codes when it comes to designing slabs with relatively large openings. The study evaluated the effect of openings and how it degrades the stiffness and strength of the slabs. The effect of different boundary conditions on behavior of slabs with

and without openings also was evaluated. Although the research presented a detailed comparison between slabs with openings and without openings, all investigated models were subjected to out-of-plane loads and effect of in-plane loads was not considered.

Piotr Rusinowski (2005) started with the concern that the proposed procedures to design slabs with relatively large holes by Swedish building codes are not accurate and underestimates the load capacity of the slabs. The study investigated effect of openings in RC two-way slabs and limitations in Swedish building codes to design them. The study was conducted on a full scale model with square openings. Two types of slabs with different boundary conditions were tested; RC slabs with square openings, and Carbon Fiber Reinforced Polymers (CFRP) slabs with sawn up openings. Non-linear FE models using ABAQUS were used to verify results obtained from experiments. Introduction of an accurate plasticity model for FE analysis of RC structures was also part of this research study. The study presented suggestion about using diagonal extra reinforcement in the corners of openings (area of stress concentration). Carbon fiber was recommended rather than traditional steel reinforcement because it yields a better load carrying capacity in tested slabs. In terms of FE analysis techniques, it was recommended to use a set of discrete springs to simulate complicated supporting conditions. Although the research presented good suggestions in terms of design procedures and FE analysis techniques of slabs with openings, both experimental and computer models were subjected to distributed out-of-plane loads only. The effect of in-plane loads was not investigated.

Paolo Casadei et al. (2009) investigated the out-of-plane failure capacity of RC two-way flat slabs with centered square openings. Three types of slabs were tested; a) two-way slabs with no openings, b) two-way slabs with centered openings and no strengthening, c) Two- way

slabs with openings and CFRP strengthening plies applied to the tensions faces around the opening. The effect of in-plane loads was not part of this study.

CHAPTER 3

EXPERIMENTAL STUDY AT LEHIGH UNIVERSITY

3.1 General

This Chapter presents a brief overview extracted from Nakashima's doctoral dissertation submitted to civil engineering department of Lehigh University (Nakashima, 1981). The study was about a number of experiments conducted on scaled RC floor slabs with different loading and support conditions. The results of those experiments provided general information about in-plane characteristics of floor slabs. The results obtained from the experiments were used to calibrate and verify the FE model in this study. After verification of the FE model, openings were added to the slabs in order to investigate the effect of openings on in-plane characteristics of RC floor diaphragms.

3.2 Design of Test Structures

3.2.1 Prototype floor system and scaled model

The prototype floor slab for test specimens was taken from a rectangular multi-story, multi-bay RC building, consisting of shear walls serving as earthquake resistance system. Structural dimensions were chosen for a low to high rise RC building. The center-to-center span length of slab panels were 7.320 m (24 ft) in both directions, the columns were 610 mm x 610 mm (24 in. x 24 in.), the slab was 180 mm (7 in.) thick, and the beams were 610 mm x 310 mm (24 in. x 12 in.) in their cross sections. A portion of the plan is shown in Figure 3.1.

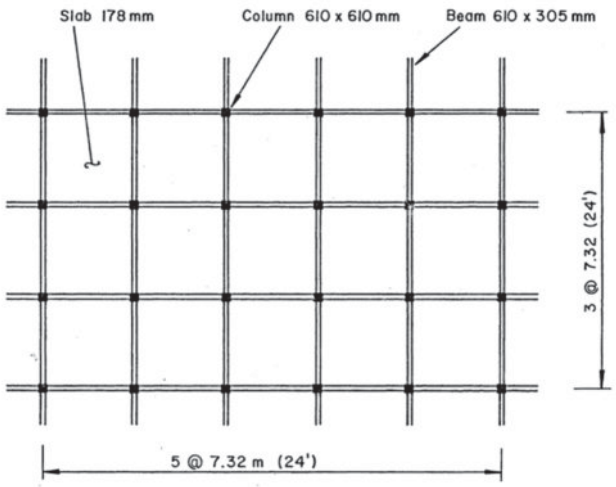

Figure 3.1: Prototype Dimensions (Nakashima, 1981)

The idea behind choosing this test specimen was to represent an interior panel of the prototype building which was supported on one edge by columns and on opposite edge by shear walls. Overhanging slabs, having a length equal to quarter of the panel dimension were added to the edges without shear walls to represent the adjacent bays. The idea of having an experimental model with full scale dimensions was dismissed because of economy, required lab space, and other factors related to the test. Also having a model with small dimensions was not acceptable because of limitations associated with modeling of aggregates, steel reinforcements, and bonding effects between them. Finally an intermediate scaling ratio of 1: 4.5 was chosen. Figure 3.2 illustrates dimensions and supporting conditions in the test specimen used in the experiment. The panel dimension was 1630 mm x 1630 mm (64 in. x 64 in.) and 39.5 mm (1.55 in.) thick.

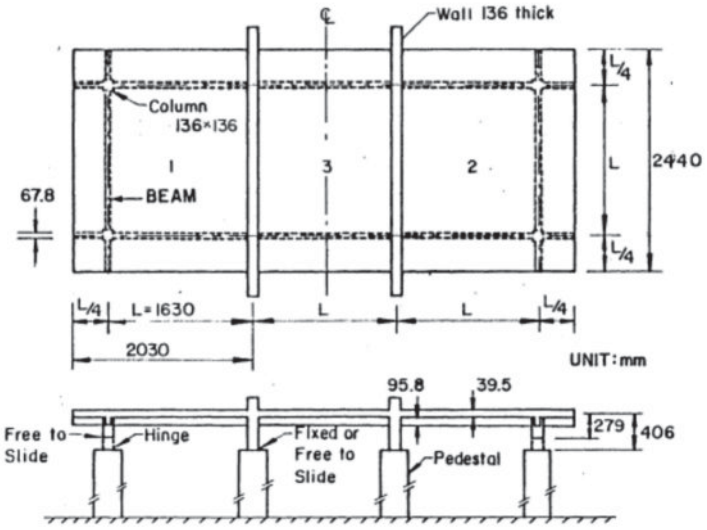

Figure 3.2: Dimension and Supporting Conditions (Nakashima, 1981)

3.2.2 Design of test specimen

The floor slab of the full scale building was designed using direct method explained in ACI Section 13.6, with service live load of 3.8 kPa (80 psf) (ACI, 1977). Columns selected from intermediate floor level, were designed for combined bending moment and axial force caused by vertical load. The shear walls however, were designed to resist maximum shear force, this was done to prevent any failure in shear walls and make sure that the failure will occur in slabs first. The results obtained from the direct method design were then scaled down to be used for test specimen. Table 3.1 lists the dimensions of test specimen.

Table 3.1: Dimensions of Test Specimen (Nakashima, 1981)

Items	Dimensions (mm)	(in.)
Center-to-Center Span Length	1630	64
Exterior Panels	2030 x 2440	80 x 96
Interior Panel	1030 x 2440	64 x 96
Slab Thickness	39.6	1.56
Beam Width	67.8	2.67
Beam Depth (projecting depth)	95.8	3.77
Column Length (from the mid-plane of the slab)	280	11.0
Column Cross Section	136 x 136	5.34 x 5.34
Wall Thickness	136	5.34
Wall Length	3000	118.0
Total Wall Height	612	24.1

Because the model was a scaled model extreme attention was paid to the size of the rebars. Figure 3.3 illustrates the way rebars were installed in slab and beams.

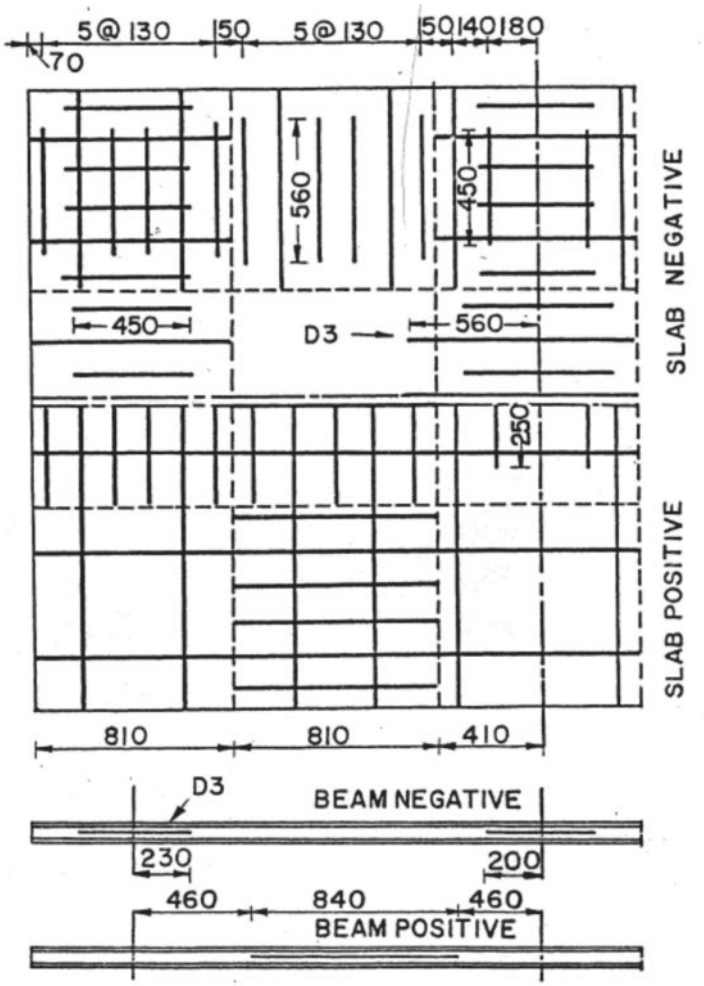

Figure 3.3: Rebar Details in Concrete slab and Beam (Nakashima, 1981)

Table 3.2 lists required and provided area of reinforcements, dimensions and design moments obtained from code. According to the design, temperature requirement (.00018 multiplied by total area of the section) determined the required rebar area in most of sections.

Table 3.2: Design Detail of Concrete Slab (Nakashima, 1981)

	Strip	Sign	A_s Required (mm^2)	A_s Provided	Required Steel Ratio	Over Reinforcement Ratio	Over-Strength Ratio
1	Column	Negative	58*	D2.0 x 6	0.0018	1.3	2.9
		Positive	58*	D2.5 x 2 + D2.0 x 4	0.0018	1.5	5.6
	Column	Negative Interior	58*	D2.0 x 6	0.0018	1.3	4.1
	Middle	Negative	61	D2.0 x 6	0.0019	1.3	1.3
		Positive	58*	D2.5 x 2 + D2.0 x 4	0.0018	1.5	5.6
	Middle	Negative Interior	120	D3.0 x 7	0.0038	1.1	1.1
2	Column	Negative	58*	D2.0 x 6	0.0018	1.3	2.8
		Positive	58*	D2.0 x 6	0.0018	1.3	5.0
	Column	Negative Interior	29*	D2.0 x 2	0.0018	1.1 ?	2.2
		Positive Interior	29*	D2.0 x 2	0.0018	1.1 ?	4.1
	Middle	Negative	67	D2.0 x 6	0.0021	1.2	1.2
		Positive	58*	D2.0 x 5	0.0018	1.1	1.9

* Controlled by temperature requirement

** Based on flexural resistance

Table 3.3 lists the amount of required and provided rebars in the beams. According to requirements in Appendix A of the ACI 318-77 code, extra rebars were placed in bottom of negative moment and top of positive moment to meet the continuity requirements.

Table 3.3: Design Detail in Concrete (Nakashima, 1981)

Region	Required Area	Actual Area	Ratio (Actual/Required)
Negative Moment (Around Columns)	54.3 mm^2 (0.0842 $in.^2$)	D3.0 x 3 (58 mm^2)	1.07
Negative Moment (Around Walls)	33.2 (0.0515)	D2.0 x 3 (39 mm^2)	1.17
Positive Moment	27.9 (0.0432)	D2.0 x 3 (39 mm^2)	1.39

3.2.3 Fabrication of specimen

Strain gages along with reinforcing bars and fifty inserts were placed in their specified locations; the inserts were used as hooks to transfer vertical loads. In order to make the construction process easier, the frame was elevated 1.2 m (4 ft) above the lab floor (Figure 3.2).

Two specimens; B-1 and B-2 were built at the same time from same concrete mix at the lab. Concrete with 27.6 MPa (4000 psi) compressive stress was selected for slab and shear walls and concrete with 34.5 MPa (5000 psi) was selected for the columns. Table 3.4 lists concrete mix properties.

Table 3.4: Concrete Mix Properties (Nakashima, 1981)

For 1.0 m^3 (1.3 cu.yd) Concrete	Concrete 27.6 MPa (4,000 psi)	Concrete 34.5 MPa (5,000 psi)
Type 1 Portland Cement	330 kg (730 lbs.)	400 kg (880 lbs.)
6.4 mm Crushed Limestone	770 kg (1700 lbs.)	770 kg (1700 lbs.)
Concrete Sand	1000 kg (2300 lbs.)	1000 kg (2300 lbs.)
Total Water	0.23 m^2 (60 gals.)	0.23 m^3 (60 gals.)
WRDA-19 Plastisizer	0.012 m^3 (110 oz.)	0.015 m^3 (130 oz.)
Water Cement Ratio	0.68	0.57

The aggregates were restricted to size of 6.4 mm (0.25 in) in order to obtain the relationship between aggregate and slab thickness in real building model.

Different concrete cylinders were created and were cured in same condition as the specimen concrete. Both test specimen and cylinder concretes were air-cured. Mechanical properties of rebars and concrete obtained from tension test for steel and concrete cylinder test for concrete are presented in Section 3.3.

3.3 Mechanical Properties of Materials

3.3.1 Reinforcing bars

Average values for mechanical properties of four tension tests of three different rebar sizes used in specimens (D2.0, D2.5, and D3.0) are given in Table 3.5.

Table 3.5: Mechanical Properties of Rebars (Nakashima. 1981)

Size	Area (mm^2)	Yield Stress (MPa)	Yield Strain (m/m)	Ultimate Stress (MPa)	Ultimate Strain (m/m)	Modulus of Elasticity (GPa)
D2.0	13.4	368	1.93×10^{-3}	411	78.3×10^{-3}	191
D2.5	17.2	609	3.11×10^{-3}	668	49.2×10^{-3}	196
D3.0	21.5	590	2.72×10^{-3}	590	62.5×10^{-3}	190

3.3.2 Concrete

For each of the two specimens B-1 and B-2 two types of concrete were utilized in the experiments: 27.6 MPa (4000 psi) for slabs, beams and shear walls; and 34.5 MPa (5000 psi) for columns. Different concrete cylinders cured in the same condition were tested to make sure the mechanical properties were accurate. Table 3.6 lists mechanical properties of concrete used at initial stages of testing.

Table 3.6: Mechanical Properties of Concrete (Nakashima, 1981)

Type		Slump (mm)	7-Day Strength (MPa)	28-Day Strength (MPa)
27.6 MPa (4,000 psi)	Batch 1 (B-1)	110	23.2	27.7
	Batch 2 (B-2)	120	24.0	28.8
34.5 MPa (5,000 psi)	Batch 1 (B-1)	110	29.9	36.1
	Batch 2 (B-2)	130	26.8	33.1

3.4 Testing Procedure

3.4.1 Test setup

As mentioned earlier in Section 3.2.3 the test specimen was elevated 1.2 m (4 ft) in order to facilitate installing the loading and measurement instruments. The model was supported on four concrete pedestals which were fully fixed to the laboratory floor, thus the wall and the columns could sit on top of the pedestals. Different supporting conditions were provided on top of these pedestals. Supporting condition for walls were provided in three ways: first was to fix the wall and prevent it from any movement about floor plane, second was to let the wall to move about any horizontal planes at top of the pedestals, third alternative was to prevent any lateral movements but let it to rotate about a vertical plane. Column bases were also provided with conditions to either have a free-to-slide condition or to be fixed. The columns with a free-to-slide support condition were completely free to slide in a way that they did not have any reaction against horizontal loads. However they were able to react

against vertical gravity loads. On the other hand, fixed- base condition provided resistance against lateral loads, and was only given the freedom to rotate about both bending axis.

3.4.2 Loading system

The in-plane loads were applied to the test specimen using a mechanical jack that applied loads to five integrated studs at equal distances of 540 mm (21.3 in.) on a steel frame attached to beam. This set up for loading was used to distribute the lateral load equally along the line of loading. Figure 3.4 illustrates the set up for lateral loading.

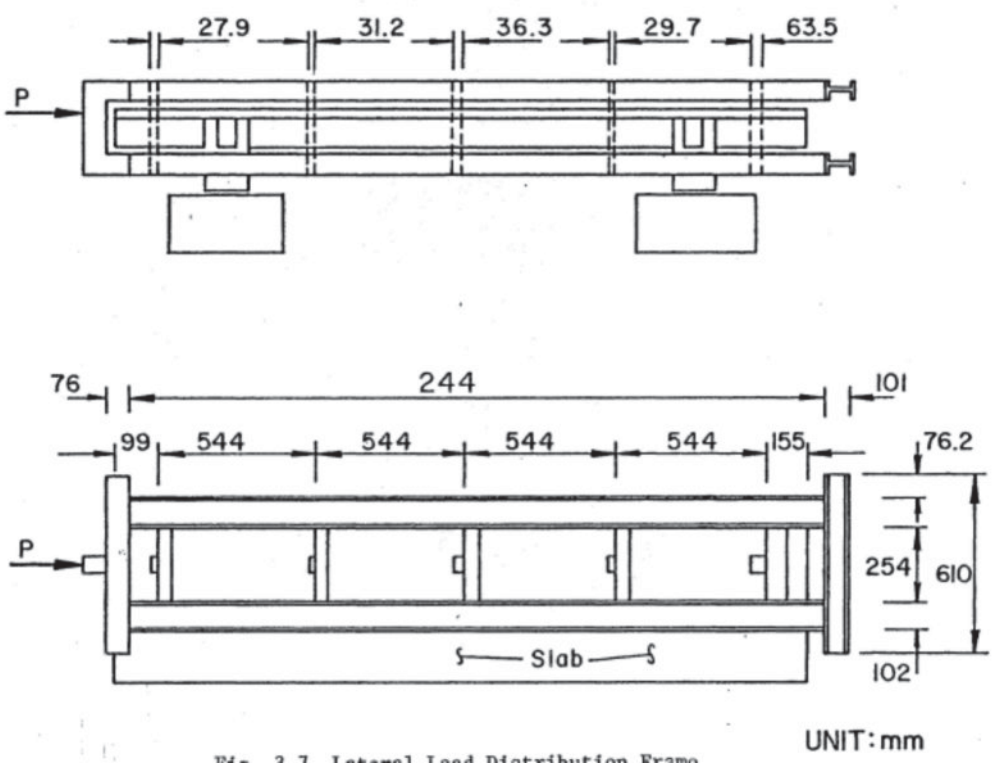

Figure 3.4: Lateral Load Set up (Nakashima, 1981)

The application of out-of-plane loads was done using inserts equally spaced at 540 mm (21.3 in.) center- to- center in both directions. Figure 3.5 illustrates application of vertical loads.

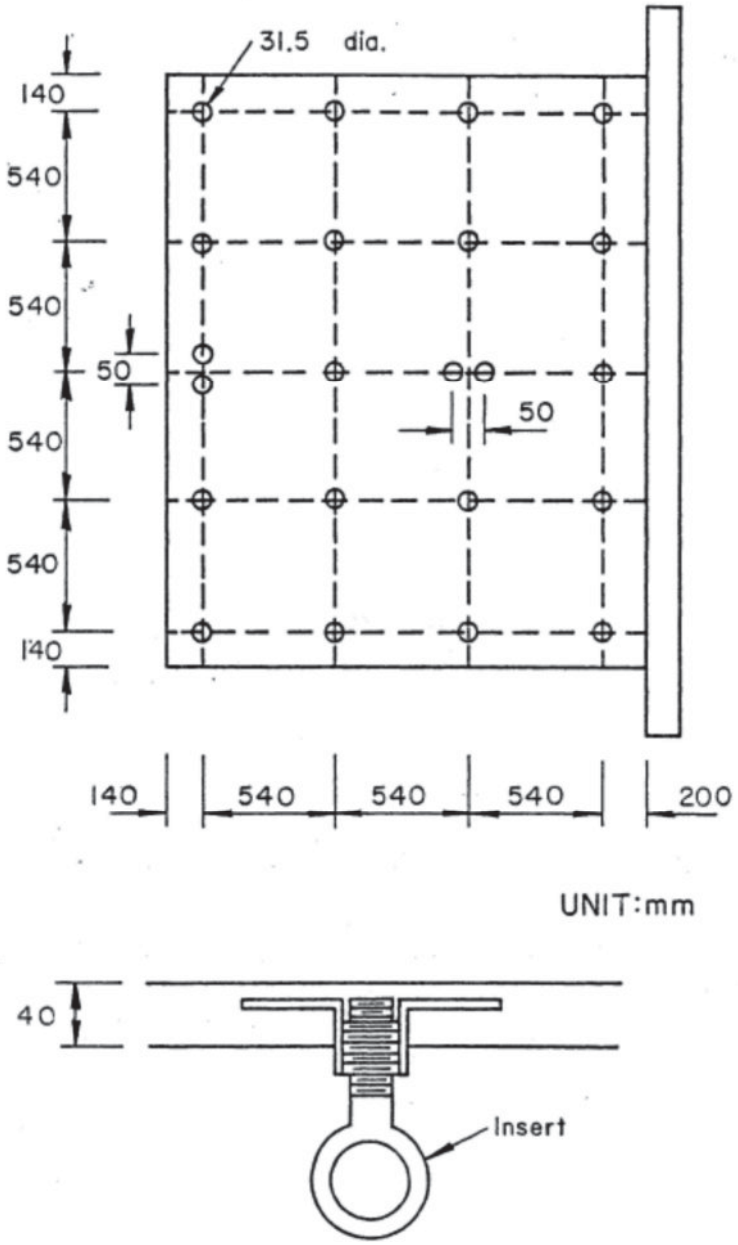

Figure 3.5: Application of Vertical Load (Nakashima, 1981)

3.4.3 Instrumentation

LVDT's were used to monitor in-plane deflections (Figure 3.6a). Vertical deflections were monitored using three fixed scales that were installed at top of the test specimen at mid-spans

of slab panels and beams perpendicular to the walls as shown in Figure 3.6b. Figure 3.6b shows the locations of LVDT's used of measuring in-plane deflections of the end panels.

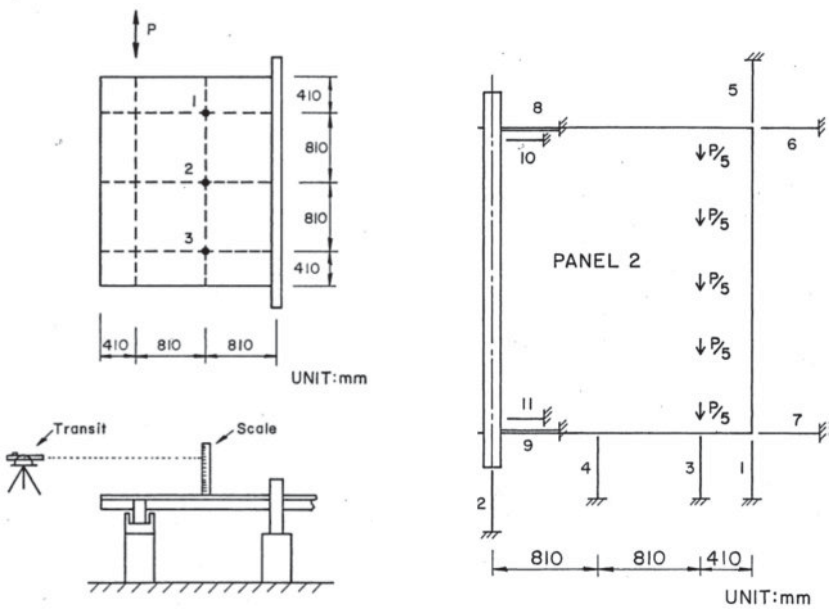

Figure 3.6: a) Vertical Deflection Measurement (left), b) Lateral Deflection Measurement (right) (Nakashima, 1981)

3.5 Programs for Testing

In order to make the most of the test specimens, series of testing sequencers were designed for each of two specimens. Four different kinds of tests were: strength test, stiffness test, free vibration and repaired strength test. Stiffness test measured elastic stiffness of the slabs. In strength test, ultimate strength, ductility and stiffness in inelastic range were measured. The damaged specimens were repaired and tested again and these tests were named repaired strength tests. In free vibration tests natural frequency and period of the slabs were investigated. However in this study the main focus was on strength tests.

3.5.1 Stiffness test

In-plane stiffness tests were performed prior to strength tests. Symmetrical and anti-symmetrical in-loads were applied along the edge beams parallel to the walls in both panels 1 and 2 (Figure 3.2) of the specimens with free-to-rotate wall condition and free-to-slide column condition (Figure 3.7). Applied loads were about 15 kN (3.5 Kip), twelve percent of the ultimate load to make sure that specimen behaves elastically.

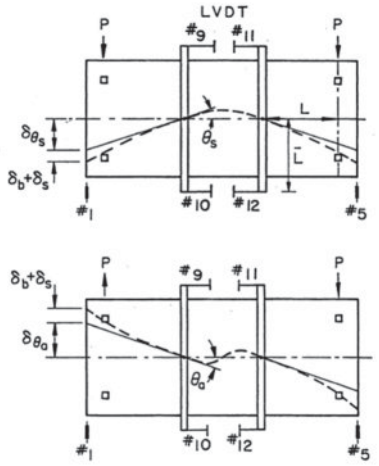

Figure 3.7: Stiffness Test Setup

3.5.2 Strength test

In the strength tests, the wall connection was completely fixed through the use of braces and bolts, the columns were provided with free-to-slide supporting condition. Application of in-plane loads were along the column line parallel to the fixed wall. Out- of-plane loads were applied using inserts in specific locations mentioned in Section 3.4.2.

In-plane loads were applied in two ways: monotonic and cyclic loading. In monotonic loading the magnitude of the in-plane loads were increased up to the ultimate strength was reached.

Cyclic loads were applied at complete cycles of various amplitudes in each cycle used to investigate the hysteresis behavior of the specimen.

For the tests involved out-of-plane loading, live and dead load was chosen to represent the service loads. Because the specimens were scaled by factor of 4.5 an extra load had to be added to simulate the real weight of the prototype. A total load of 45.8 kN (10.3 kip) was applied to the scaled model for the testing of panel 1 or 2.

3.6 Test Results

3.6.1 Behavior of test slab under service vertical load

Table 3.7 lists the vertical displacements obtained at three locations shown in Figure 3.6a after the out-of-plane service load was applied to panels 1 and 3 prior to being tested for in-plane monotonic (MN) and cyclic (CY) loads. The computed values using uncracked section properties (elastic theory in Table 3.7) underestimated these measured displacements since two lines of cracks, one along the top of the wall and the other along the top of the beams parallel to the wall were observed. Figure 3.8 illustrates the location of the cracks on top surface of the panel.

Table 3.7: Vertical Deflection under Full Service Loads (Nakashima, 1981)

Test	Scale #1 (mm)	Scale #2 (mm)	Scale #3 (mm)
BV 1MN	0.76	1.30	1.02
BV 2CY	0.76	0.89	1.52
Elastic Theory	0.42	1.17	0.42

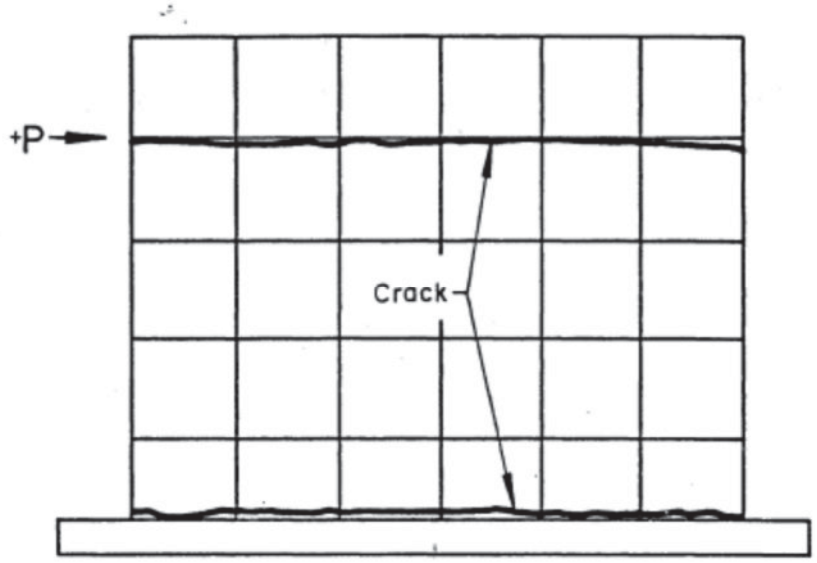

Figure 3.8: Cracks Caused by Vertical Service Loads (Dead+ Live) (Nakashima, 1981)

3.6.2 Strength test results

Ultimate in-plane loads and displacements in different tests subjected to different loads are listed in Table 3.8. Notations used in Table 3.8 are explained in detail in Section 5.1.1.

Table 3.8: Load and Displacements for Different Testing Conditions (Nakashima, 1981)

Test	Ultimate Load (kN)		Maximum Displacement (mm)	
	Positive	Negative	Positive	Negative
BH 2MN	120.0	- 88.5	8.48	- 7.44
BH 1CY	94.7	- 96.5	8.36	- 8.29
BH 3MN	56.9	- 38.7	7.32	- 6.17
BH 3CY	41.8	- 40.5	6.21	- 5.87
BV 1MN	102.0	- 89.8	9.22	- 9.22
BV 2CY	85.0	- 83.2	6.72	- 7.02

CHAPTER 4

FINITE ELEMENT (FE) MODELING

4.1 Introduction

This chapter describes analytical part of this study. The FE method was used to analyze the non-linear behavior of RC slabs with and without openings. These analyses were performed using educational version of software package ANSYS 13.0. Before modeling the prototype slab, a simple RC cantilever beam was used for verification purposes, where the cracking pattern in concrete, and stresses in steel and concrete were compared with hand calculations. Modeling of this beam helped in a better understanding of non-linear behavior of RC structures and different parameters associated with its analysis using the ANSYS software package.

4.2 Calibration Beam

This section very briefly explains the modeling and analysis of the calibration beam using ANSYS, verification of the results with hand calculations and conclusions which were very helpful for this research. However detailed procedure of FE modeling (element type, material properties, solution module and etc...) will be explained fully in the next section related to modeling of prototype beam supported slab panels (Section 4.3).

The dimensions for full size cantilever beam were 120 in. x 12 in. x 12 in. Area of steel of 0.8 in^2 was used at 1.5 in. from top; the beam was loaded with a point load at the top of the free side. Figure 4.1 illustrates the half- size FE beam model used for the calibration, taking advantage of beam and load symmetry to reduce analysis time.

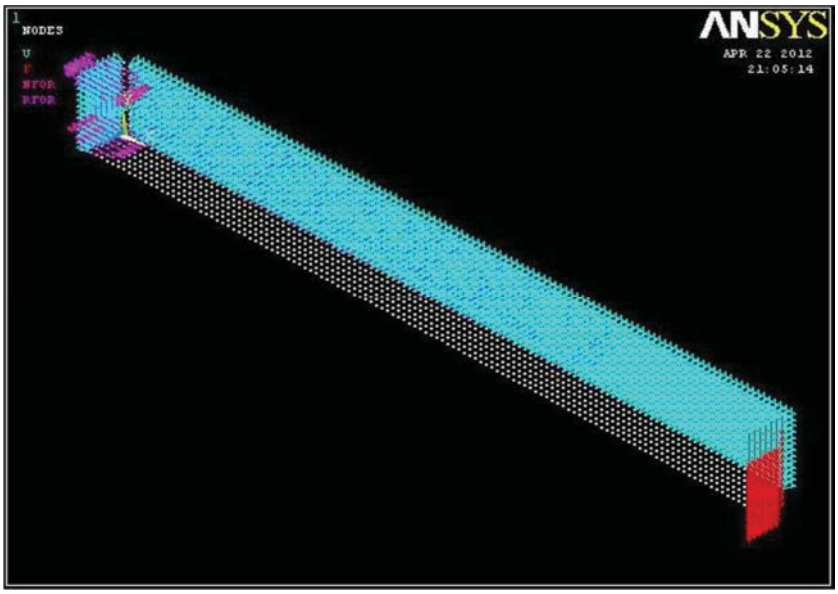

Figure 4.1: FE ANSYS Calibration Beam Model

SOLID65 brick element was used to model concrete, smeared capability of SOLID65 was used to model rebars in the longitudinal direction by providing a volumetric ratio ($\frac{Volume\ of\ Steel}{Volume\ of\ Concrete\ Element}$) in the appropriate elements. Ultimate compressive stress and modulus of rupture were defined for concrete to account for non-linear behavior. A bilinear stress-strain curve was defined for steel material properties. Performing a non-linear analysis of this beam using ANSYS entailed dealing with many parameters, each having significant contribution in results, meaning that even a slight change in those parameters led to a big error. Boundary condition was one of those parameters where extreme care was taken in assigning it. A combination of fixed-fixed and restraint only in X- direction at support were used for fixed end in a way that only one line (the midline) was fixed in all directions and the other nodes were only retrained in x-direction.

A concrete with compressive strength of 3000 psi and steel rebars with yield stress of 60 ksi were used in the model.

Analysis was performed and the results were compared with hand calculated results in three stages: linear, yield of steel and near the ultimate failure of concrete. The hand calculation procedure is presented in Appendix A of this study. Table 4.1: lists a summary of the overall results obtained from analysis of the calibration beam. As it is observed there is good agreement between the ANSYS results and hand calculations at all three loading stages.

The cracking pattern, as one of the most important aspects in non-linearity of concrete also was investigated. Figure 4.2 illustrates a comparison between cracking pattern obtained from ANSYS versus the calculated results using transformed section method at beam cracking load.

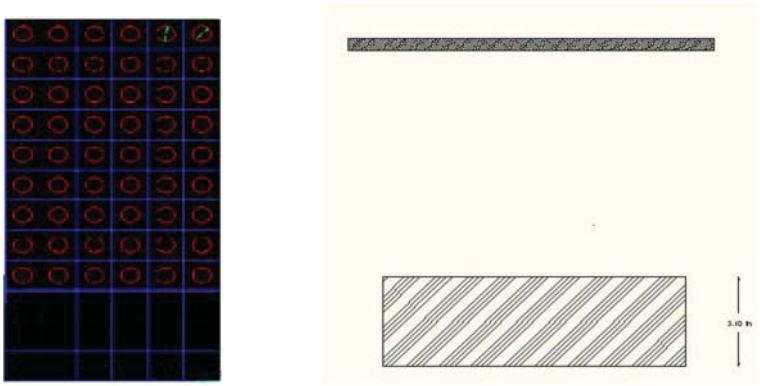

Figure 4.2: Cracking Pattern Comparison between ANSYS and Transformed Section Calculation Results

As it can be seen in Figure 4.2 the height of calculated compression block at right (Y=3.1 in.) well compares to the one from ANSYS (left). The red circles represent the cracked SOLID65 elements under tension which corresponds to the hollow section (tension area of concrete) at the right.

Table 4.1: Comparison between ANSYS and Hand Calculations

		Extreme Compression Fiber Stress (psi)	*Reinforcing Steel Stress (psi)*	*Max Defletion of the Beam (in.)*	*Applied Load (lbs.)*
Linear	*Hand Calculation Results*	309.819	2040.576	0.0786	774
	ANSYS	312.557	2027	0.0794	774
Steel Yield	*Hand Calculation Results*	2565	60000	1.266	3731
	ANSYS	2591	60443	1.31	3731
Failure	*Hand Calculation Results*	3000	60000	1.7	3886
	ANSYS	3370	60900	1.66	3886

The following conclusions were observed based on the evaluation of the analyses of the calibration model, which were helpful in modeling the prototype slab.

1. Using SOLID65 yielded good results for non-linear analysis of RC members in flexure. It simulated cracking and crushing of the concrete well.
2. Default convergence values specified by ANSYS needed to be modified to obtain a solution.
3. Open shear and closed shear coefficients used in SOLID65 had a considerable effect on results with variation up to 10% compared with hand calculated results. These factors needed to be calibrated before doing the final analysis.
4. Using the stress relaxation option (keyoption=7) for SOLID65 element helped a lot in order to have a converged solution. After concrete element reaches the tensile capacity this feature in ANSYS prevents the stresses in concrete from dropping immediately to zero, in other word it takes the stresses gradually to zero with a default slope, however this slope can be modified by user as required.

4.3 FE Modeling of the Prototype Slab

4.3.1 Scaling and similitude requirements

Because of the economic reasons, measuring, lab space and other associated problems, the experimental models were chosen to be a scaled-down of the real building prototype. They

could not choose a very small model because of limitations in rebar and aggregate size so they chose an intermediate scaling factor of 4.5 for the experimental models.

Benefiting from the numerical modeling method that does not pose any of the problems associated with an actual test and for convenience of conducting further parametric study, it was decided to use the real dimensions of the prototype for FE modeling in ANSYS.

Since the prototype beam-supported floor slab models used for FE analysis had real dimensions, in order to have a correct comparison between the experiment and the FE modeling, the experiment results had to be scaled up to match the FE results . Table 4.2 lists the conversion factors applied to the experimental test results. (S= Scaled Factor of 4.5).

Table 4.2: Prototype Scale Factor

Parameter	**Conversion Factor to Convert from Scaled to Prototype**
Length	S
Area	S^2
Force	S^2
Stress	1

For example a unit value of the displacement (1 mm)and a unit value of the load (1kN) in experimental model must be multiplied by S and S^2 (S=4.5) factors to be compared with the results of FE analysis of prototype. After scaling up the results from experimental model using the required scaling factor, they also were converted from SI to the U.S Customary unit system in order to be comparable with results obtained from ANSYS analysis. Therefore, the prototype center-to-center span length of the slab panels was 24 ft. in both directions with 7 in. slab thickness. The dimensions of columns and beams were 24 in. x 24 in. and 24 in. x 12 in., respectively. A gravity live load of 80 psf was applied. The in-plane loads applied in the

prototype structure in the lab was multiplied by a factor of 20.25 (S^2) to accurately simulate loading for full-scaled ANSYS model. The overall dimensions of the prototype structure are given in Figure 4.3.

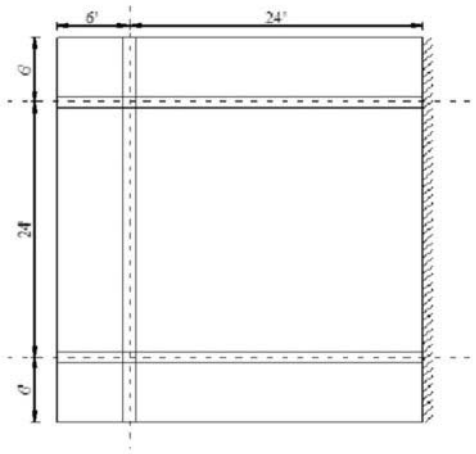

Figure 4.3: Prototype Dimensions Used in Computer Model

4.3.2 Element types

4.3.2.1 Concrete. SOLID65 (Concrete65) element was used to model the concrete. This element is a 3-D brick element. It has eight nodes with three degrees of freedom at each node and translations in X, Y and Z directions. This element can handle non-linear material properties. It also is capable of cracking in tension, crushing in compression, plastic deformation and creep. The schematic of SOLID65 element is shown in Figure 4.4

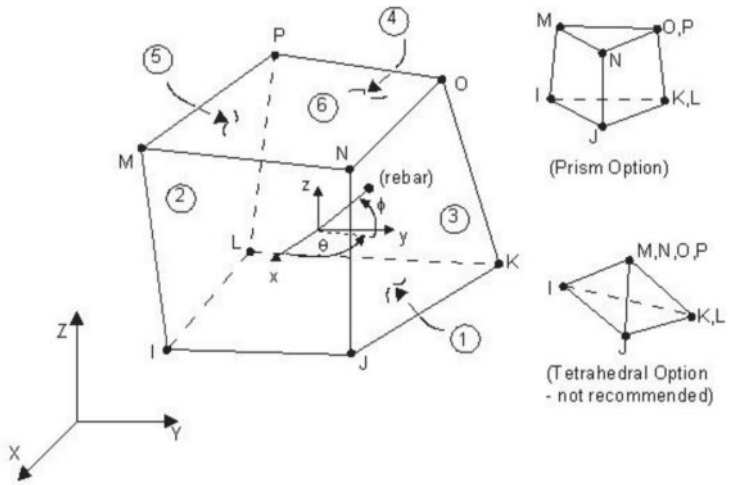

Figure 4.4: SOLID65 Element (ANSYS, 2012)

4.3.2.2 Steel reinforcements (rebars). Two methods for steel reinforcing were used to model rebars in ANSYS. A comparison between these two methods was made; advantages and disadvantages of both models were discussed.

Because of existence of too many rebars at top and bottom of slab and beams in the model, first the built-in reinforcement capability of SOLID65 called "smeared reinforcement" was used to define the rebars. In this method reinforcements must be defined as a volumetric ratio of elements and are uniformly distributed throughout the SOLID65 element. The material of the smeared reinforcement is defined as separate material (steel in this case). The direction of rebars can be defined as real constant input values for SOLID65, using two parameters representing angles (θ and φ). The θ is measured from X to Y axis, and φ is the angle between reinforcing direction and Z axis. With this method of defining reinforcements in SOLID65 every element can have up to three different reinforcements with different materials and volumes in three different directions. However, only one type of material (steel rebars) in two directions were used.

After performing analysis with smeared rebar option it was seen that a more accurate model was needed to define the reinforcements to take into account of the location of the rebars in the model. Since the models with smeared reinforcing did not converge easily, using an embedded reinforcement technique versus a smeared reinforcement was preferred. The use of REINF264 was recommended by ANSYS specialist as a new element specially designed to simulate the behavior of steel reinforcements in concrete.

REINF264 uses a discrete approach and is suitable for modeling reinforcing fibers in arbitrary orientations and locations. Each fiber is modeled as a spar that only has uniaxial stiffness. (ANSYS 13.0 Help). Figure 4.5 illustrates REINF264 geometry.

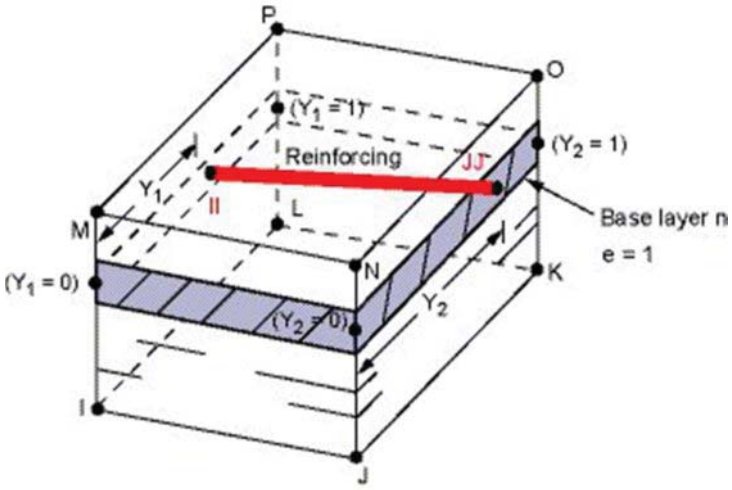

Figure 4.5: REINF264 Element Geometry (ANSYS, 2012)

First the section properties for each type of rebar must be defined. The input values are as followings:

V1 (or e) -- The number to indicate the element edge to which the offsets are measured. The default value is 1. This parameter basically determines the orientation of the reinforcement.

V2 and V3 (or Y1 and Z1) -- The normalized distances from the fiber to the first end of the specified element edge. Valid values for Y1 and Z1 are 0.0 through 1.0. The default value for Y1 and Z1 is 0.5.

V4 and V5 (or Y2 and Z2) – The normalized distances from the fiber to the second end of the specified element edge. Valid values for Y2 and Z2 are 0.0 through 1.0.

Fourteen sections had to be defined for REINF264 due to existence of three types of rebars in two directions along the slab and beams. The number of required sections was fourteen because in some locations two different reinforcements (with different areas) had to be defined for both directions which required defining of four different rebar sections.

Table 4.3 lists the rebars sizes used in the model. Figure 4.6 illustrates how to define a typical REINF264 section in ANSYS.

Table 4.3: Selected Reinforcing Bars

Items	**Bar Size**
Slab Reinforcing Bars	D2.0, D2.5, D3.0
Beam Longitudinal Bars	D2.0 , D3.0

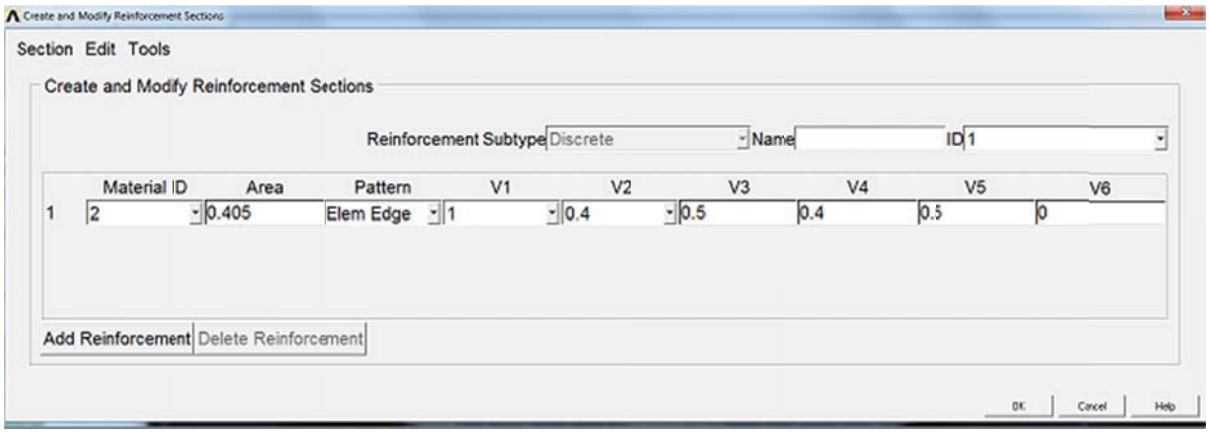

Figure 4.6: Required Values to Define a Typical Rebar Section

Figure 4.7compares the top slab reinforcing in computer model and experimental model. As it can be observed the REINF264 element allows a very detailed modeling of reinforcement. Bottom reinforcements for the slab and also top and bottom reinforcement for the beams were modeled the same way. Figure 4.8 illustrates an overall ANSYS model reinforced with REINF264 elements (purple lines in Figure 4.8).

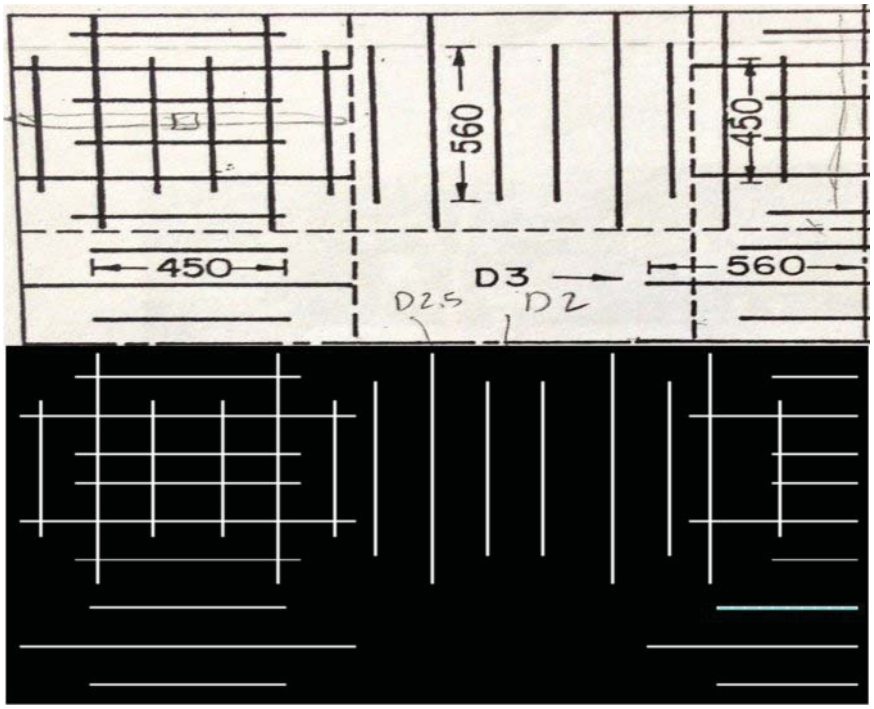

Figure 4.7: Top Slab Reinforcement Comparison between ANSYS (top) and Experimental Reinforcing Configuration (bottom)

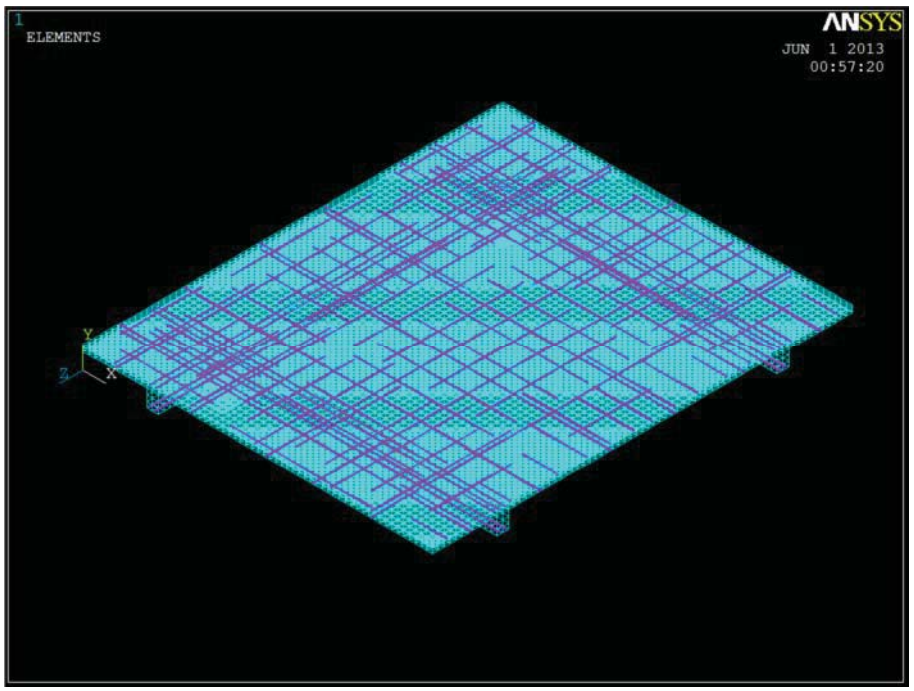

Figure 4.8: ANSYS Reinforced Model Using REINF264 Elements

Table 4.4: Real Constant for SOLID65 when REINF264 is used

Element Type	Constants			
		Real Constants for Rebar 1	Real Constants for Rebar 2	Real Constants for Rebar 3
Solid 65	Material Number	0	0	0
	Volume Ratio	0	0	0
	Orientation Angle	0	0	0
	Orientation Angle	0	0	0

Table 4.4 lists the required input values if a smeared reinforcement capability of SOLID65 is used. Material number defines the type of material used for reinforcements. Volume ratio defines the ratio of rebar volume to one for the reinforced element. Orientation angles define the angles and directions of the rebars. For the SOLID65 no real constant was used since it was decided to use the embedded reinforcing instead of smeared capability of it (Table 4.4). However, for the models having smeared rebars, seventeen real constants were defined for SOLID65 to account for the arrangement of the rebars in top and bottom of the slab and beams in two directions. A detailed calculation of all required input values to define the smeared rebars is presented in Appendix B.

4.3.3 Material properties

4.3.3.1 Concrete. Different types of material models were used for SOLID65 (concrete) in ANSYS. Mechanical properties used for concrete were directly taken from results of several concrete cylinder tests in the lab as listed in Table 3.6. Linear isotropic, multi-linear isotropic, and built-in concrete model in ANSYS (default model) were used to define the material non-linearity of concrete. At the end a comparison was made among all material models used for SOLID65 (concrete) in ANSYS, advantages and disadvantages of every model is discussed in results section. Key options were used to include specific element

functions such as tension softening behavior for SOLID65 element. For a typical concrete, stress-strain model is recommended by Vecchio and Colins (1986) as illustrated in Figure 4.9a. Since negative slope in FE solution module will not lead to a converged solution, a modified version of this model using compressive uniaxial stress-strain curve (McGregor, 1992) ignoring the portion with negative slope was used. Figure 4.9b illustrates the simplified version of this model.

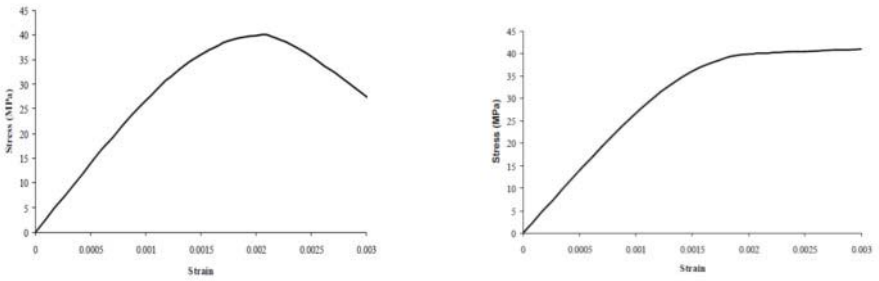

Figure 4.9: a) Actual Concrete Stress-Strain Curve (left) and b) Simplified Model Recommended for FE Analysis (right) (Vecchio and Colins, 1986)

In order to construct uniaxial stress-strain relationship for concrete (MacGregor, 1992) the following equations are used.

$$f = \frac{E_c \varepsilon}{1+\left(\frac{\varepsilon}{\varepsilon_0}\right)^2} \tag{4.1}$$

$$\varepsilon_0 = \frac{2\, f'_c}{E_c} \tag{4.2}$$

$$f = E_c\, \varepsilon \tag{4.3}$$

Where:

$f =$ Stress at Strain ε, psi

$\varepsilon =$ Strain at Stress f

$\varepsilon_{0=}$ Strain at f'_c, in/in

$E_c =$ Modulus of Elasticity of Concrete, psi

$f'_c =$ Compressive Strength of Concrete, psi

Note that the first point of the stress-strain curve must agree with Hook's law, i.e., Equation 4.3, while the remaining part of the curve will follow the parabolic relationship given in Equation 4.1.

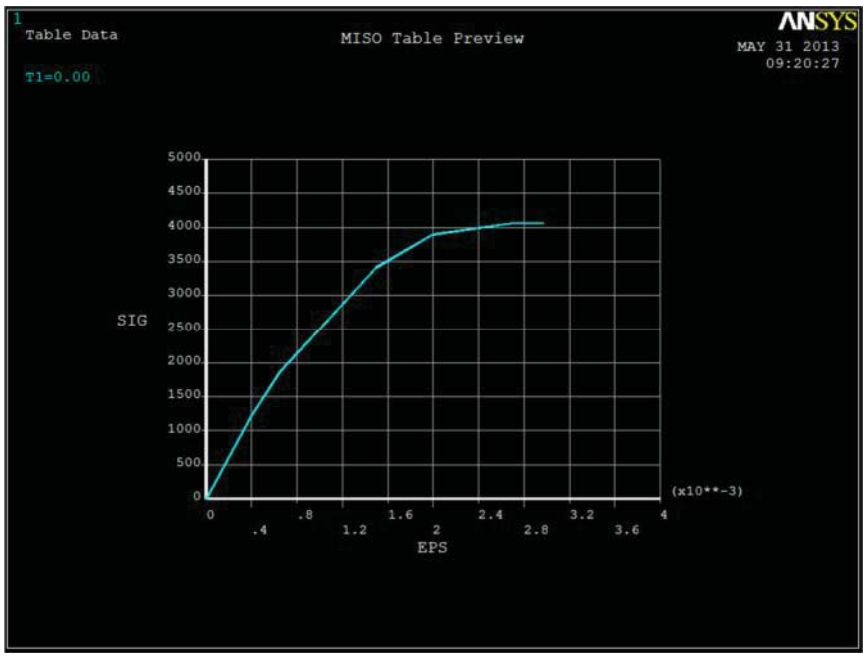

Figure 4.10: Uniaxial Compressive Stress- Strain Curve

Figure 4.10 shows the uniaxial compressive stress-strain curve used for this study. This formulation follows the study done by Kachlakev, et al. (2001). This curve is comprised of

five points; first point defined at stress of 0.3 f'_c satisfying the Hook's law (Eq. 4.3). Equation 4.1 was used to determine the coordinates of points 2, 3 and 4 while ε_0 was obtained using Equation 4.2. Stresses were selected and corresponding strains were calculated. Finally the stress at point 5 was determined using f'_c as stress in Equation 4.1. The corresponding points were used to define multi-linear isotropic material model in ANSYS.

ANSYS default concrete model uses Willam and Warnke (1974) material model that requires nine input values listed below (ANSYS, 2013):

1. Shear transfer coefficients for an open crack;
2. Shear transfer coefficients for a closed crack;
3. Uniaxial tensile cracking stress;
4. Uniaxial crushing stress (positive);
5. Biaxial crushing stress (positive);
6. Ambient hydrostatic stress state for use with constants 7 and 8;
7. Biaxial crushing stress (positive) under the ambient hydrostatic stress state (constant 6);
8. Uniaxial crushing stress (positive) under the ambient hydrostatic stress state (constant 6);
9. Stiffness multiplier for cracked tensile condition.

Shear transfer coefficients are ranged from 0.0 to 1.0, with 0.0 being a smooth crack which cannot transfer any shear force and 1.0 being a type of crack behavior that can transfer the entire shear without any loss. Numbers of studies have been done to determine best shear transfer coefficients for RC FE analysis. Studies of Bangash, (1989), Hemmaty (1998), Huyse, Hemmaty and Vandewalle (1994) and parametric study performed by Kachlakev et al

(2001) have led to the conclusion that open shear coefficient selected less than 0.2 does not lead to a converged solution so the value of 0.4 have been used with successful results.

For closed cracks, the value was chosen to be 0.8 according to studies of Kachlakev,T. Miller, Yim and Chansawat (2001), and Stehle (2002). However a parametric study was done on the calibration beam model to confirm the values recommended by mentioned researchers. Uniaxial tensile stress and uniaxial crushing stress was pulled from the lab report. With defining these two values ANSYS automatically defines constants 6, 7 and 8.

Constant 9 defines the tension softening behavior of concrete after reaching to its modulus of rupture (Figure 4.11)

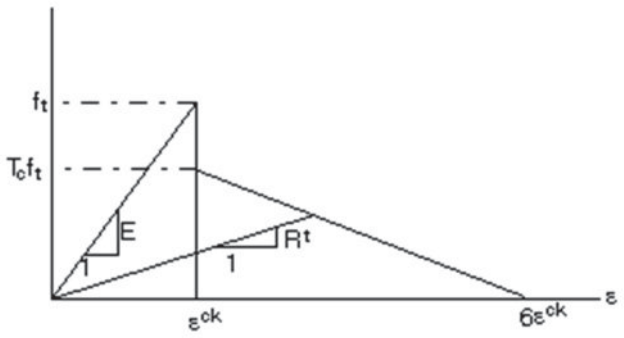

Figure 4.11: Tension Softening Behavior of Concrete

When a crack occurs in concrete, setting the key option (7) to value of 1 automatically drop the stress by a value defined by constant 9 to point $T_c f_t$ (Figure 4.11) and then gradually slopes down the value to zero. Default value of 0.6 is used in ANSYS for T_c (i.e., Constant 9=0.6). Table 4.5 lists required input values by ANSYS for SOLID65 element.

Table 4.5: Required Values for SOLID65 by ANSYS

Element Type	Material Properties				
	Linear Properties				
		Slab & Beams	Columns		
	EX (Modulous of Elastisity)	3045800 psi (28 Mpa)	4300000 psi (30 Mpa)		
	PRXY (poisson's Ratio)	0.13	0.21		
		Slab & Beams	Columns		
	Density (lb/ cu in)	0.00021	0.00021		
	Multi-Linear Isotropic				
		Slab & Beams		Columns	
		Strain	Stress (psi)	Strian	Stress (psi)
	Point 1	0.0004	1218	0.000373	1623
	Point 2	0.00065	1868	0.000605	2488
Solid65	Point 3	0.0015	3411	0.00135	4543
	Point 4	0.002	3898	0.00186	5192
	Point 5	0.0027	4061	0.00248	5409
	Concrete				
		Slab & Beams	Columns		
	ShrCf-Op (Open Shear Coeficient)	0.4	0.4		
	ShrCf-Cl (Closed Shear Coeficient)	0.8	0.8		
	UnTensSt (modulous of Rupture)	308.9 psi (2.13 Mpa)	517 psi (3.57Mpa)		
	UnCompSt (Ultimate Compresive Stress)	4061 psi (28.0 Mpa)	5409 psi (37.3 Mpa)		
	BiCompSt	0	0		
	HydroPrs	0	0		
	BiCompSt	0	0		
	UnTensSt	0	0		
	TenCrFac (Tension Softening Coeficient)	0	0		

ANSYS uses Willam and Warnke (1974) failure surface for concrete. This model develops a popular tri-axial failure surface for unconfined concrete. The suggested failure surface is shown in Figure 4.12. The major principal stress components are ordered ($\sigma_1 > \sigma_2 > \sigma_3$) in order to construct a sextant theoretical model. Hydrostatic and deviatory sections separate the failure surface as can be seen Figure 4.13. Equisectrix $\sigma_1 = \sigma_2 = \sigma_3$ included in meridianal plane forms hydrostatic section, which is orthogonal to deviatoric section (Figure 4.13).

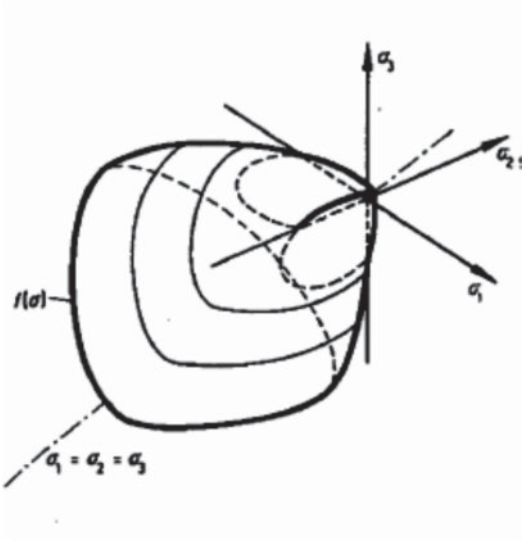

Figure 4.12: Willam and Warnke (1974) failure surface for Concrete

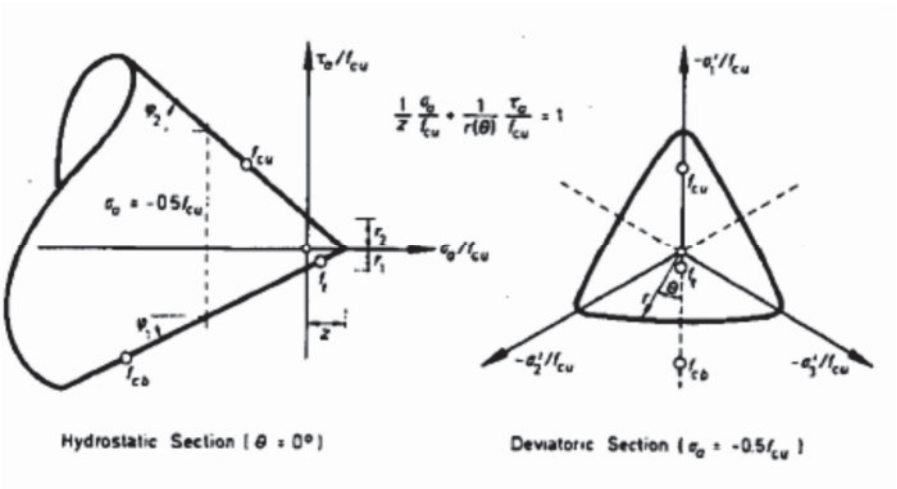

Figure 4.13: Hydrostatic and Deviatoric Sections (Willam and Warnke 1974)

Polar coordinates r and θ are used to define the deviatoric section, where r is the distance vector of the point of the failure on the surface to origin and θ is the angle of vector r. Equation 4.4 defines the failure surface:

$$\frac{1}{z}\frac{\sigma_a}{f_{cu}}+\frac{1}{r(\theta)}\frac{\tau_a}{f_{cu}}=1 \qquad (4.4)$$

Where:

σ_a and τ_a = Average Stress Components

f_{cu} = Ultimate Compressive Stress

Z= Highest Point in the Surface

Two angles of hydrostatic curve are defined by φ_1 and φ_2 as shown in Figure 4.13. Z and r values are found using ultimate compressive stress (f_{cu}), biaxial compressive stress (f_{cb}) and modulus of rupture(f_t). This model has benefits of a good match with experimental data. ANSYS creates constitutive material model for concrete based on above criteria and model defines the yield surface by three parameters for linear and five parameter for non-linear strains by utilizing a scaled function of stress$f(\sigma)=0$, the shown failure envelope in Figure 4.12.

4.3.3.2 Reinforcement. Defined material properties for the steel rebars were based on the actual tension test results on the scaled rebars used in the experimental model. Linear isotropic and bilinear isotropic properties were used to simulate the non-linear behavior of rebars in ANSYS. Self- weight of the steel material was also taken into account, defining this parameter will enable ANSYS to calculate the service dead load. Table 4.6 lists the required input values for the steel.

Table 4.6: Material Properties of Steel used in ANSYS Model

Steel	**Linear Isotropic**	
	EX (Modulus of Elasticity) (psi)	2.77E+07
	PRXY (Poisson's Ratio)	0.3
	Bilinear Isotropic	
	Yield Stress (psi)	53373
	Tang Modulus (psi)	1450000
	Self-Weight (Mass Density)	
	Steel (lb/cu in)	0.000734

Based on the given information ANSYS constructs a bilinear isotropic curve for steel, the slope of the first linear portion is equal to modulus of elasticity of steel and the slope the second portion is equal to tangent modulus. Figure 4.14 illustrates the steel bilinear curve used in ANSYS.

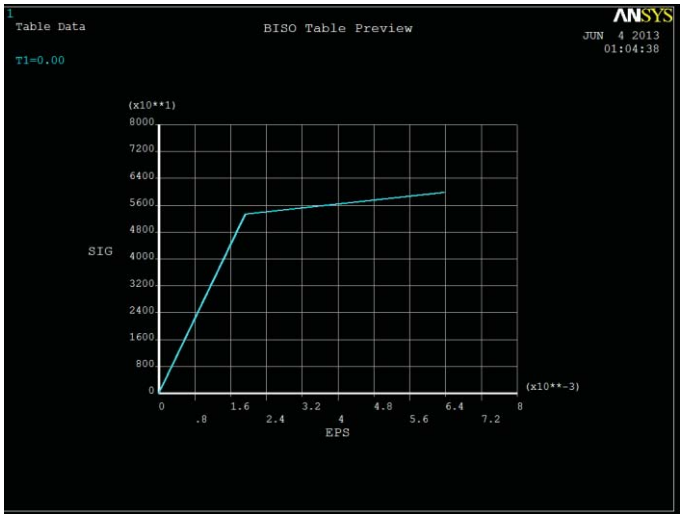

Figure 4.14: Bilinear Curve for Steel Constructed by ANSYS

4.3.4 Constructing ANSYS prototype RC slab model

Because of presence of rebars in top and bottom of slab and beams in two directions, different volumes with different sizes had to be created. Total number of seventy two

volumes was created to account for complicated arrangement of rebars in slab and beams (Figure 4.15). The part of the beams below the slab were made of two volumes to account for positive reinforcement placement, however, since the beams and the slab behaved as a T-section, the upper part of the beams were modeled within the slab depth to account for T-section behavior of the beams (Figure 4.16). The slab was made of four layers and nine volumes in each layer (except the layer containing top section of the beams) to account for top and bottom arrangement of rebars in middle strip and column strip of the slab. Figure 4.17 illustrates required number of rebars and their direction used to model the reinforcements in top and bottom of the slabs. A similar pattern was used to model rebars for beams. Table 4.7 lists the amount and location of the rebars used in the experimental model, however, because of the scaling relationship between test specimens and computer models, special care was taken in order to calculate the location and amount of steel rebars to model the prototype. As listed in Table 4.2, the length is multiplied by S (Scale factor=4.5) and the area of rebars are multiplied by S^2.

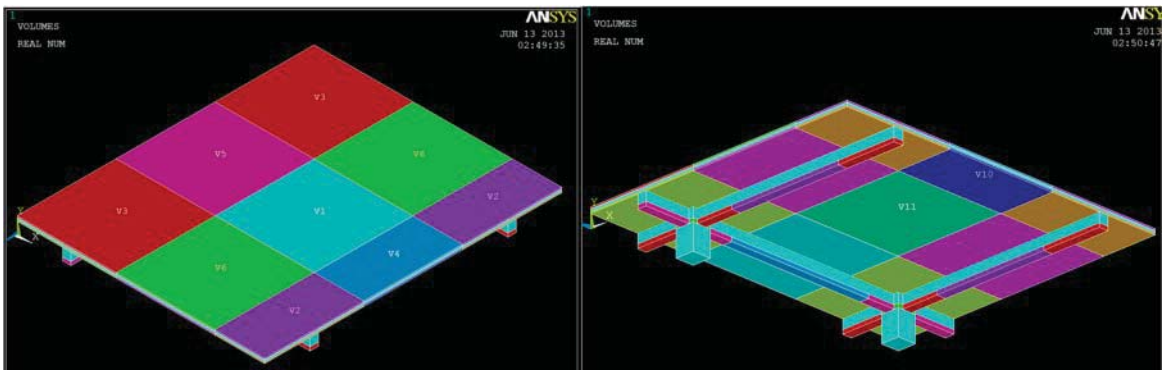

Figure 4.15: Top (left) and Bottom (right) View of ANSYS Model

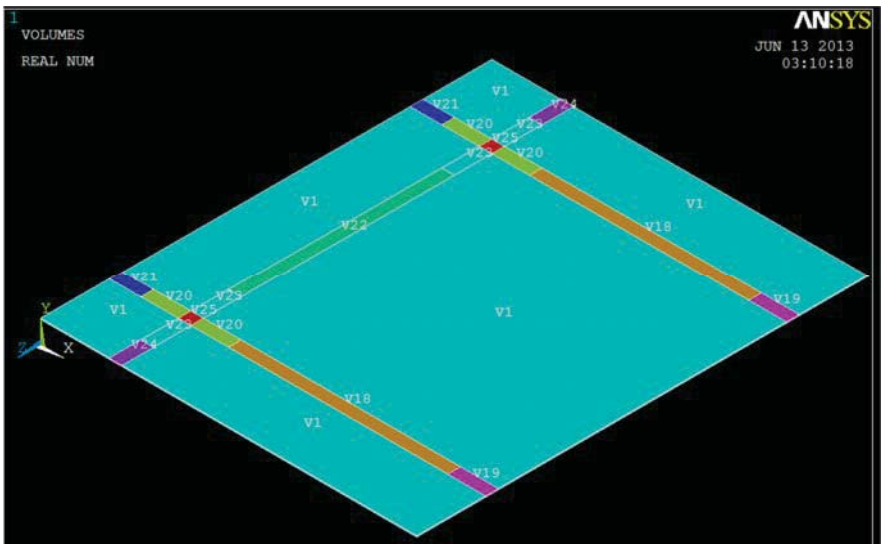

Figure 4.16: Top Portion of Beams (in slab layer) with ANSYS Model

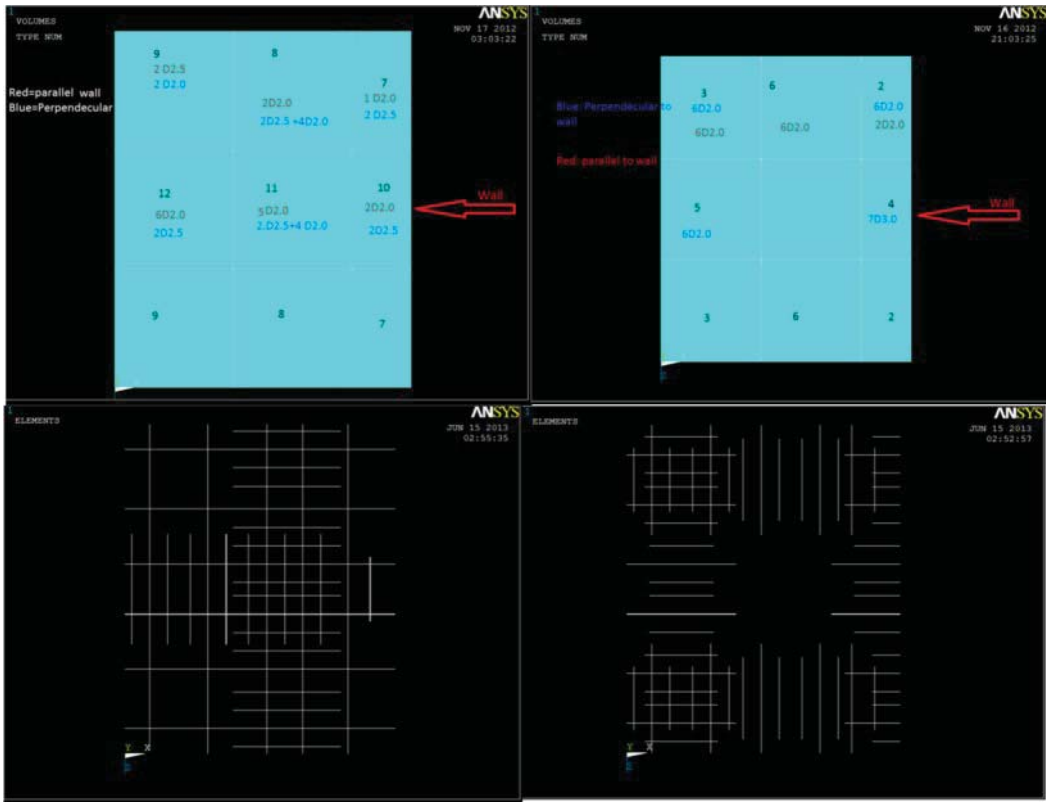

Figure 4.17: Rebar Arrangement in Top (right) and Bottom (left) Slab in ANSYS Model

Table 4.7: Rebar Arrangements in Slab (test specimen)

		Associated Numbers in Fig 4.17	Amount of Steel
Top Rebars	**Parallel to Wall**	7	1 D 2.0
		8	2 D 2.0
		9	2 D 2.5
		10	2 D 2.0
		11	5 D 2.0
		12	6 D 2.0
	Perpendicular to Wall	7	2 d 2.5
		8	2 D 2.5 +4 D 2.0
		9	2 D 2.0
		10	2 D 2.5
		11	2 D 2.5+4 D 2.0
		12	2 D 2.5
Bot Rebars	**Parallel to Wall**	2	2 D 2.0
		6	6 D 2.0
		3	6 D 2.0
	Perpendicular to Wall	2	6 D 2.0
		3	6 D 2.0
		4	7 D 3.0
		5	6 D 2.0

4.3.5 Meshing

Based on the analysis done on the calibration beam model, and as a general rule in FE analysis, the more the element aspect ratio is closer to unity the better results are obtained. A convergence study was performed to obtain the best element size. Floor slab was divided into four layers (2", 1", 2", and 2" thick) with a plan dimension of 6"x 6", and the stem of the beams below the slab were divided into three layers (6", 6", and 5" thick) with similar plan dimensions of SOLID65 elements (Figure 4.19). It was observed that reducing slab plan dimension to 3 in only made an insignificant change (<.0001%) in the displacement of the reference point, however, it increased the running time. This size of elements set up the mesh in a way that all the nodes in volumes with different sizes (nodes that were sharing the same interface) corresponded to each other. Since all the dimensions of elements were a multiple

of 6, this led to a dimensional compatibility between all the volumes. The volume sweep command then used to mesh the model. Since two types of rebar models were used, meshing was different for each of them. For smeared reinforcement, after defining the real constant for SOLID65 as described in Section 4.3.2.2 necessary mesh attributes assigned to the volumes then *vmesh* command automatically took care of the meshing smeared rebars and SOLID65 together. As for REINF264, after the volumes were meshed rebars were assigned to appropriate elements using *Secn* Command then *ereinf* command automatically meshed the reinforcements within the SOLID65 element. Figure 4.18 illustrates the two types of rebar modeling used in this study (smeared and embedded).

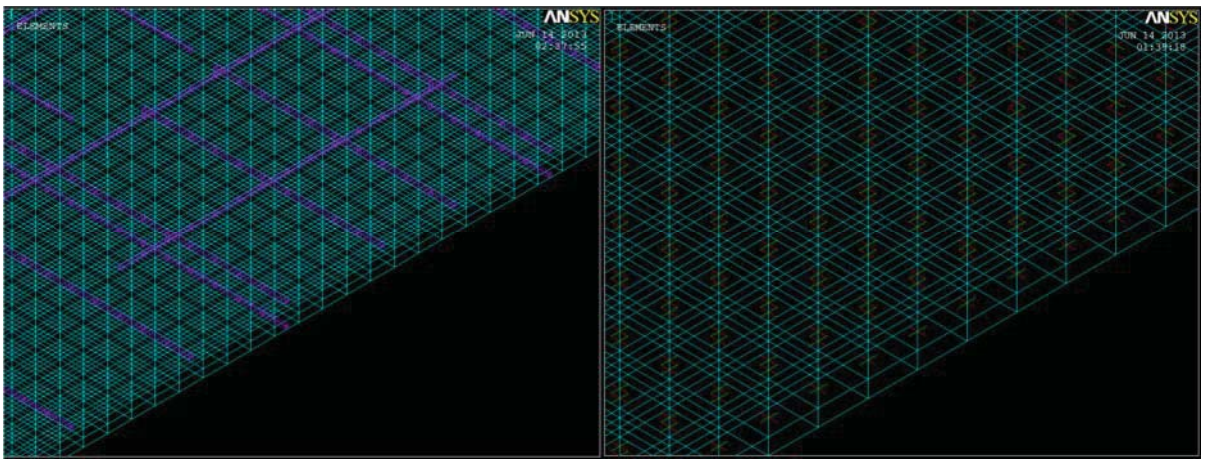

Figure 4.18: Embedded Reinforcement (left), Smeared Reinforcement (right)

4.3.6 Numbering control

Merge command merges separated entities which have components in common, for example this command will make two volumes that have common area a single entity, this command was very important in modeling procedure because the model was made of 71 different volumes with different sizes and they all needed to act as an entire entity. Special care was taken in process of merging entities.

4.3.7 Boundary conditions

The boundary condition was one of the most challenging parts in modeling procedure. The description given in the Nakashima's report (1981) was not very clear therefore variety of boundary conditions were used to capture closest results to experiments. As mentioned in the experimental report the specimen was lifted up on heavy pedestals in order to facilitate the testing procedure, the pedestals were anchored to the floor to be completely fixed. In the BH2MN (in-plane monotonic test of slab panel 2) and BV1MN (full service gravity and in-plane monotonic test of slab panel 1) (Figure 3.2) which were investigated in this study, walls were attached to the pedestal using twelve bolts and four heavy steel braces. This fixture completely prevented the slabs from moving in its floor plane. Therefore this fixture was simulated by fixed-fixed support condition along slab- wall interface (Figure 4.19). The column base was given variety of fixtures depending on the type of tests. However, in investigated cases in this study the column base was provided with a free-to-slide condition, in this set up the base did not have any resistance against sliding. To simulate this fixture, it was decided to use the roller support (restrained only in Y direction) to let the model move laterally without any resistance. A sensitivity study was done on the model with different patterns of nodes restrained in Y direction. The closest results were obtained when only a single node at bottom of columns was restrained only in Y direction (Figure 4.20). The reason that restraining all the nodes did not work was that it created a moment resistance which consequently prevented the model to behave identical to ideal free-to-slide set up.

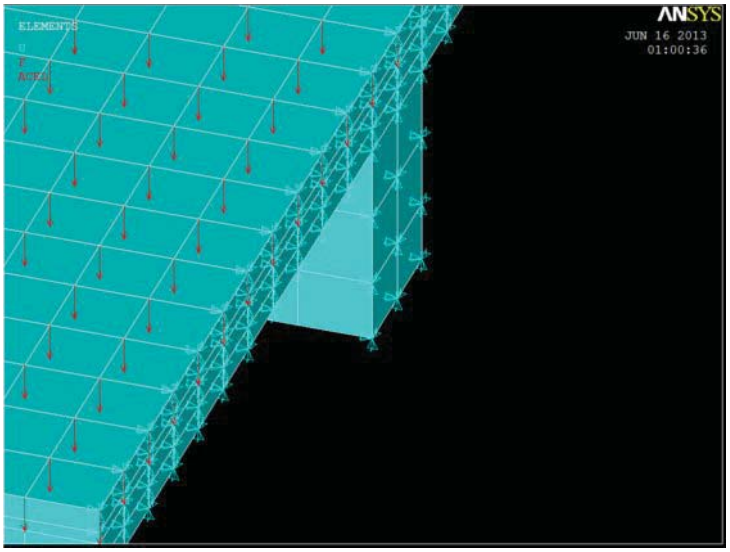

Figure 4.19: Slab and Beam Mesh Geometry and Fixed-fixed Support along the Wall

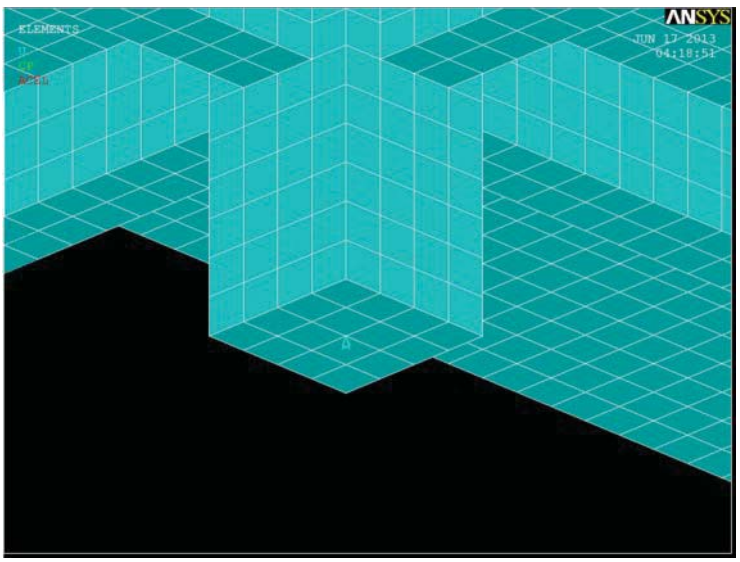

Figure 4.20: Roller support at Base of Columns

4.3.8 Analysis type

The type of analysis chosen for this model was static analysis with material non-linearity. Non-linear material properties were defined for both steel and concrete as mentioned before. Because of the way the test was set up the model had to finish an analysis and then resume another analysis with different loading conditions while keeping the effect of the previous

loads; therefore, the restart command was used to resume an unfinished run or execute next load step. Solution control command defines the parameters needed by ANSYS to run either a linear or non-linear solution. Table 4.8 lists a typical set of commands used for a non-linear static analysis. It is worth to mention that the small displacement option was utilized since it was known beforehand that there will be no buckling in the model and flexural failure will control the behavior of slab panels (i.e., no geometric non-linearity in the analysis was present).

In this type of analysis, total applied load is divided into smaller load increments (load steps). At the end of each load increment the stiffness matrix –if changed due to material non-linearity- is recalculated before moving up to the next load increment. Newton-Raphson equilibrium iterations method is used in ANSYS to adjust the change in stiffness in every load increment.

Newton-Raphson method checks for the convergence within a tolerance limit defined in the program. The force and displacement convergence criteria were used in this study, however the ANSYS default tolerance limits did not yield good convergence because of highly non-linear behavior of the model; therefore, the values were increased by a factor of 5 (0.5% for the force and 5% for the displacement). The effectiveness of using bigger tolerance values and also convergence problems associated with SOLID65 element when ANSYS default values were used were confirmed in studies done by Anthony J. Wolanski (2004).

Table 4.8: Typical Solution Controls for a Non-linear Analysis

Analysis Option	Small Displacement Static
Automatic Time Stepping	On
Number of Sub steps	200
Equation Solver	Sparse Direct
Write Items to Result File	Every Sub step

All other parameters related to non-linear algorithm in ANSYS, were set to default values. Table 4.9 lists the values ANSYS uses to solve non-linear problems. Behavior of ANSYS in case of non- convergent solution was set in a way that the solution stopped but program did not exit.

Table 4.9: ANSYS Non-linear Algorithm Parameters

Line Search	On	
DOF solution predictor	Prog Chosen	
Maximum number of iteration	100	
Cutback Control	.15	
Equiv. Plastic Strain	0.15	
Explicit Creep ratio	0.1	
Implicit Creep ratio	0	
Incremental displacement	10000000	
Points per cycle	13	
Set Convergence Criteria		
Label	F	U
Ref. Value	Calculated	calculated
Tolerance	.05	.5
Norm	L2	L2
Min. Ref.	not applicable	not applicable

4.3.9 Loading

Because the experimentally tested specimens were scaled down to represent the full service dead and live loads plus monotonic and cyclic earthquake loads, an extra vertical load had to be applied to the scaled down model to account for full service dead and live loads. The

description given in the experimental report was not very clear about the amount of load applied to the test specimen, however since the models in this study were actually the full size specimens the ambiguity of the amount of extra applied vertical load did not create any problems. Therefore the 80 psf live (as described in the report) plus dead load (the weight of actual RC slab) were used in FE model to represent the full service load condition described in the experiment. Vertical live load was distributed uniformly along all the nodes located on top of the slab as point loads (Figure 4.21). Dead load was taken care of by defining the mass density of the concrete and steel materials in ANSYS material property module. The monotonic horizontal loads were scaled up to full size specimen (by multiplying them by $S^2 = 4.5^2$) and applied along the beam parallel to the shear wall. However horizontal loads were applied in very small increments since the model experienced a high degree of non-linearity under that loading condition (Figure 4.22).

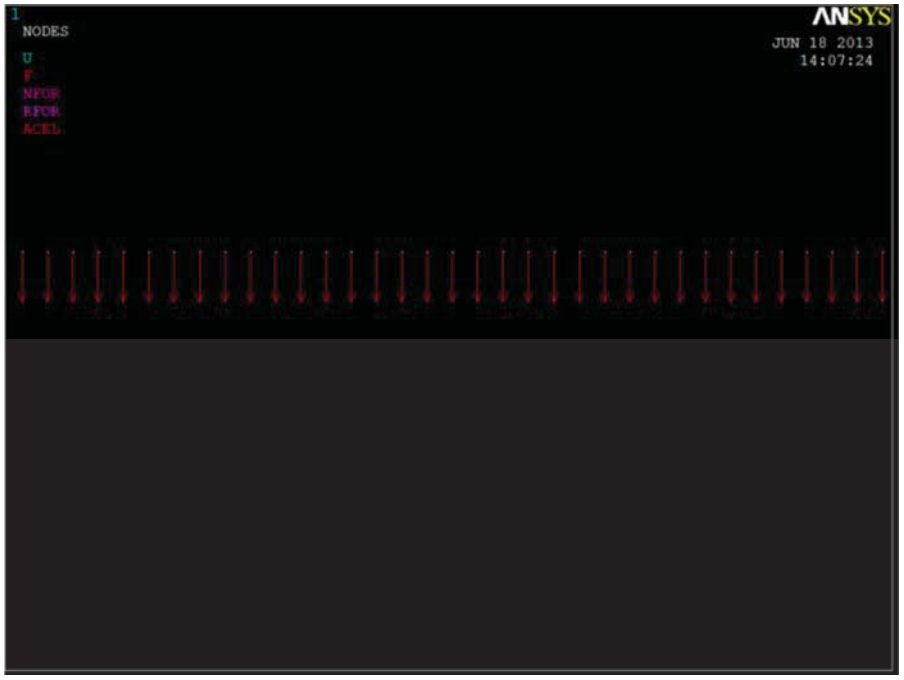

Figure 4.21: Application of Live Load in FE model

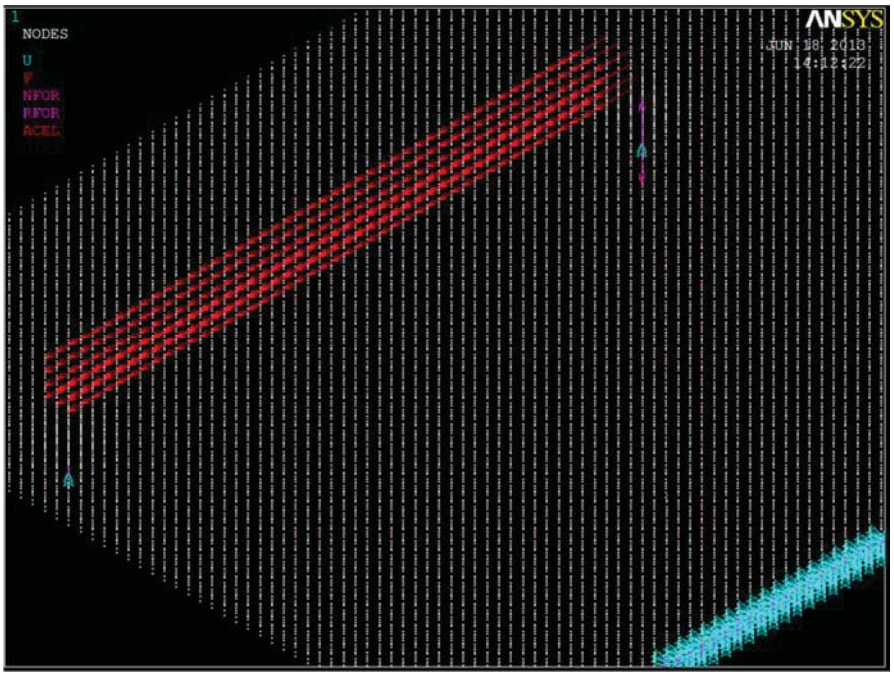

Figure 4.22: Application of Lateral Load in FE model

CHAPTER 5

FE ANALYSIS OF BEAM-SUPPORTED SLABS WITHOUT OPENING

The purpose for this section is to verify the constructed 3-D non-linear FE model for analyzing the behavior of beam-supported two-way slabs subjected to out-of-plane service loads and in-plane earthquake loads by comparing the prototype results with corresponding value obtained from testing of the scaled specimen at the Lehigh University (Nakashima, 1981). Two different material models were used in FE models: a) ANSYS default model, and b) multi-linear model. Also two different methods for reinforcing were used: a) embedded, and b) smeared. After detailed comparisons of the results of the FE models with the experimental results, the adequate material properties, real constants, convergence criteria and reinforcing technique are determined to construct the FE model of two-way beam-supported slabs with openings.

5.1 Testing Program and Sequence

5.1.1 Testing programs designation

For the sake of simplicity, each test was labeled with five alphanumeric characters. The first character was always **B**, describing the type of slab which was **B**eam-supported slab panel in this study. The second character was either **H** or **V** describing type of loading used in the test program. H means that only **H**orizontal loads (in-plane) were applied and there were no vertical loads in the testing program. **V**, on the other hand, indicated the use of both in-plane and **V**ertical loads. Third character, being a number, indicated the slab panel number being used in the test. Numbers 1, 2, and 3 referred to the use of panels 1, 2, and 3 respectively (Figure 3.2). The fourth and the sixth characters described the way that the in-plane loads were applied to the test specimen. MN strands for **M**o**N**otonic, and **CY** for **CY**clic loading

applications. However, only the results of the BH2MN and BV1MN are used for the verification of the present 3-D FE models.

5.1.2 Initial slab stiffness verification

As mentioned in Section 3.5 a series of stiffness tests were performed on scaled specimens to determine the initial in-plane stiffness of the slab panels. In order to make sure of the accuracy of FE model within the elastic range the stiffness test with very small in-plane loads (9 kN), which had taken place right before the strength test, were reproduced by ANSYS for the test specimen BH2MN. The stiffness obtained was eight percent larger than the experimental result which agreed well (within 4%) with the value obtained using the virtual work method accounting for both in-plane flexural and shear deformations, given in Appendix C. This slight difference in stiffness indicated that the model has already experienced a few minor shrinkage cracks in concrete.

5.2 Verification of the ANSYS FE Model

5.2.1 Full service gravity loads: elastic analysis

In process of verification of FE models, first step was to verify the model using the elastic analysis with full service dead and live loads. Thus, the different types of non-linear material models used do not affect the results. Lehigh report also included results for a similar linear-elastic FE analysis of the scaled specimen using SAP IV, a general-purpose FE software (Nakashima, 1981). The vertical deflections for the linear-elastic analysis using full service loads were investigated in three points (Figure 3.6a). Results obtained from the ANSYS model matched well with the ones from SAP IV (Table 5.1). It is also observed that the type of reinforcement steel (embedded versus smeared) did not change the results since the concrete remained elastic (i.e., no cracking and crushing was defined). Therefore, steel

reinforcement contribution was insignificant. Also, when these results are compared with the experimental values (given in Table 5.2), they are considerably smaller since the elastic analysis did not account for the slab cracking observed during the test.

Table 5.1*:* Linear-elastic Results Comparison for Vertical Deflections

Item	**Deflection at Reference Points**		
Analysis Type	**Point 1 (in)**	**Point 2 (in.)**	**Point 3 (in.)**
SAP Linear-Elastic Analysis (Report)	0.074	0.2073	0.074
ANSYS	0.073	0.2078	0.073

5.2.2 Full service gravity loads: non-linear analysis

Before performing the strength tests, the slab specimen BV1MN was subjected to full service gravity loads. The vertical beam and slab displacements at three points mentioned in Section 3.4.3 were recorded using fixed scales (Table 5.2). The model created in ANSYS was subjected to self-weight plus 80 psf of live load in order to simulate the full service gravity load as described in Section 4.3.9. Besides the vertical deflections recorded, the cracking pattern also was described in the lab report. Two lines of cracks were observed on top of the slab, one along the wall and the other along the beam parallel to the wall (Figure 3.8). The results obtained from FE model were in a good agreement with the experimental results (Table 5.2). Cracking pattern in ANSYS model also corresponded well to the experiment (Figure 5.1).

Table 5.2: Full Service Gravity Test results

Analysis Type	Point 1 (in)	Point 2 (in.)	Point 3 (in.)
Full Service Gravity Load (Experiment)	0.13	0.23	0.17
ANSYS	0.125	0.23	0.125

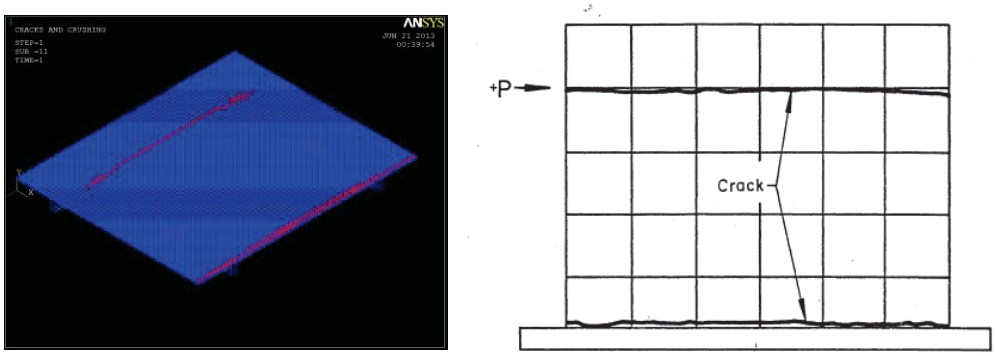

Figure 5.1: Cracking Pattern, ANSYS (left), Experiment (right)

Slight difference in deflections can be related to the initial stiffness tests conducted on the specimens discussed in Section 5.1, where some minor concrete cracking might have occurred. The difference between Point 1 and Point 2 deflections in the test can be explained due to test specimen imperfections, where the concrete in one side of the slab panel may have had more shrinkage cracks or it may have not had the same strength as the other side. Also cracking pattern in concrete is a random phenomenon; therefore, one of the beams may have cracked earlier than the other one, which led to more flexible behavior.

Using different material models or different type of reinforcing techniques did not make a considerable difference in the ANSYS analysis results. The reason was that under full service loading the reinforcing steel stress remained within the elastic range and concrete in compression essentially behaved elastically. The effect of selected concrete material models

and methods of steel reinforcing (embedded vs. smeared) becomes more significant at higher applied loads when both steel and concrete show non-linear behavior.

It is worth mentioning that there was not any load-deformation graph available from the actual test specimen for the comparison purposes. However, the global response of the test specimen was captured through the cracking pattern and vertical deflections (as shown in Figure 5.1) in the ANSYS FE analysis of the prototype slab. It was observed that the first major crack started along the wall at 58% of the full service load causing a change in stiffness and a sudden increase in vertical deflection (Figure 5.2). This crack expanded along the wall at 79% of the full load. Second major crack along the column line parallel to the wall appeared around 97% of full service load and expanded along the column line.

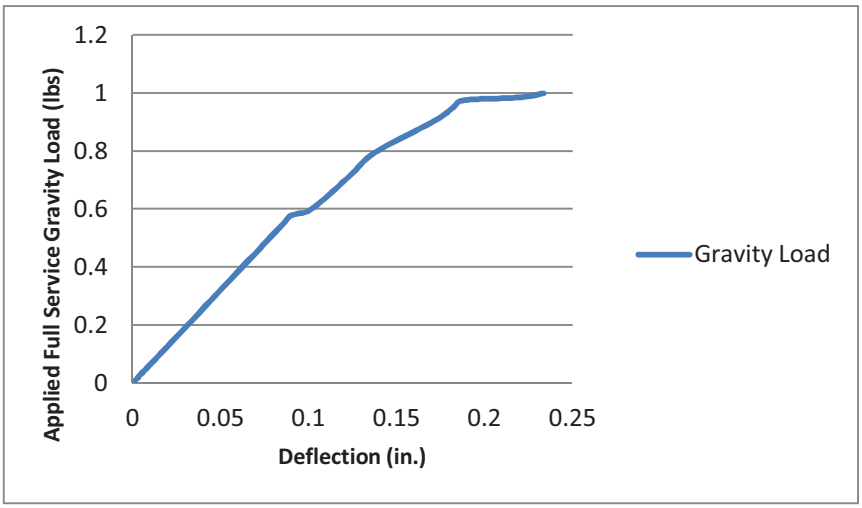

Figure 5.2: Out-of-Plane Load vs. Vertical Slab Deflection

5.2.3 Comparison between material models and steel reinforcing methods

As mentioned in Section 5.2.1, the ANSYS models were not sensitive to the type of concrete material models selected (default ANSYS model vs. multi- linear model) and also to the type of steel reinforcing methods used (smeared vs. embedded) since steel and concrete (in

compression) remained essentially elastic when out-of-plane load up to the service loads were applied. However, as the specimen were loaded further toward their in-plane capacity, the differences were significant. In this section a comparison between models with different parameters are made to determine which ones globally yield closest results to the test results.

5.2.3.1 Test with in-plane loads (BH2MN). As mentioned in Section 4.3, two types of concrete material models and two types of steel reinforcing methods were used. Figure 5.3 illustrates the in-plane load-deflection relationship for these models compared to experimental curves for the slab specimen BH2MN. It can be observed that although all the combination of models used globally capture the behavior of the slab, embedded steel with default concrete model (green curve in Figure 5.3) captured both load capacity and deflection more accurately when compared to experimental curve (blue curve in Figure 5.3).

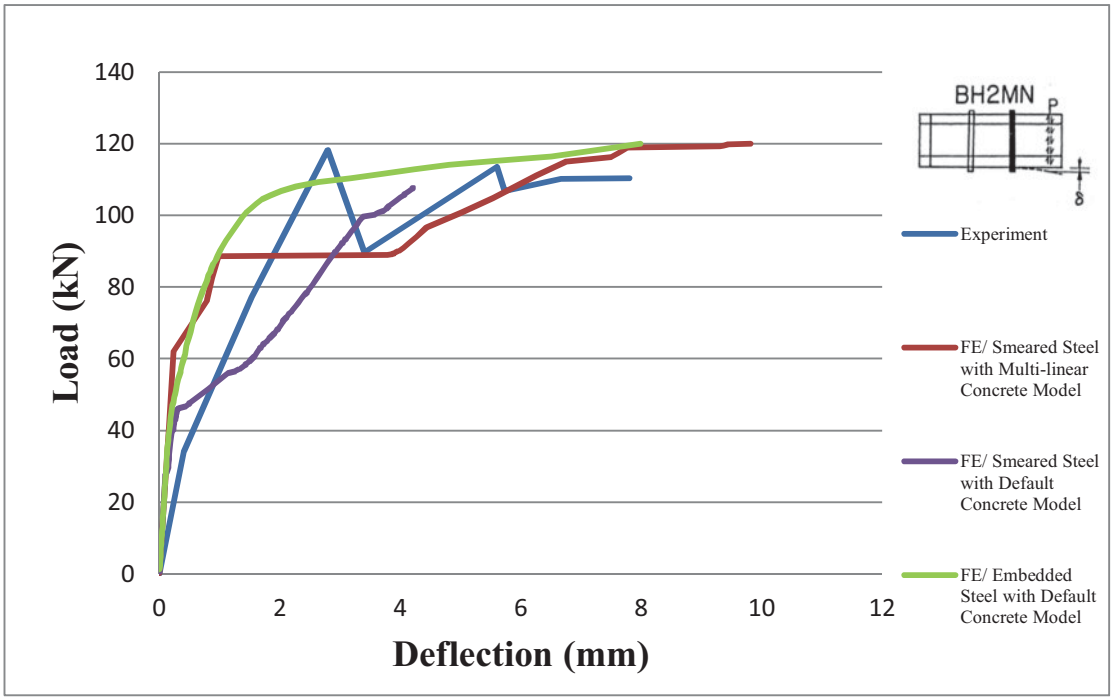

Figure 5.3*:* ANSYS vs. Experiments (BH2MN)

Furthermore, the ultimate in-plane bending moment capacity of the test specimen was estimated by hand computations using procedure typically utilized in reinforced concrete shear walls (Wight and MacGregor, 2011), given in Appendix C. The results obtained agreed well with the experimental and ANSYS results (6% difference), since the slab panel was only subjected to in-plane loads.

5.2.3.2 Test with in-plane & out-of-plane loads (BV1MN). Same variables used in Section were used to analyze the behavior of the slab panels subjected to in-plane and out-of-plane loads. Figure 5.4 illustrates the results obtained from ANSYS analysis of slab panels subjected to in-plane and out-of-plane loads compared to experimental curve. It can be seen that sensitivity of the results are more towards the selected steel reinforcing modeling procedure rather than the interaction between concrete material modeling and the reinforcement modeling used . In other words, while it is evident that the models with

embedded steel (green curve) produced closest results to load capacity and deflection compared to the experiment. In comparison, models with smeared steel- regardless of what their concrete model is- did not do well in capturing the experimental behavior. It can be concluded that when gravity load is present, the importance of embedded steel modeling is more pronounced. Therefore, when the floor slab model is subjected to in-plane and out-of-plane loads, embedded steel reinforcing is more appropriate in order to obtain the most accurate results.

Therefore, based on the above observations, the embedded steel model was chosen to do further comparisons and verifications.

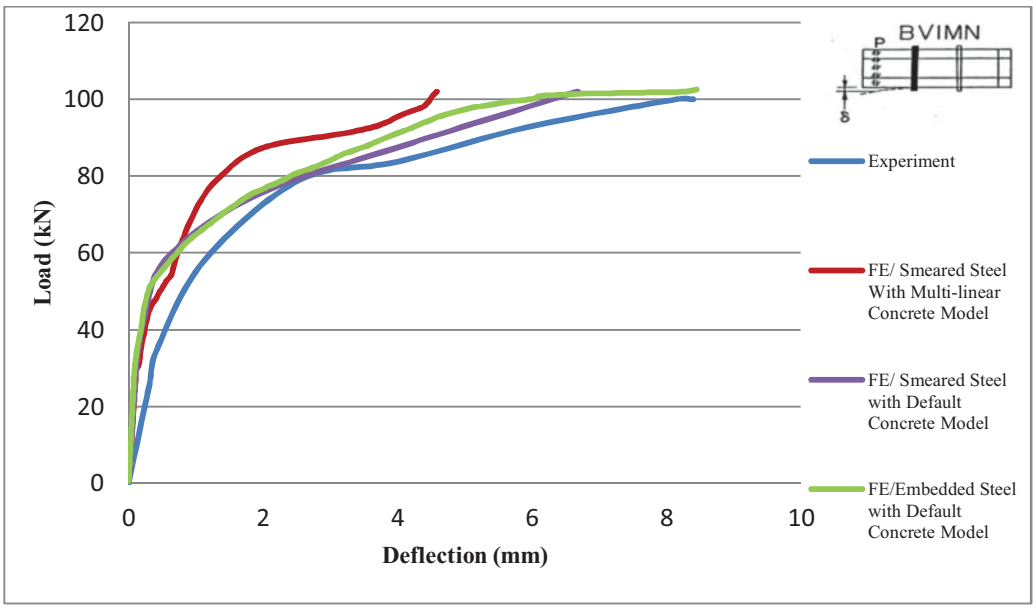

Figure 5.4: ANSYS vs. Experiment (BV1MN)

5.2.4 Discussion of the BH2MN test results and comparison to ANSYS model with embedded reinforcement

In this test, only in-plane loads were applied along the column line parallel to the wall (no vertical loads were applied). The specimen was fixed to the wall and columns were in free-to-slide condition. This test set up required in-plane loads to be applied monotonically in very small increments. Loads were gradually increased up to the point that the resistance of the test specimen dropped considerably.

As mentioned in the report, at the load value of 36 kN cracks were developed at wall-slab interface and extended towards the beam, this pattern was produced by ANSYS FE model. Figure 5.5 illustrates the extension of the cracks at wall –slab interface starting at 36 kN (0.3*120 kN).

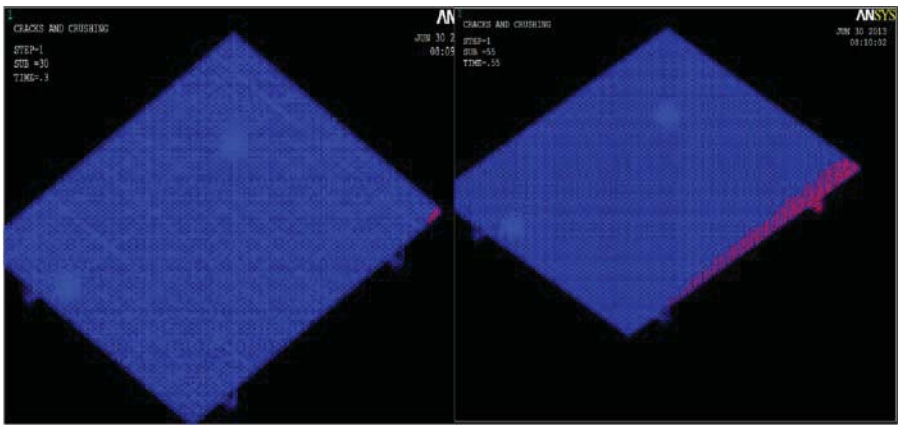

Figure 5.5: First Crack Extension

According to the report the ultimate load of 120 kN (27 kip) was reached when several cracks which were developed at lower load levels started to grow bigger. Soon after a significant loss of resistance of approximately 31 kN (7 kip) was followed, dropping the load

from 120 kN to 89 kN. After this significant loss, the system regained its equilibrium and reached to the ultimate load level of 116 kN (Nakashima, 1981). According to experimental report, another significant loss in resistance took place where one of the cracks rapidly extended inwardly through depth of the test slab. This crack was labeled the major crack, and soon after a few numbers of rebars broke at the deflections 7.6 mm (1.35 in.) (Figure 5.8). This was reproduced accurately with ANSYS model. As it can be seen in Figure 5.6 yielding of the rebars at load value of 89 kN, as mentioned in the report, is produced in ANSYS model at 0.74 of ultimate load (showed with blue arrows in Figure 5.6) caused a loss in slab resistance. A significant loss due to the braking of the rebars caused a mechanism which controlled the failure behavior of the slab in the experiment. In other words, the section where the major crack occurred acted as a plastic hinge region where it was captured by extensive yielding of the rebars at that location as shown in Figure 5.7. This section of the slab model nearly coincided with boundary between middle strip and column strip, where number of reinforcing bars were cut off. Also, the load-deflection curve obtained by Nakashima using a 2-D FE model (dashed lines in the Figure 5.8) agrees well with the ANSYS curve (green line in Figure 5.3). In both Nakashima's and present ANSYS FE models, it is observed that a considerably higher stiffness than the real test result curve obtained at the initial loading stage (i.e., at the start of the load-deflection curve). This difference in the initial stiffness can be attributed to small cracks caused by random loads applied to the model during the transportation, cracks caused by shrinkage and cracks caused due to other tests performed on the specimens before initiation of the strength tests (Nakashima, 1981).

Figure 5.6: Breaking of the Rebars

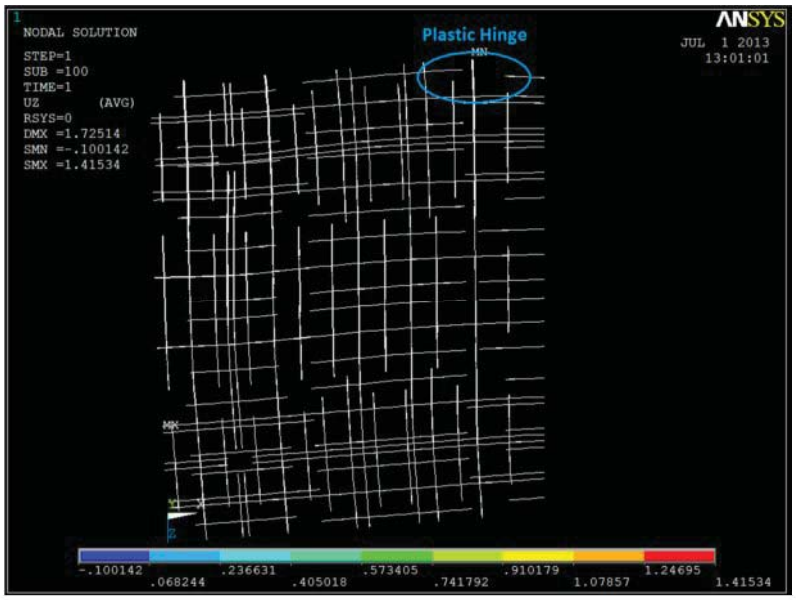

Figure 5.7: Plastic Hinge Location

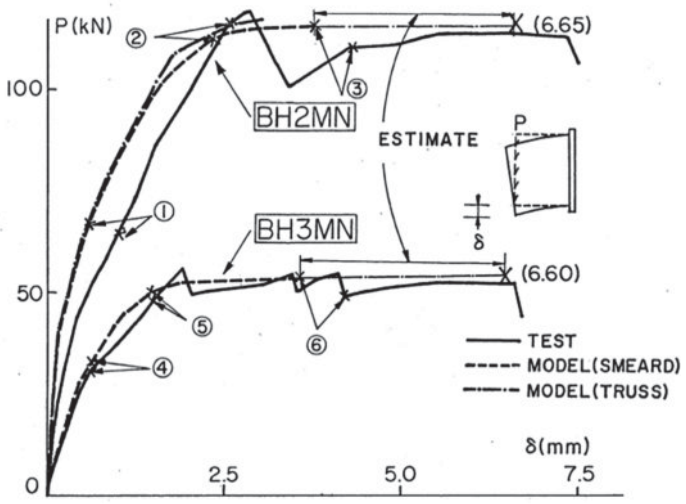

Figure 5.8: Analytical Load-Deflection Curves in Lab Report

Furthermore, all experiment results were obtained using the displacement control procedure while FE results were obtained by load controlled procedure. In other words, in load-controlled analysis by ANSYS the zigzag nature of experimental curve representing sudden loss and recovery of the resistance at post-ultimate load region cannot be created. However, in summary the correlation between the ANSYS and experimental curves were considered reasonable.

5.2.5 Discussion of the BV1MN test results and comparison to ANSYS model with embedded reinforcement

In this test first the gravity service loads were applied to test panel as explained in Section 5.2.2. The next step was to apply the in-plane loads. The types of in-plane loads used in this test were monotonic loads. In-plane loads were applied incrementally until the panel reached its ultimate strength of 102 kN with the corresponding displacement of 8.8 mm. ANSYS model (green curve in Figure 5.4) produced load capacity of 102.6 kN with the corresponding displacement of 8.45 mm which were almost the same as experiment results.

As mentioned in Section 5.2.2, the gravity service load created two lines of cracks on top of the slab. The line of cracks located at the wall-slab interface was extended inward until it reached the bottom surface at 21% of the ultimate load (22kN). Figure 5.10 illustrates the cracking pattern obtained from the ANSYS model in a section located near the wall-slab junction at 100% of gravity loads (Figure 5.9 left), where the cracks are created only at the top surface of the slab, and at 22% of the ultimate in-plane loads (in addition to 100% of gravity loads) where the cracks extended all the way to the bottom surface of slab. According to the experimental observations, cracking pattern was significantly different at top and bottom of the slab. Most of the cracks on the top surface were confined near the slab-wall interface while many of the cracks at the bottom extended radially from center of the slab. This pattern was produced accurately in the ANSYS model as shown in Figure 5.9 where the top left and bottom right surface patterns are compared.

As mentioned in the report (Nakshima, 1981) no substantial loss of in-plane load resistance was observed in the test. The stiffness decreased gradually and smoothly until the ultimate capacity was reached. The reason was that the service gravity loads already started the development of some of the cracks at the plastic hinge region (the region between the end wall where the top slab and beam rebars were cut off) before the application of in-plane loads. In other words, existing cracks due to gravity loads made the transfer of the loads from cracked concrete to rebars more gradual when in-plane loads are applied. However, the same phenomena (presence of cracks due to gravity loads) caused a 15% drop in in-plane load carrying capacity of the floor slab system.

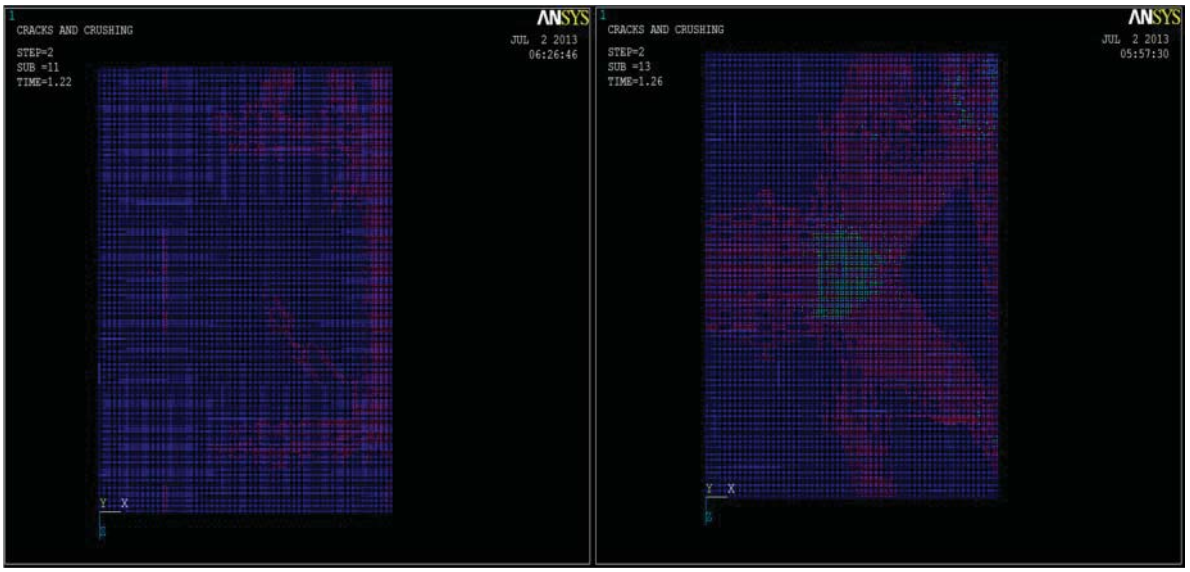

Figure 5.9: Cracking Pattern at Top (left) and Bottom (right) of Slab

Figure 5.10: Extension of Cracks Inwardly (in depth of slab)

Figure 5.4 compares the load-deflection curves obtained from ANSYS with the experimental curve. It can be seen that the model with embedded rebars (green curve) accurately captured the load capacity as well as the displacement comparing to experimental curve (blue curve). The significant reduction in the in-plane stiffness of the initial part of the experimental curve

was due to additional cracking which had occurred in pretests prior to ultimate in-plane strength tests (Nakashima, 1981). However, the ANSYS results are in a close agreement with test results for the remaining part of the curve.

5.3 Concluding Remarks

The following conclusions were obtained on the evaluation of the solid RC slab models subjected to in-plane and out-of-plane loads.

5.3.1 Modeling and FE techniques

Following observations are made with regard to the FE modeling of RC beam-supported two-way floor slab systems:

1. In linear-elastic stage, the use of different material models for concrete and different methods for rebar modeling had insignificant effect on the results.
2. In the BH2MN test model, the results were more sensitive to the interaction between the selected concrete material models and type of steel reinforcing models (Section 5.2.3.1).
3. In the BV1MN test model, results were more influenced with the steel reinforcing method used (smeared vs. embedded). Thus, in the slab models subjected to biaxial bending use of embedded rebars yielded more accurate results (Section 5.2.3.2).
4. ANSYS cracking model for concrete –being a smeared crack model- is efficient enough to provide results with a good correlation with experimental ones in terms of cracking patterns.
5. Boundary condition modeling played an important role in the FE analysis process. An extreme care must be taken to accurately simulate the boundary conditions. A slight change can lead to wrong results.

5.3.2 Behavior of floor slabs under in-plane and out-of-plane loads

Following observations are made based on FE analysis of RC slabs subjected to in-plane and out-of-plane loads:

1. In both strength test models (BH2MN and BV1MN) behavior of the slabs were controlled by forming the major crack at the plastic hinging location where many of the top slab and beam rebars were cut off (Figure 3.3). This implies that ultimate strength of the slabs was controlled by in-plane flexural rather than shear capacity.
2. Vertical loads, as expected, lowered the ultimate capacity of the slabs. The ratio for the load capacity of BH2MN (green line in Figure 5.3) to the BV1MN (green line in Figure 5.4) was 1.17. This difference originated from the fact that vertical loads (service dead & live) in BV1MN test model created two lines of cracks in the slabs (Figure 5.1) which caused more gradual transformation of concrete stress to the reinforcing steel (smoother load-deformation curve) and a lower ultimate in-plane load capacity, both of which were reproduced by the FE analysis model.
3. In both cases significant differences in initial in-plane stiffness between the theoretical and tested specimen were observed. This was attributed to preloading tests conducted on the test specimens (BH2MN and BV1MN) before actual strength tests, accidental forces applied due to transportation of the specimens and shrinkage and creep cracks in the concrete, as explained in experimental report (Nakashima, 1981).
4. The cracking pattern of the top and bottom of the slab in BV1MN test was different, while the pattern was the same throughout the slab for BH2MN. This was due to the fact that in the BV1MN tests, gravity load application created tensile stress at the bottom of the slab and compressive stress at the top; therefore, by the time that in-

plane loads were applied, further cracking occurred in the pre-stressed beam surface of the slab. This was also reproduced by present FE analysis. Thus, in general it is concluded that the ANSYS 3-D non-linear models provided accurate results which were in a rescannable agreement with experimental values.

CHAPTER 6

TWO-WAY RC SLABS WITH OPENINGS

6.1 General

The motivation for this study originated from the fact that the presence of openings in building structures is sometimes inevitable, and they can easily change the behavior of floor slabs. At present, routine design procedures ignore the in-plane deformations of the floor slabs, and the current building standard ASCE 7-10 requires that RC floor slabs to act as elastic deep beams sitting on the shear walls when the aspect ratio of the floor diaphragm is greater than 3:1. With diaphragms deforming in an inelastic manner, contrary to what is assumed, the distribution of the shear force to lateral force resisting members (such as shear walls and frames) may significantly change. This can be even more pronounced when floor openings are present resulting in a behavior completely different than what was expected of the structure when subjected to seismic loads.

Consequently, considerable (and unaccounted) loss of in-plane stiffness may result in a change in the redistribution of the lateral loads resisted by the vertical members in frames, overloading some of them (such as columns) to failure.

Kunnath et al. (1990) investigated the inelastic response of floor slabs by developing IDARC2 an enhanced numerical model; Reinhorn et al. (1988) and Panahshahi et al. (1991) confirmed the accuracy of the model through conducting shake table tests on two single-story RC scaled model structures. These series of studies confirmed the possibility of the structure's failure (collapse) due to diaphragm yielding in low-rise buildings with shear walls. IDARC2 is a non-commercial macro-model computational tool having the capability

of performing inelastic analysis of RC buildings with rigid, elastic, or inelastic floor slabs subjected to static and dynamic loads, however, the effect of floor openings was not included.

Alharash (2011) enhanced IDARC2 to handle floor diaphragms with openings and conducted non-linear time-history analysis of RC buildings with different opening sizes at different locations, enabling the user to over-ride the default idealized moment-curvature in the program.

In this chapter the verified FE model was used to investigate the effect of openings with different sizes in two-way RC slabs subjected to in-plane and out-of-plane loads. Three different openings in terms of their sizes with respect to whole panel area were investigated. The obtained results then are recommended for the use in the enhanced IDARC2 in order to define more accurately the user specified moment-curvature curves for the slabs with openings.

6.2 Floor Slab Openings: Design Code Requirements and FE Modeling

The ACI code permits openings of any size in slabs if the required serviceability and strength conditions shown by acceptable analysis methods are met (Section 13.4.1). The analysis procedure can sometimes be difficult and require experimental verifications. As an alternative to the detailed required analysis, the Section 13.4.1 of the code gives simple guidelines for selecting opening size and location to make the designing procedure simpler for engineers only in flat slabs, when beams are not present.

In summary, according to the ACI code in order to be able to have an opening in slabs supported on beams (the type of slabs investigated in this study), a detailed analysis showing

that the strength and serviceability requirements are maintained is required. The prototype slab model used in previous chapters was used to incorporate the openings. Three different sizes of openings (25%, 14% and 6.25%) were placed in the mid-region of the slab panel. The ratio was calculated ignoring the overhanging parts of slab panel. The embedded steel reinforcing model with default concrete material properties were used in the ANSYS models with openings since their accuracy was verified with experimental results in the previous Chapter.

As a routine design procedure described by ACI 318-11, Section 13.4.1, the missing rebars at bottom of slab where the opening is placed were added to the boundary of the openings (Figure 6.1) to maintain full out-of-plane bending capacity of the slab panel. This was also helpful in a way that it could prevent local failure of concrete elements in that region. Figure 6.1 illustrates a top view of the rebar arrangement's on slabs with openings.

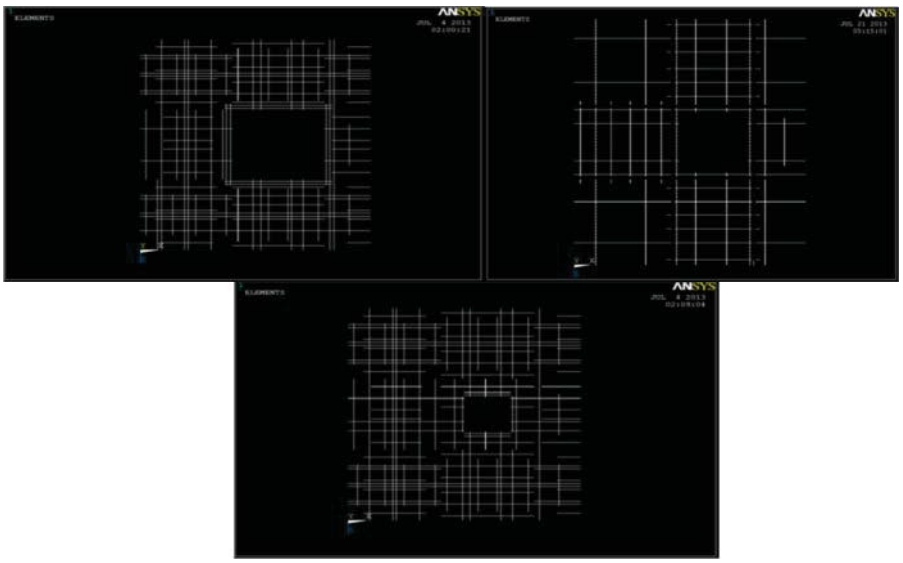

Figure 6.1: Openings with 25% (top left), 14% (top right) and 6.25% (bottom)

Boundary conditions, loading method and non-linear solver settings were chosen the same as described in Chapter 4.

6.3 Results and Discussions

6.3.1 Behavior at service loads (dead & live)

When the slab models with openings were subjected to service loads (dead & live), they demonstrated a different behavior than slabs without openings under the same loading conditions. Presence of the openings actually reduced concrete stresses to the point that no cracks were observed with the largest opening size (25%). In the slab with 25% opening at service gravity loading stage, stresses at concrete were under cracking stress value of 308 psi and steel stresses were multiples of modular ratio of steel to concrete (Figure 6.2). In other words the model with 25% opening size remained elastic under gravity service loads. The reason was that the relatively big opening size (25%) took away the dead and live loads at the mid-panel region, thus, significantly reduced the total load applied on slab panel. However, with using smaller opening sizes, more cracks and stresses started to appear and the behavior approached to that of solid slabs (without opening). In the slab with 14% opening size a line of cracks started to appear in slab-wall junction. The stresses at steel rebars at that location increased to about 14500 psi, indicating that since concrete non-linearity started to be introduced into the system, and steel was picking up more stresses.

In the slab with the smallest opening size (6.25%) also a line of cracks parallel to the wall at slab-wall junction were observed (similar to 14% opening with more stress values); however, stresses at steel rebars at cracking section were about 10% higher. Note that service gravity loads on solid slab created two lines of cracks in slabs, as it was presented in Section 5.2.2 (see Figure 5.1).

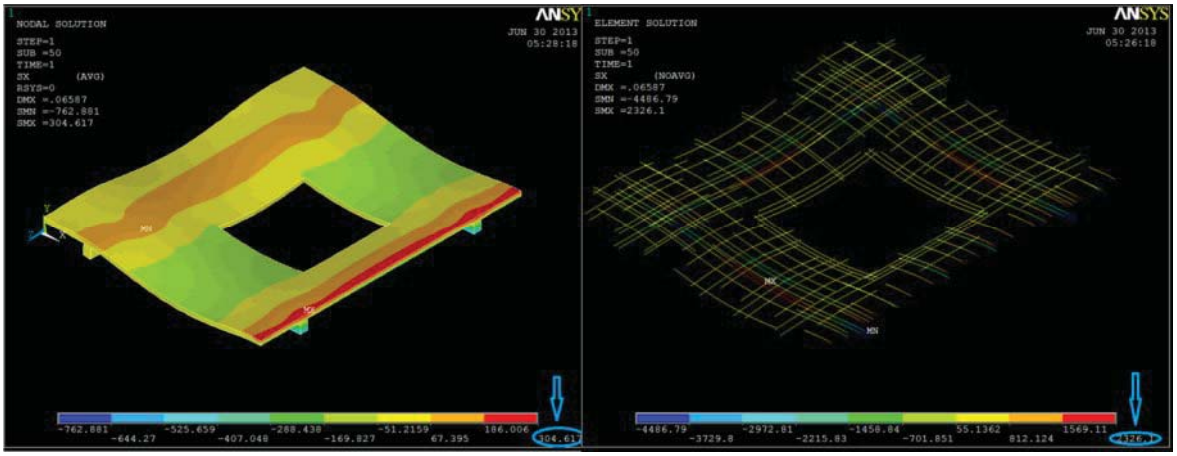

Figure 6.2: Stress in Concrete (left), and Stress in Steel (right) in Slab with 25% Opening

6.3.2 Behavior of slabs with openings subjected to in-plane loads

Under in-plane loading condition the slab model with 25% opening size demonstrated a different behavior compared to the solid slab. The first cracking occurred at about 12kN at the top left and bottom right corners of the opening. However, these cracks did not create a major loss of stiffness in the slab (Figure 6.5). As these cracks started to expand diagonally, second set of cracks appeared at about 31.2 kN at slab-wall junction, which resulted in the first major loss in stiffness in this model (Figure 6.5). At this stage maximum steel stress of 36000 psi (68% of the yield strength) occurred at the slab-wall junction, which was almost 1.6 times the stress value in the rebars located at the opening corners. This means that the contribution of the cracks at the slab-wall junction were more on the in-plane stiffness loss of the slab panel than the cracks at opening corners. Figure 6.3 illustrates the cracking pattern and stresses at steel rebars at first major stiffness loss.

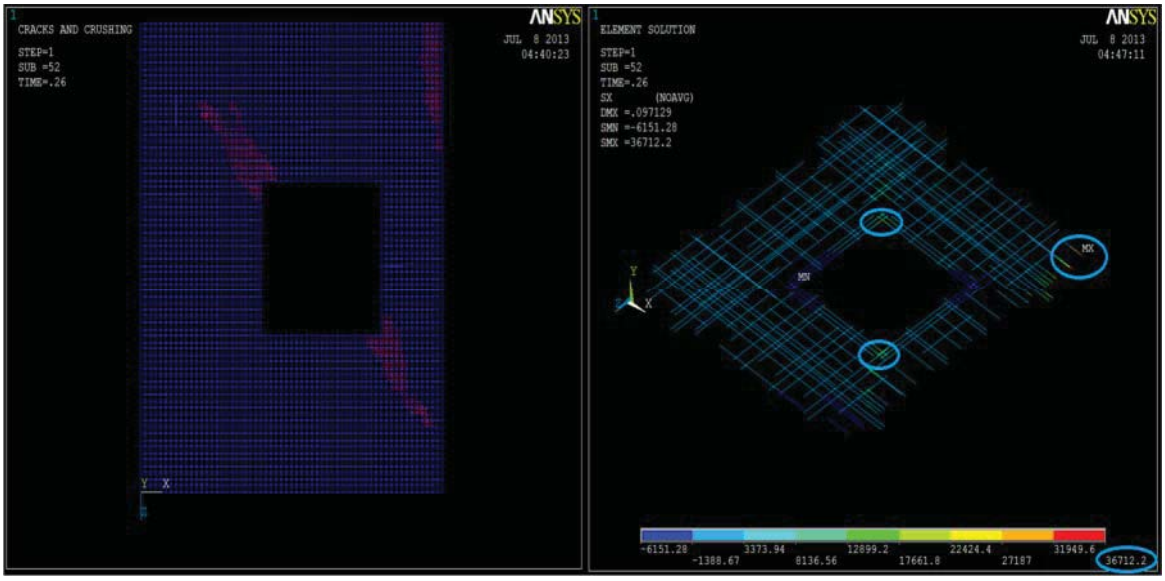

Figure 6.3: Cracking Pattern (left), and Stresses in Steel Rebars at First Major Stiffness Loss (right)

At the load value of 51.6 kN the scenario was vise-versa, where the stresses in the rebars at the corners of the opening were larger than the rebars at slab-wall junction. In fact the corner rebars reached the yield stress first, which marked the second major loss of stiffness in Figure 6.5. The stresses of the rebars at opening corners were approximately 1.4 times the stresses at the slab-wall junction (Figure 6.4). Finally at the load value of 81 kN the slab with 25% opening experienced failure by crushing of the concrete elements where an ultimate in-plane displacement of 20.7 mm was obtained, as shown in Figure 6.5.

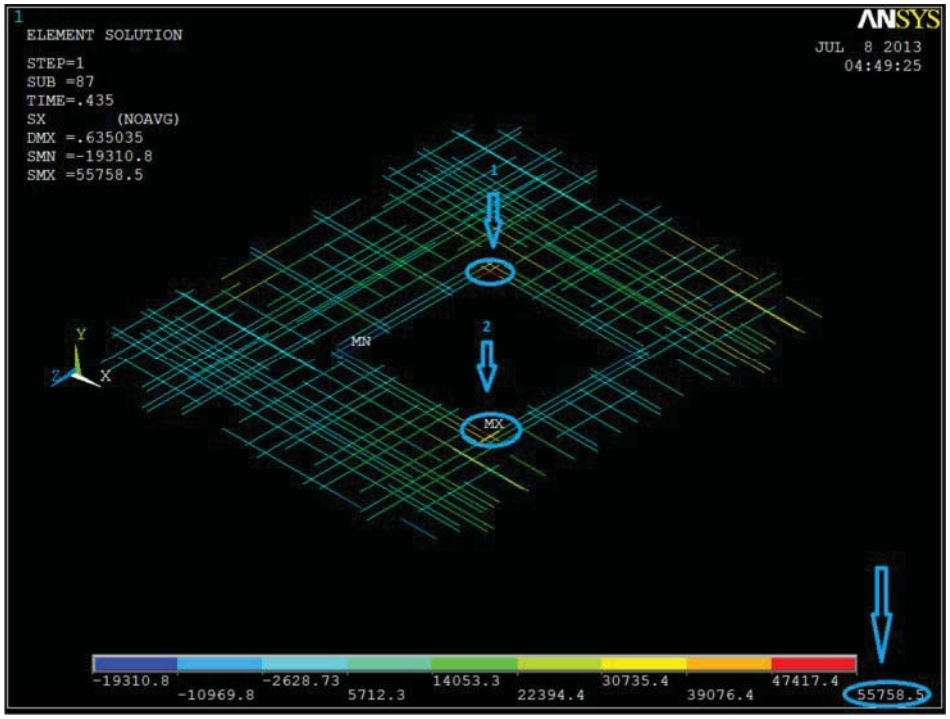

Figure 6.4: Stresses in Steel at Second Major Stiffness Loss

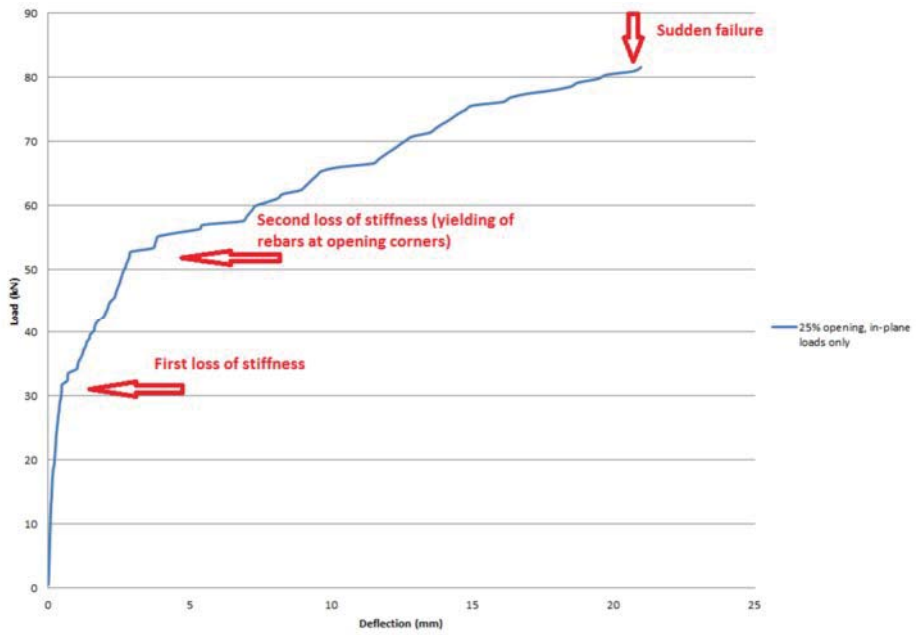

Figure 6.5: Load- Deformation Curve for Slab with 25% opening, In- Plane Loads only

Comparing these results (Figure 6.5) with the ones obtained from solid slab analysis (Figure 5.3), it was concluded that the presence of opening reduced the load carrying capacity 30% (from 117 kN to 81 kN). It also changed the failure mechanism of the slab in a way that the yielding of the steel rebars around the corners played a significant role of causing a major stiffness degradation of the slab.

In the slab with 14% opening size, the ultimate displacement was smaller than slab with 25% opening (11.3 mm compared with 20.7 mm) ; however, the load capacity was increased; from 81kN to 93 kN. The opening seemed to still be affecting the flexural behavior of the slab especially towards the failure. The load-deformation curve is shown in Figure 6.6. At the load value of 28.8 kN (30% of ultimate load), Figure 6.7 shows the first concrete cracks started to appear at opposite corners of the opening, however this did not create a significant loss of stiffness in the slab as seen in the Figure 6.6 (point 1). At this load level the maximum steel stress was 11000 psi, which occurred at opening corners. At the load value of 48 kN the cracks at opening corners were accompanied by a set of cracks at slab-wall region to mark the first major loss of stiffness (point 2 at Figure 6.6). At the load value of 76.2 kN rebars at the opening corners exceeded the yield stress value of 53000 psi, similar behavior as in the slab with 25% where the rebars at opening corners reached the yielding stress first (Figure 6.8).

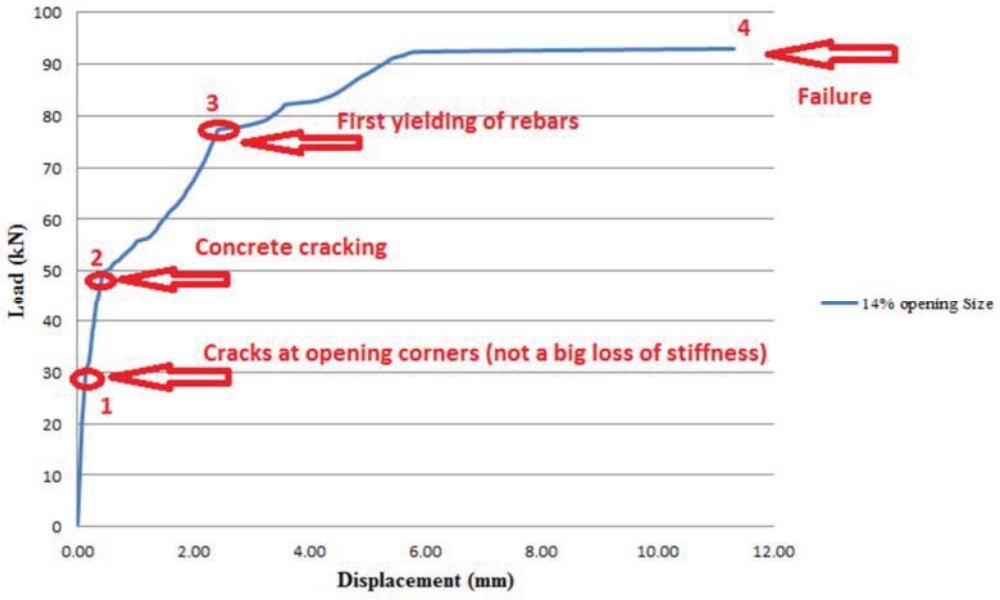

Figure 6.6: Load- Deformation Curve for Slab with 14% Opening, In- Plane Loads only

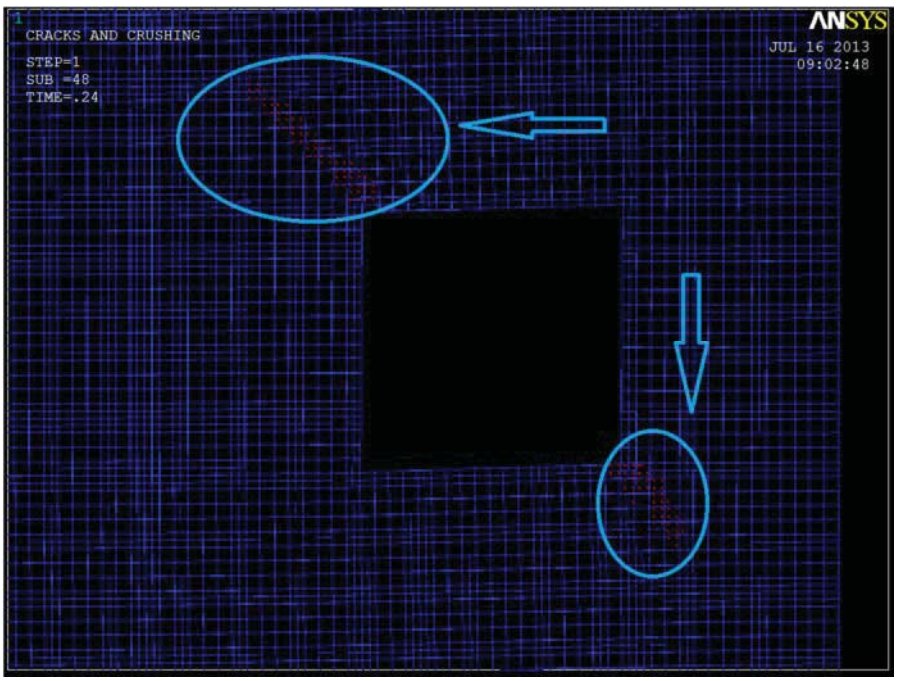

Figure 6.7: Concrete Cracks at Opening (14%) Corners, at Load of 28.8 kN

Figure 6.8: First Yielding of Steel Rebars at Opening (14%) Corners, at Load of 76.2 kN

The global behavior of the slab with 6.25% was similar to the solid slab behavior for in-plane load but with slightly larger lateral deflection due to the reduced in-plane stiffness of the location of the opening. The load carrying capacity was dropped from 117 kN to 102 kN (13% reduction). The small opening size of 6.25% also did not affect the failure mechanism of the slab compared to solid slab (with no opening). The shape of the load-deformation curves were similar and no major loss of stiffness was observed until the complete failure. Failure occurred shortly after rebar yielding at plastic hinge area near the wall (same behavior was observed in solid slab).

Table 6.1 lists the results obtained from FE models of slabs with openings subjected to in-plane loads. As it can be seen with larger opening size the ultimate displacement increased and the load capacity decreased.

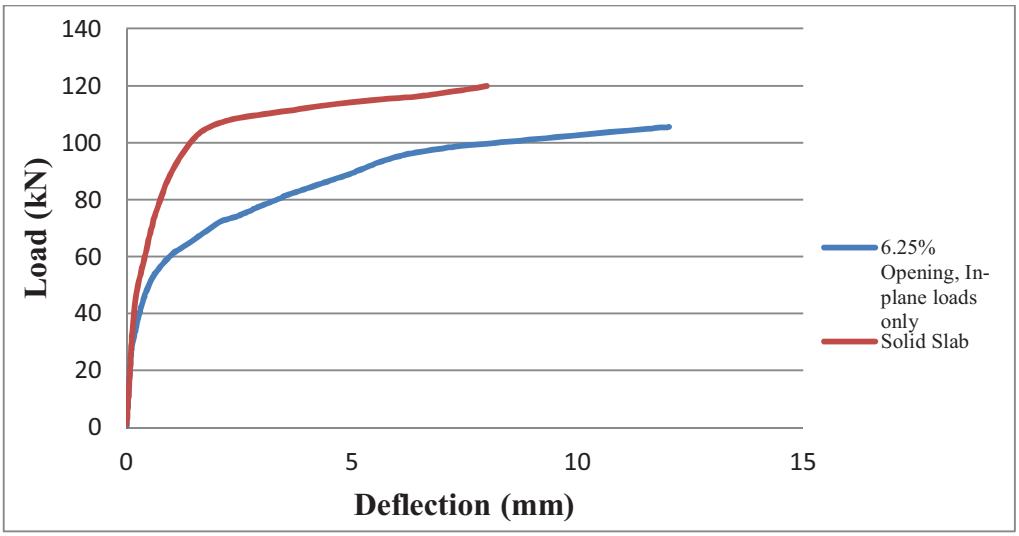

Figure 6.9: Slab with 6.25% Opening Load- Deformation Curve Compared with Solid Slab

Table 6.1*:* Results for Slab with Openings Subject to In-plane

Models with In-plane loads only		
Opening Size	Load Capacity (kN)	Displacement (mm)
25%	81	20.7
14%	93	11.3
6.25%	102	9.48
0% (solid slab)	117	8.04

6.3.3 Behavior of slabs with openings subjected to in-plane and out-of-plane loads

In FE analysis of the slab with 25% opening, a considerable change in behavior was observed compared to solid slab when in-plane load was applied after the slab was subjected to out-of-plane service loads. The relatively big opening size of 25% decreased the load

capacity to 78 kN, about 23% less than capacity of the solid slab. However, the load carrying capacity was slightly reduced (about 4%) compared to the slab with 25% opening with in-plane loads only. The behavior of the slab was very similar to the model with in-plane loads only (Figure 6.10). The only major difference was occurrence of the less sudden failure at slab with in-plane and out-of-plane loads which can be attributed to the minimal effect of gravity loads in creating more concrete cracks helping to transfer concrete stresses to reinforcing steel.

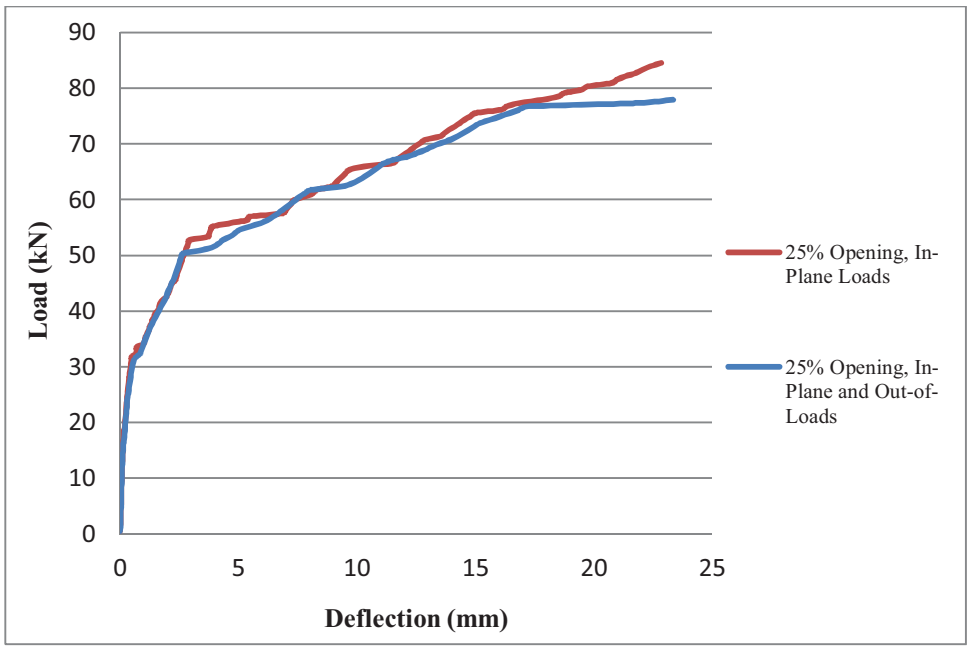

Figure 6.10: Load- Deformation Curve Comparison for Slab with 25% opening

In the slab with 14% opening the analysis showed that the behavior was moving towards the solid slab as the opening size reduced (from 25%) where the sudden changes in stiffness were not obvious in the slab. In other words, the stiffness decreased gradually until the ultimate load value of 86 kN with corresponding displacement of 13.72 mm reached (Figure 6.13). Comparing to the slab with 25% opening, the load capacity increased 10 % (from 78 kN to 86 kN), and the ultimate displacement was decreased from 20.7 mm to 13.7mm.

While comparing to the same model with in-plane loads only, it was seen that the load capacity decreased from 93 kN to 86 kN (10% drop) and the displacement increased from 11.3 mm to 13.72 mm. First change in stiffness occurred at load value of 26 kN (30% of load capacity) where stress of the concrete elements exceeded the value of 308 psi (modulus of rupture). At the load value of 60 kN the rebars at opposite sides of the opening and near slab-wall junction started to yield simultaneously (Figure 6.11). This caused a relatively significant loss of stiffness in the slab.

Finally at the ultimate load value of 86 kN the rebars at plastic hinge locations yielded significantly resulting in-plane failure of the slab panel (Figure 6.12). Figure 6.13 compares the load-deformation curve for slab with 14% opening subjected to in-plane and out-of-plane loads with the curve for solid slab. It is observed that the behavior of the slab is affected significantly by steel yielding at 60 kN and extensive damage at opening corners and wall-slab junction at 86 kN.

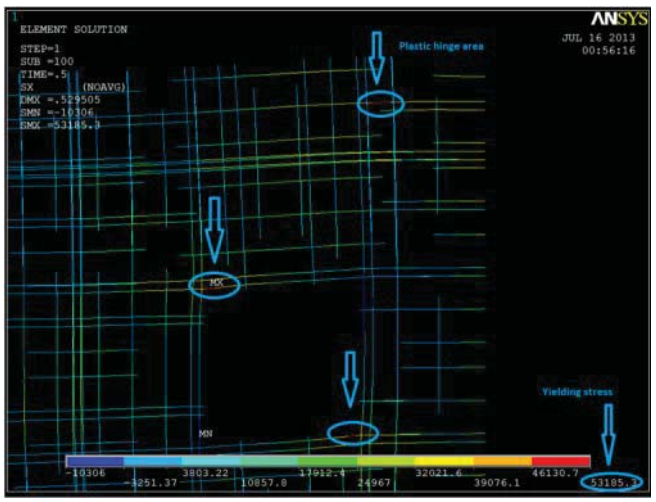

Figure 6.11: Yielding of Steel Rebars at Corner of Opening

Figure 6.12: Failure of the Slab With 14% Opening

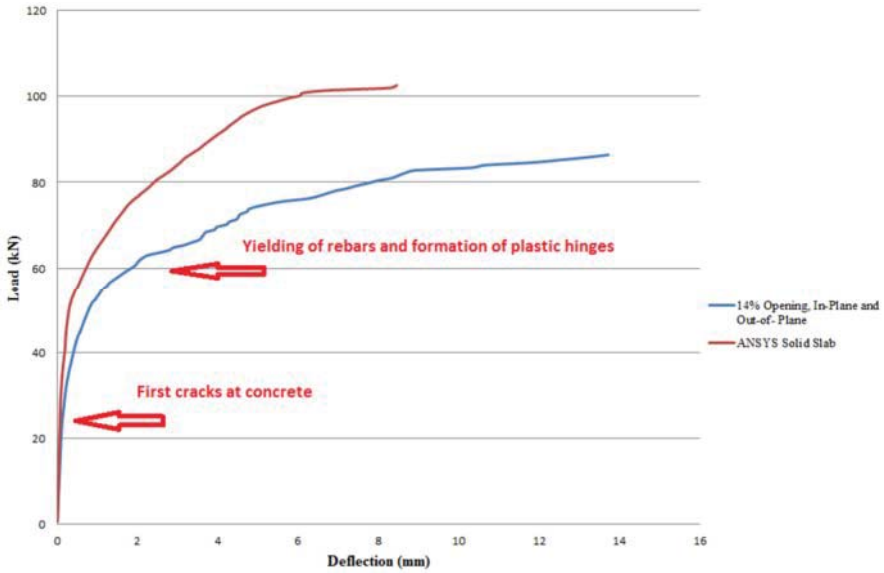

Figure 6.13: Load- Deflection Curve for Slab with 14% Opening, In-plane and Out-of-Plane Loads

In slab with 6.25 % opening the behavior was almost identical to the solid slab. The load capacity reduced 9% compared to solid slab (from 102 kN to 92 kN). The small opening size of 6.25% also did not change the failure mechanism of the slab compared to solid slab. However, the opening caused a slight drop in load capacity and an increase in deflection (from 8.8 mm to 10.2 mm).

Table 6.2 lists the results obtained from FE analysis of slabs with openings subjected to both in-plane and out-of-plane loads. As it can be seen with increasing opening sizes the load capacity decreased significantly and the ultimate displacement increased considerably. Although this pattern indicates that the slab panel with openings behaves in a more ductile manner as the opening size increases (compared to the solid slab), however, since the in-plane strength in the slabs with 25% openings dropped considerably (by 24%), it was decided to strengthen this slab by adding diagonal reinforcement at corners of the openings (as recommended by Enochsson et al., 2006) in order to meet the Section 13.4 requirements of the ACI code. The result of the strengthened slab panel is presented in the following section.

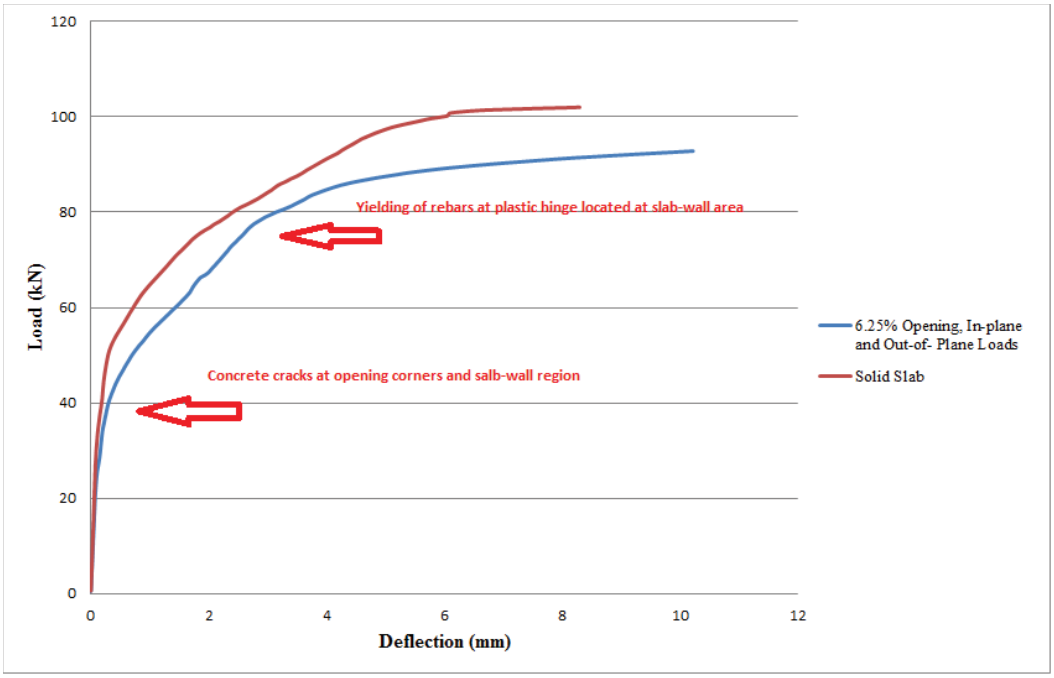

Figure 6.14: 6.25% Opening, In-Plane and Out-of-Plane Loads

Table 6.2: Results for Slab with Openings Subject to In-plane and out of-Plane Loads

Models with In-plane and Out-of-Plane Loads		
Opening Size	Load Capacity (kN)	Displacement (mm)
25%	78	23.9
14%	86	13.7
6.25%	92	10.21
0% (solid slab)	102	8.8

6.3.4 Behavior of strengthened slab panel with 25% openings

ACI code Section 13.4.1 requires that in slabs with openings the moment capacity (in-plane and out-of-plane) should meet the strength requirement of the code. Moving of the rebars in the opening region to the edges of the openings (as done in previous sections) provides adequate out-of-plane moment capacity of the slab panel. However, detailed analysis (Section 6.3.3) indicated that additional strengthening is needed to obtain the in-plane moment capacity.

In the slab panel with 25% opening two diagonal rebars (with a total cross-section area of 1.12 in^2) were added to opening corners where concrete crack and extensive yielding of the opening edge rebars were observed. Figure 6.15 illustrate the arrangements of rebars in strengthened slab with 25% opening. The non-linear ANSYS analysis results of the strengthened slab panel are given in Figures 6.16, where its load-deformation curve is compared with the one obtained from analysis of the solid slab (without opening) and un-strengthened slab panel with openings. As it can be seen adding the diagonal rebars at opening corners helped to recover the load capacity of 103 kN, meeting the ACI strength requirements in Section 13.4.1 successfully. In summary, it is concluded that adding diagonal reinforcement to the slab corners not only improves the out-of-plane load carrying capacity of the slabs as recommended by Enochsson (2006), but also it is effective in strengthening the in-plane load capacity.

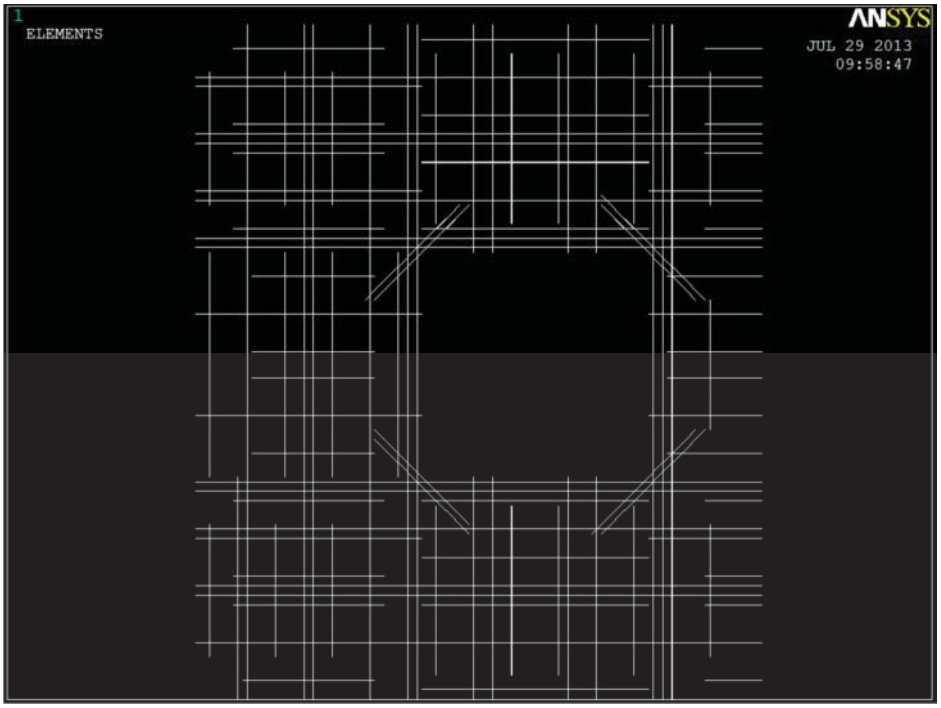

Figure 6.15: 25% Opening with Diagonal Rebars at Corners

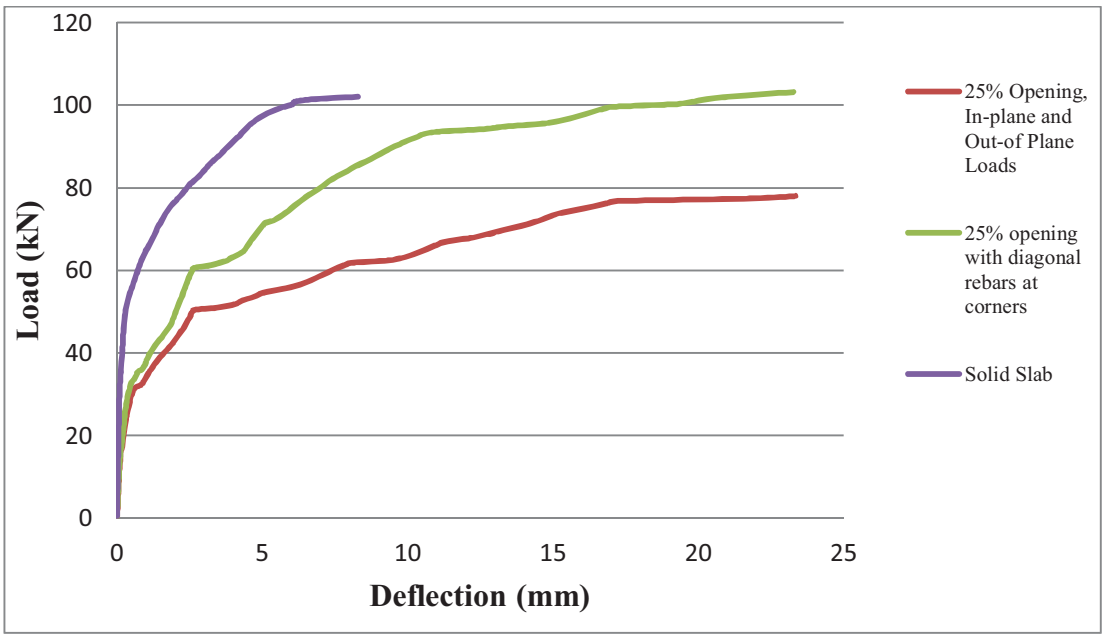

Figure 6.16: Load-Deformation Curve for the Strengthened Slab with 25% opening

CHAPTER 7

SUMMARY AND CONCLUSIONS

7.1 General

A parametric use of FE method was evaluated to analyze in-plane and out-of-plane characteristics of RC slabs. First a RC cantilever beam was modeled and analyzed for the purpose of calibration, and becoming familiar with the behavior of RC members where the steel area was close to the minimum amount. The model was calibrated and the ANSYS results compared with hand calculations. Results obtained at loads of concrete cracking, yielding of steel, and crushing of concrete. Comparison of the stresses in concrete, steel and maximum deflection of the beam obtained using ANSYS model with hand calculations provided a good agreement. The knowledge obtained from calibration beam analysis was used to model the actual two-way beam-supported concrete slab experimentally investigated by Nakashima at Lehigh University (1981). After verification of the FE slab models subjected to in-plane and out-of-plane loads with the experimental results, the verified FE models were used to analyze the effect of openings on the behavior of RC floor slabs subjected to in-plane and out-of-plane loads.

7.2 Conclusions

7.2.1 Solid slabs, in-plane and out-of-plane loads

The following conclusions are obtained based on non-linear FE analysis of two-way RC slabs subjected to in-plane and out-of-plane loads:

1. Use of ANSYS REINF264 element for rebar modeling (embedded) accurately simulated the complicated rebars arrangement and behavior in slabs. However

smeared reinforcing model was not able to capture the load capacity and corresponding displacement accurately. Therefore the use of the ANSYS embedded reinforcing bar is recommended for a three dimensional analysis of RC two-way floor slabs.

2. Comparing the results obtained from accepted hand calculation methods (beam theory for deflection and limit stage equations for ultimate moment capacity) yielded an almost exact (within 3%) correlation with ANSYS results (Appendix C) when the floor slabs are subjected to in-plane loads. The slight difference can be attributed to the assumption of having a uniform distribution of steel rebars at top and bottom of the slab in order to calculate the moment capacity of the floor section.
3. In all cases the failure was followed after formation of the plastic hinge at a section near the wall, where numbers of positive and negative rebars were cut off. This section was approximately at the boundary between column and middle strips of the slab panel.
4. As expected, out-of-plane loads (full service dead and live loads) decreased the in-plane capacity of the solid slabs by 13%, and slightly increased the ultimate in-plane displacements. The reduction in load capacity is attributed to having two lines of cracks occurred at the top of the slab due to application of the out-of-plane loads (Figure 5.1).
5. In the ANSYS models with in-plane and out-of-plane loads (simulating the behavior of BV1MN experiment), the load-deflection curve was much smoother than the one obtained for the model with in-plane loads only (as in BH2MN experiment). That is, the stiffness of the BV1MN models decreased gradually until the ultimate load was reached, unlike in BH2MN model because of sudden occurrence of in-plane cracking,

yielding of steel rebars, and breaking of rebars at plastic hinge region, which triggered the failure.

7.2.2 Slabs with openings, in-plane and out-of-plane loads

Slab models with three different opening sizes (25%, 14% and 6.25% of the panel) subjected to in-plane and out-of-plane loads were investigated. The following conclusions were obtained:

1. In all cases the presence of the openings changed the failure mechanism of the slabs with yielding of the steel rebars at opening corners leading to formation of several plastic hinges resulting in a more ductile failure (in comparison with the solid slab). Thus, the sequence of the first cracking in concrete, yielding of steel and the location of plastic hinge regions are clearly affected with presence of the openings.
2. The presence of the openings also changed the cracking patterns. The larger the opening size the less cracks and stresses were observed due to out-of-plane loads. However, with application of the in-plane loads cracks at opposite sides of the opening corners were initiated in all cases, and also the rebars at opening corners and at slab-wall junction region yielded. This emphasized importance of the effect of opening corners in changing behavior of the slabs.
3. The larger the opening size the effect of out-of-plane loads became minimal, in other words in the slab with largest opening size (25%) the behavior of the slab (load capacity and deflections) was almost the same in both loading scenarios (in-plane vs. in-plane and out-of-plane loads). The reason was that the larger opening size reduced the associated dead and live loads at the panel, minimizing gravity effect, which consequently reduced the concrete stresses and cracking.

4. Larger opening sizes caused larger in-plane deflections due to reduced floor panel stiffness. This pattern was maintained for both loading scenarios. In the cases with in-plane and out-of-plane loads, the slab with 25% opening size increased the ultimate in-plane deflection by a factor of 2.7compared to solid slab, while in slabs with 14% and 6.25% the deflection increased by a factor of 1.56 and 1.16, respectively.
5. Larger opening sizes reduced the in-plane load carrying capacity compared with solid slab. This pattern was maintained in both loading scenarios. The reduction for the slabs with 25%, 14% and 6.25% opening sizes were 23%, 16% and 10%, respectively.
6. Introduction of out of-plane loads in all cases reduced the load carrying capacity (by a maximum of 10% in slab with 6.25% opening) and increased the deflection. However, the capacity reduction was less pronounced with larger opening size.
7. The ACI code requirements for openings in RC two-way slabs investigated. Based on the analysis performed on slabs with openings, it was concluded that placement of the openings at intersection of the middle strips in floor panels with additional rebars placed around the opening including the diagonal rebars at the opening corners will recover load capacity of the floor panels.
8. These results clearly indicate that there is a need for further research on the subject of in-plane floor diaphragms with openings. It is believed that ignoring the inelastic behavior of such diaphragms can lead to inaccurate results.

REFERENCES

ACI Committee 318 (2011), "ACI 318-08 Building Code Requirements for Structural Concrete," American Concrete Institue, Chicago, IL.

Al Harash, M. (2011), "Inelastic Seismic Response of Reinforced Concrete Buildings with Floor Diaphragm Openings," Doctorate's Thesis, Washington University in St. Louis, St. Louis, Missouri

American Society of Civil Engineers (2010), "Minimum design loads for building and other structures (ASCE 7-10)," Structural Engineering Institute of the American Society of Civil Engineers, Reston, VA.

ANSYS (2012), Academic Research, Release 13.0, ANSYS, Inc.

ASCE (2000) Pre-standard and Commentary for the Seismic Rehabilitation of Buildings (FEMA-356) (Report No. FEMA 356). Reston, VA: American Society of Civil Engineers prepared for the Federal Emergency Management Agency.

Bangash, M. Y. H. (1989), "Concrete and Concrete Structures: NumericalModeling and Applications." Elsevier Science Publishers Ltd., London, England.

Barron, M.J; and Hueste, D.B. (2004)," Diaphragm Effects in Rectangular Reinforced Concrete Buildings" ACI Structural Journal Title no. 101-S60

Boon, H.K.; Diah, M.B.; and Loon, Y.L. (2009), " Flexural Behaviour of Reinforced Concrete Slab with Opening" Proceedings of MUCEET2009

Casadei, P.; Ibell , T.J.; and Nanni, A. (2009), "Two-Way RC Slabs with Openings 1 Strengthened with CFRP Laminates," ACI Structural Journal, University of Missouri- Rolla, Rolla, Missouri

Daham, A.H. (2010), "Analytical Study of Reinforced Concrete Two-Way Slabs with and without Opening Having Different Boundary Conditions," Civil Engineering Department – University of Tikrit, Tikrit, IRAQ

Enochsson, O.; Lundqvist, J.; Taljsten, B.; Rusinowski, P.; and Olofsson, T. (2006), "CFRP Strengthened Openings in Two-Way Concrete Slabs- An Experimental and Numerical Study." Elsevier Journal, Construction and Building Materials 21 (2007) 810-826

Fanning, P. (2001), "Nonlinear Models of Reinforced and Post-tensioned Concrete Beams," Electronic Journal of Structural Engineering, University College Dublin, Earlsfort Terrace, Dublin 2, Ireland, Sept.12.

Hemmaty, Y. (1998), Modeling of the Shear Force Transferred Between Cracks in Reinforced and Fibre Reinforced Concrete Structures, Proceedings of the ANSYS Conference ,Vol. 1, Pittsburgh, Pennsylvania

Huyse, L.; Hemmaty, Y.; and Vandewalle,L. (1994), Finite Element Modeling of Fiber Reinforced Concrete Beams. Proceedings of the ANSYS Conference, Vol. 2, Pittsburgh, Pennsylvania.

Jiangt, J.; and Mirzaf, A.F. (1993), "Nonlinear Analysis of Reinforced Concrete Slabs by A Discrete Finite Element Approach" Compukw & Stucrures Vol. 65, No 4, pp. 585-592, 1991

Kachlakev, D.I.; Miller, T.; Yim, S.; Chansawat, K.; and Potisuk, T. (2001), "Finite Element Modeling of Reinforced Concrete Structures Strengthened With FRP Laminates," California Polytechnic State University, San Luis Obispo, CA and Oregon State University, Corvallis, OR for Oregon Department of Transportation, May 2001.

Kunnath, S. K.; Reinhorn, A. M.; and Park, Y. J. (1990), "Analytical Modeling of Inelastic Seismic Response of RC Structures," J. Struct. Engrg. ASCE 116 (4), pp. 996-1017.

MacGregor, J.G. (1992), Reinforced Concrete Mechanics and Design, Prentice-Hall, Inc., Englewood Cliffs, NJ.

Nakashima, M. (1981), "Seismic Resistance Characteristics of Reinforced Concrete Beam-Supported Floor Slabs in Building Structures." Doctoral Dissertation, Lehigh University, Bethlehem, PA.

Nakashima, M.; Huang, T.; and Lu, L. W. (1984), "Effect of Diaphragm Flexibility on Seismic Response of Building Structures," 8th World Conference on EQ. Eng., San Francisco, CA, Vol. 4, pp. 735-742.

Nakashima, M.; Huang, T.; and Lu, L. W. (1982), "Experimental Study of Beam-Supported Slabs Under In-plane loading," ACI Journal, Tiltle no. 79-8

Panahshahi, N.; Reinhorn, A. M.; Kunnath, S. K.; Lu, L. W.; Huang, T.; and Yu, K. (1991), "Seismic Response of a 1:6 Reinforced Concrete Scale-Model Structure with Flexible Floor Diaphragm," ACI Struct. J. 88-S34, pp.315-324

Panahshahi, N.; Reinhorn, A.M.; and Kunnath, S.K. (1994), "Earthquake Simulation Study of a One-Sixth Scale-Model RC Building with Flexible Floor Diaphragms," Proceedings, The Fifth U.S. National Conference on Earthquake Engineering, Chicago, IL.

Philips, T. L.; Itani, R. Y.; and McLean, D. I. (1993), "Lateral Load Sharing by Diaphragms in Wood-Framed Building," J. Struct. Engrg. ASCE 119 (5), pp. 1556-1571.

Reinhorn, A. M.; Kunnath, S. K.; and Panahshahi, N. (1988), "Modeling of RC Building Structures with Flexible Floor Diaphragms (IDARC2)," Technical Report NCEER-88-0035, State University of New York at Buffalo, Buffalo, NY.

Rusinowski, P. (2005), "Two-Way Concrete Slabs with Openings Experiments, Finite Element Analyses and Design", M.Sc. Thesis, Lulea University of Technology, Swedish, 2005.

Shing, P.B.; and Tanabe, T.A. (2001), Modeling of Inelastic Behavior of RC Structures under Seismic Loads, American Society of Civil Engineers

Stehle, J. S. (2002). The Seismic Performance of Reinforced Concrete Wide Band Beam Frames: Interior Connections, University of Melbourne, Australia.

Tavarez, F.A. (2001), "Simulation of Behavior of Composite Grid Reinforced Concrete Beams Using Explicit Finite Element Methods," Master's Thesis, University of Wisconsin-Madison, Madison, Wisconsin.

Vecchio, F. J.; and Collins, P.M. (1986), "The Modified Compression Theory for Reinforced Concrete Elements Subjected to Shear." ACI Structural Journal, Proceedings V. 83, No. 2, March-April 1986, pp. 219-231.

Wight and MacGregor (2011) (Book)

Willam, K..; and Tanabe, T.A., . (2001), "Finite Element Analysis of Reinforced Concrete Structures", American Concrete Institute, Farmington Hills, MI.

Willam, K.J.; and Warnke, E.P. (1974), "Constitutive Model for Triaxial Behaviour of Concrete," Seminar on Concrete Structures Subjected to Triaxial Stresses, International Association of Bridge and Structural Engineering Conference, Bergamo, Italy, p.174.

Wolanski, A.R. (2004), 'Flexural Behavior Ofreinforced and Prestressed Concrete Beams Using Finite Element Analysis' Marquette University, Milwaukee, Wisconsin May, 2004

APPENDIX A

THEORETICAL CALCULATIONS FOR CANTILEVER BEAM (CALIBRATION BEAM)

Section 1: Stress and Deflection Calculations at Linear and First Concrete Cracking :

$b := 12$ width of cross section(in)

$h := 12$ height of cross section(in)

$d := 10.5$ depth(in)

$L := 120$ length of the beam(in)

$E_c := 3.05 \cdot 10^6$ Modulos of elasticity of concrete(psi)

$E_s := 29 \cdot 10^6$ Modulos of elasticity of steel(psi)

$A_s := .8$ Area of steel(in^2)

$f_y := 60000$ yield stress of steel(psi)

$f_r := 300$ modulos of rupture of concrete(psi)

$f_c := 3000$ compressive stress of concrete(psi)

$n := \frac{E_s}{E_c} = 9.5082$ ratio of modulos of elasticity

$c := \frac{h}{2} = 6$

$I_g := \frac{b \cdot h^3}{12} = 1728$ uncracked moment of inertia(in^4)

$y := 1$

Finding the Moment of Inertia of Composite Section, Considering Steel Rebars (No Cracking):

$$y_{uncracked} := root\left[\left[(12)(12-y)\left(\frac{12-y}{2}\right) + (n-1)(A_s)(d-y) - b\cdot\left(\frac{y^2}{2}\right)\right], y\right] = 6.2031$$

$y_{uncracked} = 6.2031 \quad s(in)$

$$I_{uncracked} := I_g + (b\cdot h)\left(y_{uncracked} - c\right)^2 + (n-1)(A_s)\left(d - y_{uncracked}\right)^2 = 1859.61179$$

$$M_{crack} := \frac{f_r \cdot I_{uncracked}}{c} = 92980.58962$$

$$P_{crack} := \frac{M_{crack}}{L} = 774.83825$$

Finding the Steel and Concrete Stress(uncracked/ elastic):

$p := 774$ applied force (lbs)

$M := p\cdot 120$ moment at critical section (lbs.in)

$$\sigma_c := \frac{M\cdot y_{uncracked}}{I_{uncracked}} = 309.81969$$ stress in extreme concrete fiber(psi)

$$\sigma_{steel} := \frac{M\cdot\left(d - y_{uncracked}\right)n}{I_{uncracked}} = 2040.57637$$ stress in steel fiber(psi)

$$\Delta_{uncracked} := \frac{\left(p\cdot L^3\right)}{\left(3.E_c\cdot I_{uncracked}\right)} = 0.0786$$ Deflection of the beam when elastic load of 774 lbs was applied (in.)

Finding the Moment of Inertia in Cracked Phase (transformed section):

$y := 1$

$$y_{crack} := root\left[\left[\left(\frac{b \cdot y^2}{2}\right) - (d - y)\left(n \cdot A_s\right)\right], y\right] = 3.06926$$

Netural axis in cracked phase

$$I_{crack} := \left(\frac{b \cdot y_{crack}^3}{3}\right) + \left(n \cdot A_s\right)\left(d - y_{crack}\right)^2 = 535.65699$$

cracked moment of inertia(in^4)

$$I_e := \left(\frac{M_{crack}}{M}\right)^3 \cdot I_g + \left[1 - \left(\frac{M_{crack}}{M}\right)^3\right] \cdot I_{crack} = 1731.87814$$

ACI formula for deflection at service phase

Finding the Steel and Concrete Stresses at Cracked Phase :

$$f_{ccrack} := \frac{M \cdot y_{crack}}{I_{crack}} = 532.19376$$

Extreme concrete fiber stress at cracked phase(psi)

$$F_{scrack} := \frac{M \cdot \left(d - y_{crack}\right) \cdot n}{I_{crack}} = 12250.82631$$

steel stress at cracked phase(psi)

Finding deflection:

$$\Delta_{uncracked} := \frac{\left(p \cdot L^3\right)}{\left(3.E_c \cdot I_{uncracked}\right)} = 0.0786$$

Deflection at Linear Range (in.)

$$\Delta_{crack} := \frac{p \cdot L^3}{3.E_c \cdot I_e} = 0.0844007$$

Deflection at First Concrete Cracking (in.)

Section 2:Finding the Yield Moment and the Neutral Axis Location at Yielding of Steel:

$$\delta := f_c\left[2\left(\frac{\varepsilon}{\varepsilon_0}\right) - \left(\frac{\varepsilon}{\varepsilon_0}\right)^2\right]$$

Concrete nonlinear equation (MacGregor, 1992)

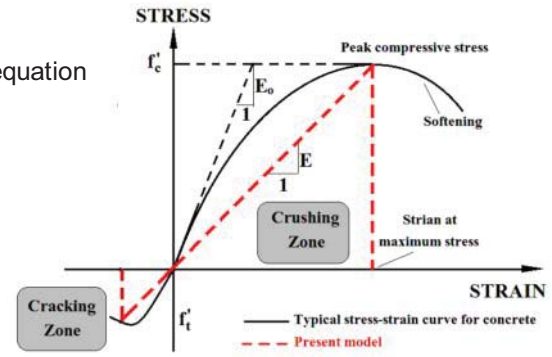

Figure A1: Concrete Stress-Strain Curve (non-linear)

$A_s := .8$ Area of steel

$F_y := 60000$ Steel yiel stress (psi)

$$\int 3000\left[2\left(\frac{y}{10.5 - c}\right) - \left(\frac{y}{10.5 - c}\right)^2\right] \cdot 12\, dy \rightarrow -\frac{36000 \cdot y^2}{c - 10.5} - \frac{12000 \cdot y^3}{(c - 10.5)^2}$$

$y := 1$

$$d := \text{root}\left[\left[-\frac{36000 \cdot y^2}{y - 10.5} - \frac{12000 \cdot y^3}{(y - 10.5)^2} - (A_s \cdot F_y)\right], y\right]$$

$d = 3.36021$ Compreesion block height (in.)

$$\gamma := \frac{\left[-\frac{2000 \cdot d^3}{d - 10.5} - \frac{750 \cdot d^4}{(d - 10.5)^2}\right]}{\left[-\frac{3000 \cdot d^2}{d - 10.5} - \frac{1000 \cdot d^3}{(d - 10.5)^2}\right]} = 2.18804$$

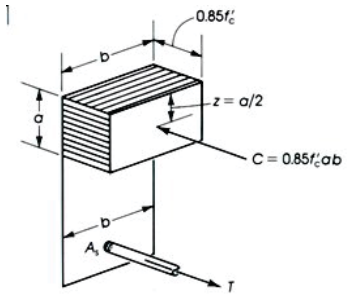

0

$z := \gamma + (10.5 - d) = 9.32783$ Coupling moment arm (in.)

$M_y := z \cdot A_s \cdot F_y = 447735.71536$ Yield Moment (lb.in)

$P_y := \frac{M_y}{120} = 3731.13096$ yield load(lbs)

Section 3: Deflection Calculations Using Curviture:

At Steel Yield:

$f_r := 300$

$E_c := 3.05 \cdot 10^6$

$d := 10.5$

$y := 3.36$

$f_s := 60000$

$E_s := 29000000$

$M_{cr} := 92980.59$ cracking moment

$P_y := 3731.13096$ yielding load calculated in A.2

$\varepsilon_y := \frac{f_s}{E_s} = 2.069 \times 10^{-3}$ yield strain of steel

$\varepsilon_{rupture} := \frac{f_r}{E_c} = 9.836 \times 10^{-5}$ strain at rupture

$\varepsilon_c := \frac{\varepsilon_y \cdot y}{d - y} = 9.736 \times 10^{-4}$ concrete strain

$\phi_{yield} := \frac{\varepsilon_c}{y} = 2.898 \times 10^{-4}$ yield curviture

$\phi_{elastic} := \frac{\varepsilon_{rupture}}{5.798} = 1.696 \times 10^{-5}$ elastic curviture

$X_{cr} := \frac{M_{cr}}{P_y} = 24.92$ elastic span of the beam

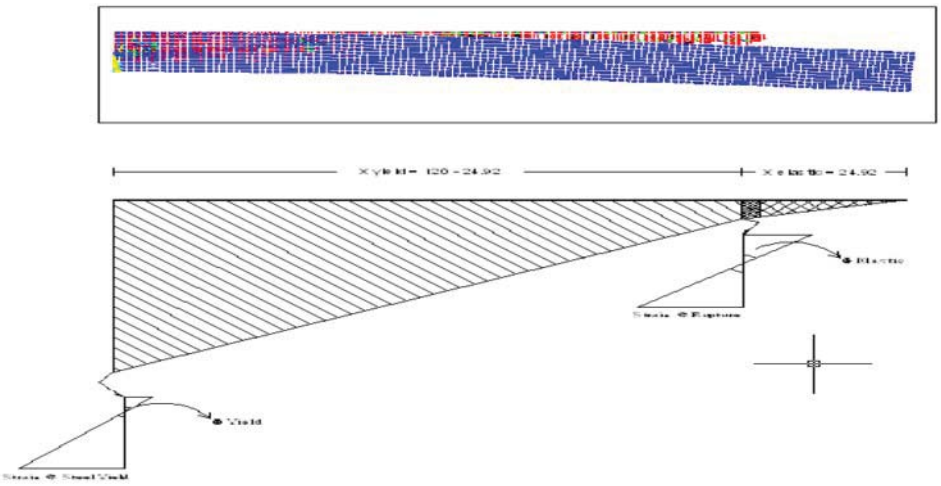

Figure A2: Graph in dicating Cracking Pattern and Elastic Section at Yielding of Steel

$$\Delta_{yield} := \left(\frac{X_{cr}\cdot\phi_{elastic}}{2}\right)\cdot\left(\frac{X_{cr}\cdot 2}{3}\right) + \left[\left[\left(120 - X_{cr}\right)\phi_{elastic}\right]\cdot\left[X_{cr} + \frac{\left(120 - X_{cr}\right)}{2}\right]\right] + \left[\left[\left(1\right.\right.\right.$$

$\Delta_{yield} = 1.266$ Maximum deflection at yield

At failure Using Whitney's Rectangular Stress Block:

$A_s := .8$ Area of steel (in^2)

$f_y := 60$ Yield stress of steel (ksi)

$f_c := 3$ Ultimate compressive stress of concrete (ksi)

$b := 12$ Compressive width of the beam (in)

$$a := \frac{A_s\cdot f_y}{.85\cdot f_c\cdot b} = 1.569$$

$$P_u := \frac{\left[A_s\cdot f_y\cdot\left(d - \frac{a}{2}\right)\right]}{120\cdot 10^{-3}} = 3.886\times 10^{3}$$ load capacity at failure (lbs)

$$c := \frac{a}{.85} = 1.845$$

$$\phi_{ultimate} := \frac{.003}{c} = 1.626\times 10^{-3}$$

$$X_{cr} := \frac{M_{cr}}{P_u} = 23.925$$

$$M_{yield} := P_y \cdot 120 = 4.477 \times 10^5$$

$$X_{yield} := \frac{M_{yield}}{P_u} = 115.209$$

$$X_{ult} := 120$$

$$\Delta_{failure} := \left(\frac{X_{cr} \cdot \phi_{elastic}}{2}\right) \cdot \left(\frac{X_{cr} \cdot 2}{3}\right) + \left[\left[\frac{(X_{ult} - X_{cr})}{2} + X_{cr}\right] \cdot \frac{(X_{ult} - X_{cr}) \phi_{elastic}}{1}\right] + \left[\frac{(X}{}\right.$$

$\Delta_{yield} = 1.266$ Deflection of the beam when yielding load value was applied (in)

$\Delta_{failure} = 1.709$ Deflection of the beam when ultimate capacity was applied (in)

APPENDIX B

CALCULATIONS OF VOLUMETRIC RATIO OF STEEL REINFORCEMENT FOR ANSYS MODELS WITH SMEARED REBAR MODELING

Section 1: Caculationg Volumetric Ratio of Steel Rebars Needed for ANSYS Smeared Steel Modeling

Ngative moment (top Slab):

(top slab) perpendicular to the wall column strip interior: 6 D2.0

$A_{srequirednperi} := 6 \cdot .02 \cdot 4.5^2 = 2.43$ and to prototype(4.5 *4.5)

Assuming that the strip is 144" long and &" depth (dimensions of cross section) and element length is equal to 6"

$$v_{eachelement} := \frac{\frac{A_{srequirednperi}}{\left(\frac{144}{6}\right)}}{12} = 8.4375 \times 10^{-3}$$

Number 2 in Figure B1

(top slab) parallel to the wall column strip interior: 2 D2.0

$A_{srequirednpari} := 2 \cdot .02 \cdot 4.5^2 = 0.81$

Assuming that the strip is 72" long and &" depth (dimensions of cross section) and element length is equal to 6"

$$\frac{\frac{A_{srequirednpari}}{\frac{72}{6}}}{12} = 5.625 \times 10^{-3}$$ Volumetric ratio of each element

Number 2 in Figure B1

(top slab) parallel to the wall middle strip: 6 D2.0

$A_{srequirednparm} := 6 \cdot .02 \cdot 4.5^2 = 2.43$ and to prototype(4.5 *4.5)

Assuming that the strip is 144" long and &" depth (dimensions of cross section) and element length is equal to 6"

$$V_{requirednparm} := \frac{\frac{A_{srequirednparm}}{\left(\frac{144}{6}\right)}}{12} = 8.4375 \times 10^{-3}$$

Number 6 in Figure B1

(top slab) perpendicular to the wall middle strip interior: 7 D3.0

$A_{sreuirednperm} := 7 \cdot .03 \cdot 4.5^2 = 4.2525$ Required steel converted to inches and to prototype(4.5 *4.5)

Assuming that the strip is 144" long and &" depth (dimensions of cross section) and element length is equal to 6"

$$V_{requirednperm} := \frac{\frac{A_{sreuirednperm}}{\left(\frac{144}{6}\right)}}{12} = 0.0148$$ Volumetric ratio of each element

Number 4 in Figure B1

(top slab) perpendicular to the wall middle strip: 6 D2.0

$A_{srequirednperm} := 6 \cdot .02 \cdot 4.5^2 = 2.43$ Required steel converted to inches and to prototype(4.5 *4.5)

Assuming that the strip is 144" long and &" depth (dimensions of cross section) and element length is equal to 6"

$$V_{requirednperm} := \frac{\frac{A_{srequirednperm}}{\left(\frac{144}{6}\right)}}{12} = 8.4375 \times 10^{-3}$$ Volumetric ratio of each element

Number 5 in Figure B1

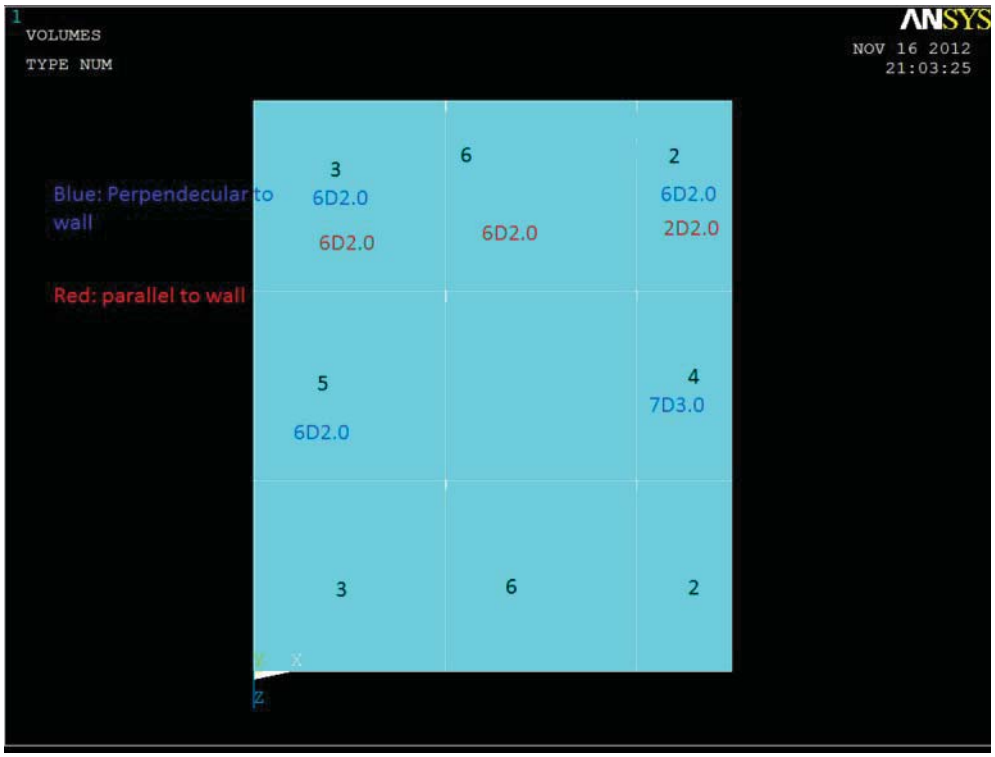

Figure B1: Real Constatnt Numbers Assigned to Top Slab (negative moment)

Positive Moment (bot slab):

(bot slab) perpendicular to wall column strip interior: 2D2.5

$A_{sreuiredpperci} := 2 \cdot .025 \cdot 4.5^2 = 1.0125$ Required steel converted to inches and to prototype(4.5 *4.5)

Assuming that the strip is 144" long and 7" depth (dimensions of cross section) and element length is equal to 6"

$$V_{requiredpperci} := \frac{\frac{A_{sreuiredpperci}}{\left(\frac{144}{6}\right)}}{12} = 3.5156 \times 10^{-3}$$ Volumetric ratio of each element

Number 7 in Figure B2

(bot slab) Parallel to wall column strip interior: 1D2.0

$A_{srequiredpparci} := 1 \cdot .02 \cdot 4.5^2 = 0.405$ Required steel converted to inches and to prototype(4.5 *4.5)

Assuming that the strip is 72" long and &" depth (dimensions of cross section) and element length is equal to 6"

$$V_{requiredpparci} := \frac{\frac{A_{srequiredpparci}}{\left(\frac{72}{6}\right)}}{12} = 2.8125 \times 10^{-3}$$ Volumetric ratio of each element

Number 7 in Figure B2

(bot slab) Perpendecular to wall column strip: 2D2.5+4D2.0

$A_{sreuiredpperc} := (2 \cdot .025 + 4 \cdot .02) \cdot 4.5^2 = 2.6325$ Required steel converted to inches and to prototype(4.5 *4.5)

Assuming that the strip is 144" long and 7" depth (dimensions of cross section) and element length is equal to 6"

$$V_{requiredpperc} := \frac{\frac{A_{sreuiredpperc}}{\left(\frac{144}{6}\right)}}{12} = 9.1406 \times 10^{-3}$$ Volumetric ratio of each element

Number 8 in Figure B2

(bot slab) Parallel to wall column strip exterior: 2D2.5

$A_{sreuiredpperce} := 2 \cdot .025 \cdot 4.5^2 = 1.0125$ Required steel converted to inches and to prototype(4.5 *4.5)

Assuming that the strip is 144" long and 7" depth (dimensions of cross section) and element length is equal to 6"

$$V_{requiredpperce} := \frac{\frac{A_{sreuiredpperce}}{\left(\frac{144}{6}\right)}}{12} = 3.5156 \times 10^{-3}$$ Volumetric ratio of each element

Number 9 in Figure B2

(bot slab) parallel to wall column strip exterior: 2D2.0

$$A_{srequiredpparce} := 2 \cdot .02 \cdot 4.5^2 = 0.81$$

Assuming that the strip is 144" long and 7" depth (dimensions of cross section) and element length is equal to 6"

$$V_{requiredpparce} := \frac{\frac{A_{srequiredpparce}}{\left(\frac{144}{6}\right)}}{12} = 2.8125 \times 10^{-3}$$ Volumetric ratio of each element

Number 9 in Figure B2

(bot slab) perpendicular to wall middle strip interior : 2D2.5

$$A_{srequiredppermi} := 2 \cdot .025 \cdot 4.5^2 = 1.0125$$

Assuming that the strip is 144" long and 7" depth (dimensions of cross section) and element length is equal to 6"

$$V_{requiredppermi} := \frac{\frac{A_{srequiredppermi}}{\left(\frac{144}{6}\right)}}{12} = 3.5156 \times 10^{-3}$$ Volumetric ratio of each element

Number 10 in Figure B2

(bot slab) parallel to wall middle strip interior : 2D2.0

$A_{srequiredpparci} := 2 \cdot .02 \cdot 4.5^2 = 0.81$

Assuming that the strip is 72" long and 7" depth (dimensions of cross section) and element length is equal to 6"

$$V_{rrequiredpparci} := \frac{\frac{A_{srequiredpparci}}{\left(\frac{72}{6}\right)}}{12} = 5.625 \times 10^{-3}$$ Volumetric ratio of each element

Number 10 in Figure B2

(bot slab) perpendicular to wall middle strip : 2D2.5+4D2.0

$A_{srequiredppc} := (2 \cdot .025 + 4 \cdot .02) \cdot 4.5^2 = 2.6325$

Assuming that the strip is 144" long and 7" depth (dimensions of cross section) and element length is equal to 6"

$$V_{rrequiredpparci} := \frac{\frac{A_{srequiredppc}}{\left(\frac{144}{6}\right)}}{12} = 9.1406 \times 10^{-3}$$ Volumetric ratio of each element

Number 11 in Figure B2

(bot slab) parallel to wall middle strip : 5D2.0

$$A_{srequiredpparm} := (5 \cdot .02) \cdot 4.5^2 = 2.025$$

Assuming that the strip is 144" long and 7" depth (dimensions of cross section) and element length is equal to 6"

$$V_{requiredpparci} := \frac{\frac{A_{srequiredpparm}}{\left(\frac{144}{6}\right)}}{12} = 7.0312 \times 10^{-3}$$

Volumetric ratio of each element

Number 11 in Figure B2

(bot slab) perpendicular to wall middle strip exterior : 2D2.5

$$A_{srequiredpperme} := (2 \cdot .025) \cdot 4.5^2 = 1.0125$$

Assuming that the strip is 144" long and 7" depth (dimensions of cross section) and element length is equal to 6"

$$V_{srequiredpperi} := \frac{\frac{A_{srequiredpperme}}{\left(\frac{144}{6}\right)}}{12} = 3.5156 \times 10^{-3}$$ Volumetric ratio of each element

Number 12 in Figure B2

(bot slab) parallel to wall middle strip exterior : 6D2.0

$$A_{srequiredpparce} := (6 \cdot .02) \cdot 4.5^2 = 2.43$$

Assuming that the strip is 144" long and 7" depth (dimensions of cross section) and element length is equal to 6"

$$V_{srequiredpparei} := \frac{\frac{A_{srequiredpparce}}{\left(\frac{144}{6}\right)}}{12} = 8.4375 \times 10^{-3}$$

Number 12 in Figure B2

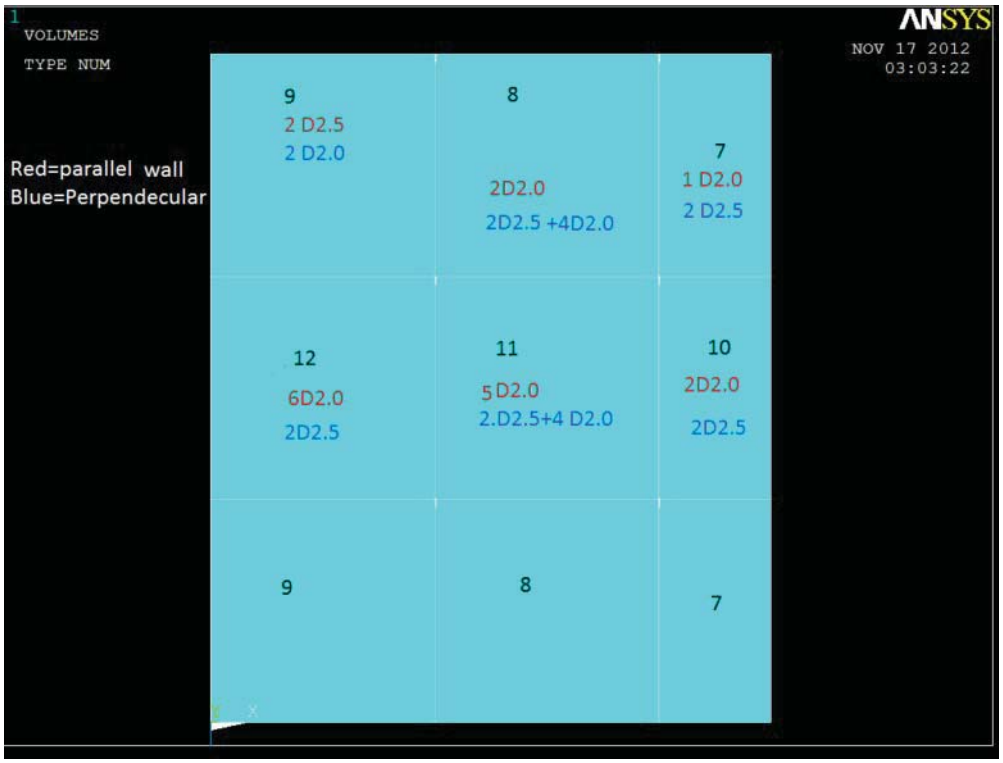

Figure B2: Real Constatnt Numbers Assigned to Top Slab (negative moment)

Beam Positive reinforcement:

Middle section (maximum flexure) x direction: 3D2.0

$$\frac{\left(3 \cdot .02 \cdot 4.5^2\right)}{60} = 0.0202$$

assuming the beam with 12" width and 6" element size

Number 13 in Figure B3

Ende sections (integrity and continuity requirements) x direction: 2D2.0

$$\frac{2 \cdot .02 \cdot 4.5^2}{60} = 0.0135$$

Number 14 in Figure B3

Middle section (maximum flexure) y direction: 3D2.0

$$\frac{\left(3 \cdot .02 \cdot 4.5^2\right)}{60} = 0.0202$$

assuming the beam with 12" width and 6" element size

Number 14 in Figure B3

Ende sections (integrity and continuity requirements) y direction: 2D2.0

$$\frac{2 \cdot .02 \cdot 4.5^2}{60} = 0.0135$$

Number 15 in Figure B3

Column Beam Intersection: 2D2.0 in both x & y directions

Number 17 in Figure B3

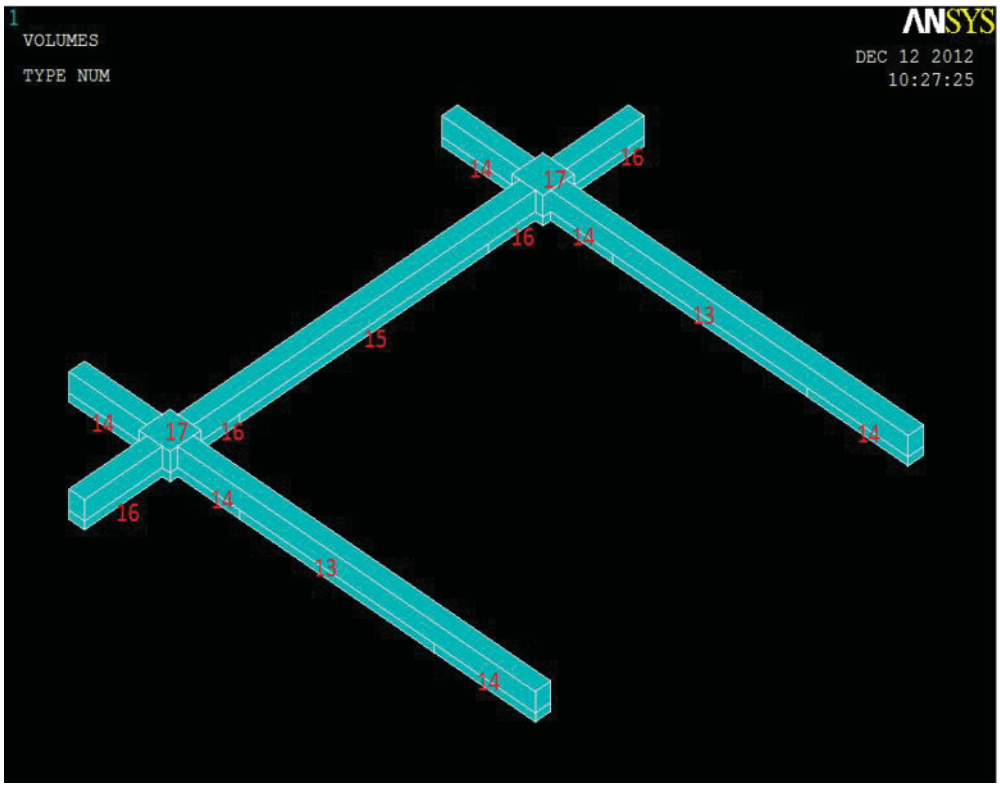

Figure: B3: Real Constants Assigned to Positive Rebars

Beam Negative:

Middle section x direction: 2D2.0

assuming 12" lenghth of beam and 6" length of element

$$\frac{2 \cdot .02 \cdot 4.5^2}{2 \cdot 6} = 0.0675$$

Required area for each eleemnt

Number 15 in Figure B4

Around the wall x direction: 3D2.0

$$\frac{3 \cdot .02 \cdot 4.5^2}{2 \cdot 6} = 0.1012$$

Number 19 in Figure B4

Aroun the columns x direction: 3D3.0

$$\frac{3 \cdot .03 \cdot 4.5^2}{2 \cdot 6} = 0.1519$$

Number 20 in Figure B4

Left End(extreme end) x direction: 2D3.0

$$\frac{2 \cdot .03 \cdot 4.5^2}{2 \cdot 6} = 0.1012$$

Number 21 in Figure B4

Middle section y direction: 2D3.0

$$\frac{2 \cdot .03 \cdot 4.5^2}{2 \cdot 6} = 0.1012$$

Number 22 in Figure B4

around the columns y direction: 3D3.0

$$\frac{3 \cdot .03 \cdot 4.5^2}{2 \cdot 6} = 0.1519$$

Number 23 in Figure B4

Around the column extreme ends: 2D3.0

$$\frac{2 \cdot .03 \cdot 4.5^2}{2 \cdot 6} = 0.1012$$

Number 24 in Figure B4

Beam column intersection: 3D3.0 in both direction

$$\frac{3 \cdot .03 \cdot 4.5^2}{2 \cdot 6} = 0.1519$$

Number 24 in Figure B4

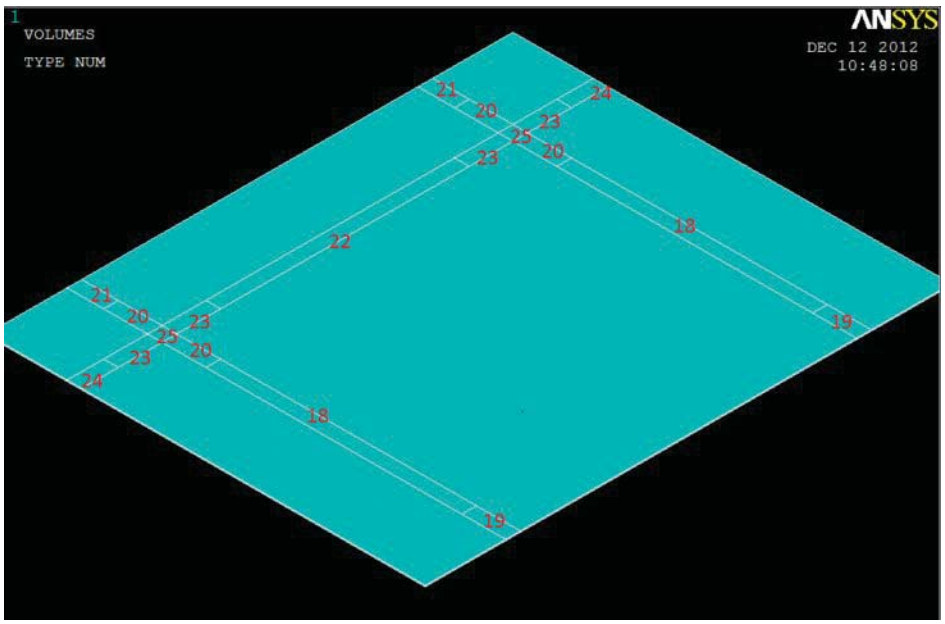

Figure B4: Real Constatnts Assigned to Negative Beam

Section 2: Constructing Stress-Strain Curves for Concrete used in Slab, beams, shear walls and Columns

Slab, Beams and Shear Wall Concrete (4061psi)

$E_c := 3.0458E+006$

$f_c := 4061$

$f_r := 308.9$

$\varepsilon_0 := \frac{2f_c}{E_c} = 2.667 \times 10^{-3}$ Strain at ultimate stress

Point 1 must satisfy hook's law:

$f_1 := .3 \cdot f_c = 1.218 \times 10^{3}$

$\varepsilon_1 := \frac{f_1}{E_c} = 4 \times 10^{-4}$

Point 2, 3 & 4 are calculated using equation

$$f := \frac{E_c \cdot \varepsilon}{1 + \left(\frac{\varepsilon}{\varepsilon_0}\right)^2}$$ (MacGregor, 1992)

f= Stress at any strain
ε= Strain at stress f
ε_0= Strain at ultimate compressive strength f_c

f_2= .46 f_c =1868.86 ε_2= .00065
f_3= .84 f_c = 3411 ε_3= .0015
f_4= .96 f_c = 3898 ε_4= .002
f_5= f_c =4061 ε_5= . 0027

$$\varepsilon := \begin{pmatrix} .0004 \\ .00065 \\ .0015 \\ .002 \\ .0027 \end{pmatrix} \qquad f := \begin{pmatrix} 1218 \\ 1868 \\ 3411 \\ 3898 \\ 4061 \end{pmatrix}$$

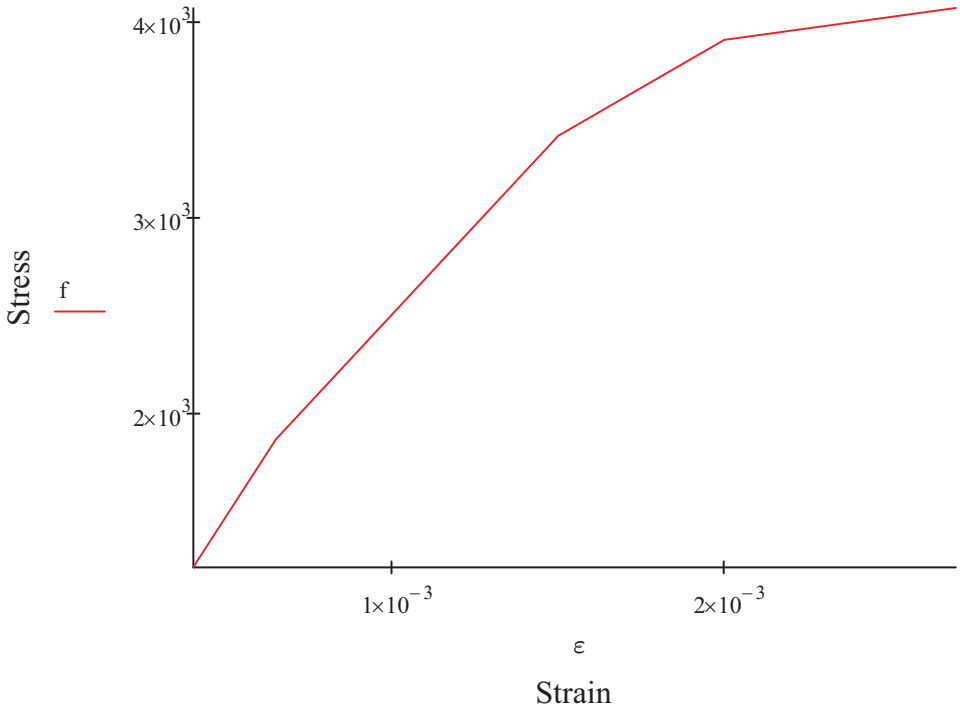

Coulmn Concrete (5409 psi):

$E_c := 4.35 \cdot 10^6$

$f_c := 5409$

$f_r := 517$

$\varepsilon_0 := \frac{2 f_c}{E_c} = 2.487 \times 10^{-3}$ Strain at ultimate stress

Point 1 must satisfy hook's law:

$f_1 := .3 \cdot f_c = 1.623 \times 10^3$

$\varepsilon_1 := \frac{f_1}{E_c} = 3.73 \times 10^{-4}$

Point 2, 3 & 4 are calculated using equation

$$f := \frac{E_c \cdot \varepsilon}{1 + \left(\frac{\varepsilon}{\varepsilon_0}\right)^2}$$

f= Stress at any strain
ε= Strain at stress f
ε_0= Strain at ultimate compressive strength f_c

$f_2 = .46\ f_c = 1868.86$ $\varepsilon_2 = .00065$
$f_3 = .84\ f_c = 3411$ $\varepsilon_3 = .0015$
$f_4 = .96\ f_c = 3898$ $\varepsilon_4 = .002$
$f_5 = f_c = 4061$ $\varepsilon_5 = .0027$

$$\varepsilon := \begin{pmatrix} .000373 \\ .000605 \\ .00135 \\ .00186 \\ .00248 \end{pmatrix} \quad f := \begin{pmatrix} 1623 \\ 2488 \\ 4543 \\ 5192 \\ 5409 \end{pmatrix}$$

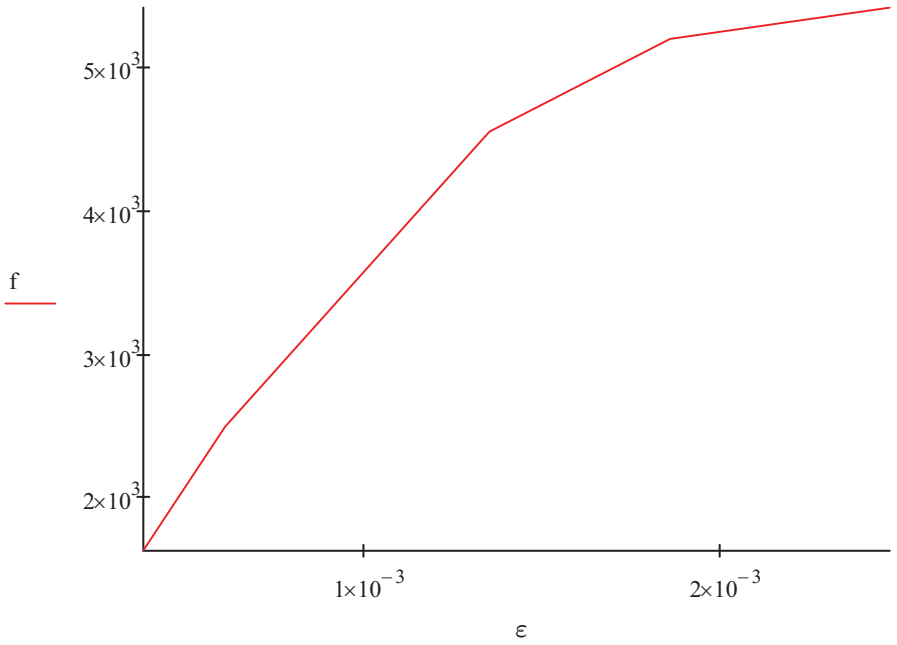

APPENDIX C

DEFLECTION CALCULATIONS (BEAM THEORY) AND ULTIMATE LOAD CALCULATIONS FOR SLABS SUBJECTED TO IN-PLANE LOADS

Section 1: Ultimate In-Plane Load capacity of Slab without Opening

In this method we assume that the steel is uniformly distributed at top and bottom slab

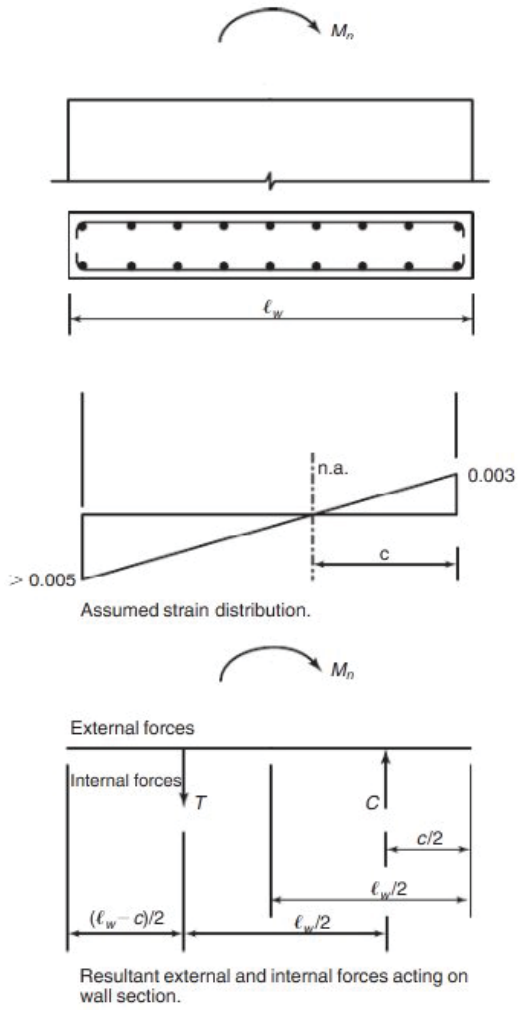

Figure C1: Illustration of Procedure to Compute Moment the Capacity of the Slab Panel With Openings when Subjected to In-Plane Loads

$A_s := 7.8 \quad in^2$ provided steel area (scaled) in each face of slab, assuming the distribution is uniform

$A_{st} := 2 \cdot A_s = 15.6 \quad in^2$ Total uniform area in the section

$L_w := 432 \quad in$ Depth of slab section

$f_y := 53373 \quad psi$ Yield stress of steel

$f_c := 4061 \quad psi$ Ultimate compressive stress of concrete

$\beta_1 := .85$

$d := 7 \quad in$ Depth of the slab

$L_r := 288 \quad in$ The distance from application of in-plane loads to the wall (moment arm)

$S := 4.5$ Scale factor

By equalling compressive and tensile forces in the section the c (neutral axis distance to compressive fiber) was calculated as follows:

$$c := \frac{A_{st} \cdot f_y}{.85 \cdot f_c \cdot d \cdot \beta_1 + \frac{A_{st} \cdot f_y}{L_w}} = 37.062 \quad in$$ Distance from extreme compressive fiber to neutral axis

$a := .85 \cdot c = 31.502 \quad in$ Depth of compressive stress block

$$T := A_{st} \cdot f_y \cdot \left(\frac{L_w - c}{L_w}\right) = 7.612 \times 10^5 \quad lbs$$ Tensile force of the section

$C_c := .85 \cdot f_c \cdot d \cdot a = 7.612 \times 10^5 \quad lbs$ Compressive force coming from concrete

$$C_s := A_{st} \cdot f_y \cdot \left(\frac{c}{L_w}\right) = 7.143 \times 10^4 \quad lbs$$ Compressive force coming from rebars at compression zone

$$M_n := T \cdot \left(\frac{L_w - c}{2}\right) + C_s \cdot \left(\frac{c}{2}\right) + C_c \cdot \left(c - \frac{a}{2}\right) = 1.679 \times 10^8 \quad lb.in$$ Moment cpacity at yield stage

$$P_n := \frac{M_n}{L_r} = 5.828 \times 10^5 \quad lbs$$

$$P_w := \frac{P_n}{S^2} \cdot \frac{4.45}{1000} = 128.079 \quad kN$$ Ultimate load capacity scaled down to the lab model (ultimate load for lab model was 120 kN)

$P_u := 120 \quad kN$

Ultimate load of tested slab and reproduced resultby ANSYS

$Ratio := \frac{P_n}{P_u} = 1.067$

This method overestimated the capacity in the test specimen by 7% more

Section 2: In- Plane Deflection Calculation Using Beam Theory Method:

In this section a theoritical method will be applied to calculate the deflection of the slab subjected to In-plane loads in linear range to verify the accuracy of the ANSYS model.

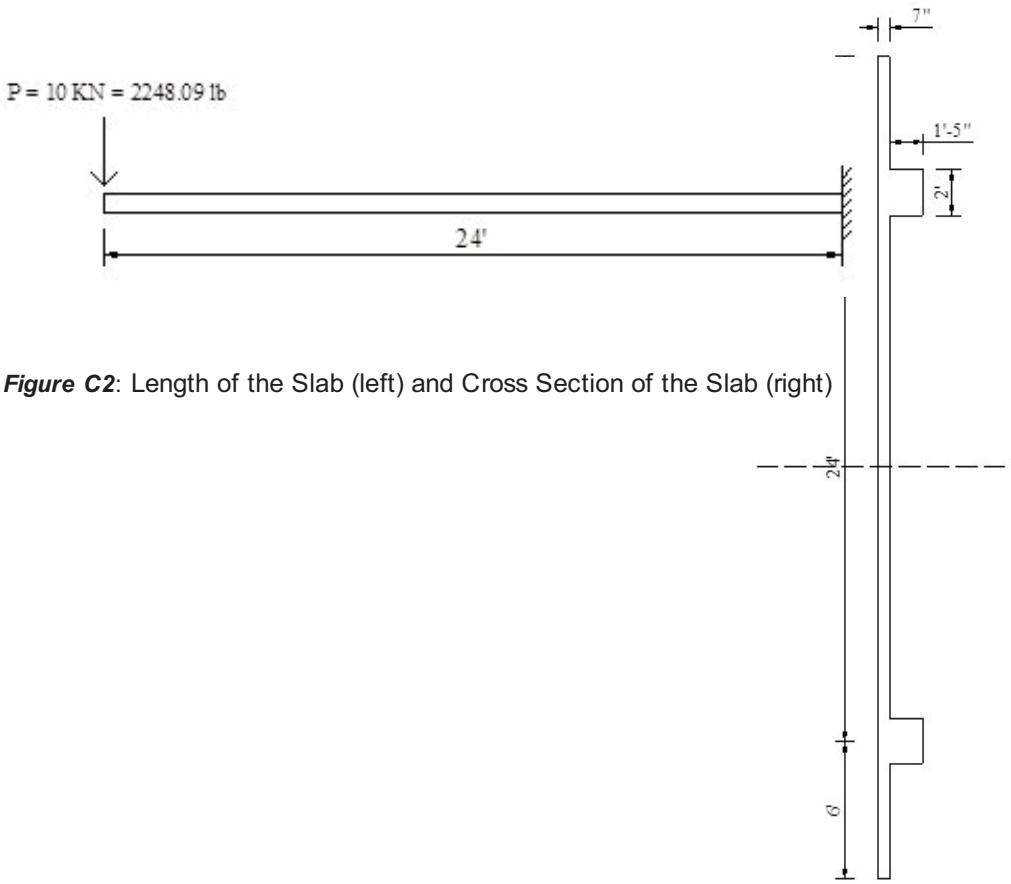

Figure C2: Length of the Slab (left) and Cross Section of the Slab (right)

The deflections due to bending moment and the shear force are calculated below:

$E := 3045800 \quad psi$ — Modulud of elasticity of concrete

$\nu := .13$ — Poisson's ratio of concrete

$I := \frac{7 \cdot 432^3}{12} + 2\left(\frac{17 \cdot 12^3}{12} + 17 \cdot 12 \cdot 144^2\right) = 5.549 \times 10^7 \ in^4$ — Moment of inertia of the section

$P := 10 \quad kN$ — Amount of load that slab remained elastic according to the report

$P := 2248.09 \quad lbs$ — The load value being converted from SI units to British units

$S := 4.5$ — Scaling factor used to convert values from lab to ANSYS model

$P := P \cdot S^2 = 4.552 \times 10^4 \quad lbs$ — Equivalant of 10 kN load converted to British units and scaled up prototype dimensions (ANSYS model)

$\Delta_{Bending} := \int_0^{288} \frac{x^2 \cdot P}{E \cdot I} dx = 2.145 \times 10^{-3} \quad in$ — Deflection due to bending moment

$G := \frac{E}{2(1+\nu)} = 1.348 \times 10^6 \quad psi$ — Shear modulus

$A := 7 \cdot 432 = 3.024 \times 10^3 \quad in^2$ — Shear area of the section

$\upsilon := 1$

$\Delta_{Shear} := \int_0^{288} \frac{K \cdot \upsilon \cdot P}{G \cdot A} dx = 3.217 \times 10^{-3}$

$\Delta_{Total} := \Delta_{Bending} + \Delta_{Shear} = 5.362 \times 10^{-3} \quad in$ — Total bending due to shear and bending moment

ANSYS Results

Deformation (in)	Load (kN)
3.94E-03	7.8
4.24E-03	8.4
4.54E-03	9
4.85E-03	9.6
5.15E-03	10.2
5.45E-03	10.8
5.76E-03	11.4
6.06E-03	12
6.36E-03	12.6

$\Delta_{ANSYS} := 5.15 \cdot 10^{-3}$ in

Note that 10 kN is approximately 8.33% of 120 kN

$Error := \frac{\Delta_{Total}}{\Delta_{ANSYS}} = 1.041$ Approximately 4% larger

$Stiffness_{Beam} := \frac{10}{\left(\Delta_{Total} \cdot \frac{25.4}{4.5}\right)} = 330.432$ Beam Theory Stiffness (kN/mm)

$Stiffness_{ANSYS} := \frac{10.2}{\left(\Delta_{ANSYS} \cdot \frac{25.4}{4.5}\right)} = 350.891$

The analysis result showed approximiately 4% larger displacement which well agreed with the results obtained from ANSYS analysis.